

RECEIVED: April 12, 2024

ACCEPTED: September 11, 2024

PUBLISHED: October 8, 2024

Search for Higgs boson pair production with one associated vector boson in proton-proton collisions at $\sqrt{s} = 13 \text{ TeV}$



The CMS collaboration

E-mail: cms-publication-committee-chair@cern.ch

ABSTRACT: A search for Higgs boson pair (HH) production in association with a vector boson V (W or Z boson) is presented. The search is based on proton-proton collision data at a center-of-mass energy of 13 TeV, collected with the CMS detector at the LHC, corresponding to an integrated luminosity of 138 fb^{-1} . Both hadronic and leptonic decays of V bosons are used. The leptons considered are electrons, muons, and neutrinos. The HH production is searched for in the $b\bar{b}b\bar{b}$ decay channel. An observed (expected) upper limit at 95% confidence level of VHH production cross section is set at 294 (124) times the standard model prediction. Constraints are also set on the modifiers of the Higgs boson trilinear self-coupling, k_λ , assuming $k_{2V} = 1$, and vice versa on the coupling of two Higgs bosons with two vector bosons, k_{2V} . The observed (expected) 95% confidence intervals of these coupling modifiers are $-37.7 < k_\lambda < 37.2$ ($-30.1 < k_\lambda < 28.9$) and $-12.2 < k_{2V} < 13.5$ ($-7.2 < k_{2V} < 8.9$), respectively.

KEYWORDS: Hadron-Hadron Scattering, Higgs Physics, Vector Boson Production

ARXIV EPRINT: [2404.08462](https://arxiv.org/abs/2404.08462)

JHEP10(2024)061

Contents

1	Introduction	1
2	The CMS detector	4
3	Data and simulated samples	5
4	Event reconstruction	8
5	Event selection	9
6	Categorization and analysis strategy	12
7	Background estimation methods	16
8	Systematic uncertainties	20
8.1	Theoretical uncertainties	21
8.2	Experimental uncertainties	22
9	Results	24
10	Summary	31
	The CMS collaboration	38

1 Introduction

Since the discovery of the Higgs boson (H) with a mass (m_H) of 125 GeV by the ATLAS and CMS Collaborations at the CERN LHC in 2012 [1–3], the focus of the Higgs boson experimental and phenomenological communities has shifted towards precise measurements of the properties of this particle and its interactions. The measured properties of this Higgs boson so far are consistent with the standard model (SM) predictions [4, 5]. The production of a pair of Higgs bosons (HH) is a rare process that provides unique access to so far unmeasured Higgs boson couplings. Of particular interest is the trilinear self-interaction coupling λ , that is embedded in the HH production in the SM, where $\lambda_{\text{SM}} = m_H^2/(2v^2)$ is 0.13 for $m_H = 125$ GeV and a vacuum expectation value, v , of 246 GeV.

The study of coupling modifications provides a probe of the shape of the scalar Higgs potential. Variations from their SM values are parametrized as $\kappa_\lambda = \lambda/\lambda_{\text{SM}}$. The implications of a beyond-the-SM (BSM) Higgs potential are profound. With a BSM potential, the electroweak phase transition in the early universe may not be a smooth transition from unbroken to broken electroweak symmetry as predicted by the SM, but rather, the transition would be abrupt [6]. In the presence of charge-conjugation and parity violation, the origins of baryon asymmetry could arise from electroweak baryogenesis [7, 8]. These models often

Production mode	Cross section (fb)	Scale uncertainty	PDF+ α_S uncertainty	m_t uncertainty
ggF	31.05	+2.2%/-5.0%	$\pm 3\%$	+4%/-18%
VBF	1.726	+0.03%/-0.04%	$\pm 2.1\%$	—
ZHH	0.363	+3.4%/-2.7%	$\pm 1.9\%$	—
W^+HH	0.329	+0.32%/-0.41%	$\pm 2.2\%$	—
W^-HH	0.173	+1.2%/-1.3%	$\pm 2.8\%$	—
$t\bar{t}HH$	0.775	+1.5%/-4.3%	$\pm 3.2\%$	—

Table 1. The cross sections and uncertainties of different HH production modes [11–14], where PDF is the parton distribution function, α_S is the strong coupling constant, and m_t is the top quark mass.

require deviations from the SM expectation for λ , and measuring κ_λ can provide valuable insights into the underlying physics and the existence of new phenomena beyond the SM.

In the SM, there are two other couplings whose modification could enhance some HH production channels involving vector bosons V (denoting either a W or Z boson) [9, 10]: the coupling of two vector bosons with a single Higgs boson (c_{VVH}), and two vector bosons with two Higgs bosons (c_{VVHH}). Their coupling modifiers relative to the SM are κ_V and κ_{2V} , respectively. In this paper, we investigate the VVHH couplings in two scenarios: the case where the couplings to W and Z are scaled together and the case where the couplings to W and Z are scaled independently. In the former case, the coupling modifier κ_{2V} represents both κ_{2W} and κ_{2Z} . In the latter case, they are uncorrelated. Measurements of single Higgs boson production by the ATLAS and CMS Collaborations have constrained both κ_W and κ_Z independently with a precision of 6–8%, and measured values are compatible with the SM predictions within that precision [4, 5]. No process arising from either c_{VVHH} coupling has been observed yet.

The HH production modes at the LHC are, in order of decreasing SM cross section, gluon-gluon fusion (ggF), vector boson fusion (VBF), vector boson associated production (VHH), and top quark associated production ($t\bar{t}HH$). In the SM with $m_H = 125$ GeV, the cross section of different HH production modes are shown in the table 1. The HH cross section is small due to the destructive interference of the contributing Feynman diagrams at leading order (LO). The total SM cross sections for VHH production is $\sigma_{VHH} = 0.865^{+5.4\%}_{-5.0\%}$ fb, computed at next-to-next-to-LO (NNLO) in quantum chromodynamics (QCD) [11, 12], and is approximately half the cross section of VBF HH production.

The CMS Collaboration has searched for the HH production process in the $b\bar{b}\gamma\gamma$ [15], $b\bar{b}b\bar{b}$ [16, 17], $b\bar{b}\tau\tau$ [18], $b\bar{b}ZZ$ [19], and multilepton [20] final states. A combination of these searches is presented in ref. [4], where the HH production cross section is constrained at 95% confidence level (CL) to 3.4 times the cross section predicted by the SM. In this combination, κ_λ and κ_{2V} are constrained from searches that target both ggF and VBF HH production channels. The allowed values at 95% CL of κ_λ and κ_{2V} are $-1.24 < \kappa_\lambda < 6.49$ (assuming $\kappa_{2V} = 1$) and $0.67 < \kappa_{2V} < 1.38$ (assuming $\kappa_\lambda = 1$). Moreover, the $\kappa_{2V} = 0$ coupling strength is excluded with a significance of 6.6 standard deviations while assuming SM values for all other couplings [4].

The ATLAS Collaboration has searched for the HH production process in the $b\bar{b}\gamma\gamma$ [21], $b\bar{b}\tau\tau$ [22], $b\bar{b}b\bar{b}$ [23], and $b\bar{b}WW$ [24] final states. These HH production searches have

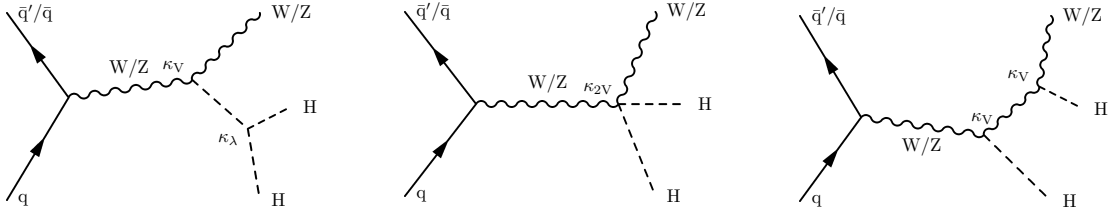


Figure 1. The three leading-order quark-initiated Feynman diagrams above result in a final state with two Higgs bosons and a W or Z boson. The left diagram requires one κ_V coupling vertex and one κ_λ coupling vertex. The middle diagram requires only one κ_{2V} coupling vertex, and the right diagram requires two κ_V coupling vertices.

been combined with the primary single Higgs boson decay channels [5] in a global search for κ_λ and κ_{2V} couplings [25]. Various HH analyses have been combined in a global search for κ_λ and κ_{2V} couplings [25], the former of which gains sizable contribution from the combination from single Higgs boson measurements [5]. The 95% CL limit on the inclusive HH production cross section is 2.4 times the SM expectation, while the 95% CL allowed range for κ_λ is $-0.4 < \kappa_\lambda < 6.3$.

Figure 1 shows representative Feynman diagrams for VHH production illustrating the dependence on the Higgs boson coupling modifiers. These three types of Feynman diagrams exhibit constructive interference when all the coupling modifiers are positive, leading to a significant enhancement in the cross section for VHH production [9, 10]. The VHH production cross section continues to steadily increase for positive coupling modifiers ($\kappa_\lambda > 0$ and $\kappa_{2V} > 0$), whereas other HH production channels have sizably reduced cross sections at approximately $\kappa_\lambda = 2$ because of the destructive interference. As a result, VHH stands out as an interesting channel for studying deviations from the predictions of the SM, given its sustained enhancement and absence of a minimum in the region $\kappa_\lambda > 0$. Notably, in the range of $4 < \kappa_\lambda < 7$ where the matrix element level interference is destructive for leading production mechanisms, VHH has constructive interference, and the sensitivity of the VHH search is near other subleading HH searches.

The ATLAS Collaboration recently published a search for VHH production [26] providing a 95% CL observed (expected) limit on VHH production at 183 (87) times the SM cross section. Only the leptonic channels were considered and 95% CL limits were set on the coupling modifiers κ_λ and κ_{2V} . The observed (expected) allowed ranges from the ATLAS VHH search are $-34.4 < \kappa_\lambda < 33.3$ ($-24.1 < \kappa_\lambda < 22.9$) (assuming $\kappa_{2V} = 1$) and $-8.6 < \kappa_{2V} < 10.0$ ($-5.7 < \kappa_{2V} < 7.1$) (assuming $\kappa_\lambda = 1$).

This paper reports on a search for VHH production in the final states with both Higgs bosons decaying into a bottom quark-antiquark pair, with a total branching fraction of $\mathcal{B}(\text{HH} \rightarrow b\bar{b}b\bar{b}) = 33.9 \pm 0.9\%$ [11]. The analysis is based on data from proton-proton (pp) collisions produced by the CERN LHC at $\sqrt{s} = 13$ TeV. To compensate for the low cross section of VHH production with SM coupling strengths, this analysis includes all the leptonic decay modes of the Z and W bosons except for those into tau leptons and is the first analysis to include a fully hadronic V decay channel in the search for nonresonant VHH

production. These decay modes encompass $Z \rightarrow v\bar{v}$, $W \rightarrow \ell\bar{\nu}$, $Z \rightarrow \ell\ell$, and $Z/W \rightarrow q\bar{q}/q\bar{q}'$, respectively, where ℓ corresponds to electrons or muons.

Experimentally, the V boson decay modes listed above are identified by their specific characteristics, including the presence of a large missing transverse momentum (\vec{p}_T^{miss}), the presence of one charged lepton, the presence of two charged leptons, and the presence of two hadronic showers (jets). The vector \vec{p}_T^{miss} is defined as the projection onto the plane perpendicular to the beam axis of the negative vector momenta sum of all reconstructed particles in an event. Its magnitude is referred to as p_T^{miss} . These characteristics help in distinguishing and categorizing the different decay modes.

The Higgs boson decaying to $b\bar{b}$ can be reconstructed as two small-radius jets. In the case where the Higgs boson has a large Lorentz boost, a single, large-radius jet provides better reconstruction efficiency than the small-radius jet reconstruction. All channels in this paper utilize the four small-radius jets topology to select events with two Higgs boson candidates, while two of the channels (large p_T^{miss} and one charged lepton channels) utilize the two large-radius jets topology as well.

This paper is organized as follows: section 2 provides a description of the CMS detector. In section 3, the data sets and simulated event samples utilized in the study are presented. The event reconstruction techniques are discussed in section 4. Section 5 outlines the event selection criteria used to identify the events of interest. The categorization scheme and overall analysis strategy are presented in section 6, providing insights into the methodology employed. The estimation and modeling of background contributions are addressed in section 7. Systematic uncertainties and their impact on the analysis are discussed in section 8. The final analysis results are presented in section 9. Finally, section 10 provides a comprehensive summary and conclusion of the analysis. The tabulated results are provided in a HEPData record [27].

2 The CMS detector

The central feature of the CMS apparatus is a superconducting solenoid of 6 m internal diameter, providing a magnetic field of 3.8 T. Within the solenoid volume are a silicon pixel and strip tracker, a lead tungstate crystal electromagnetic calorimeter (ECAL), and a brass and scintillator hadron calorimeter (HCAL), each composed of a barrel and two endcap sections. Forward calorimeters extend the pseudorapidity (η) coverage provided by the barrel and endcap detectors. Muons are detected in gas-ionization chambers embedded in the steel flux-return yoke outside the solenoid. A more detailed description of the CMS detector, together with a definition of the coordinate system used and the relevant kinematic variables, can be found in refs. [28, 29].

Events of interest are selected using a two-tiered trigger system. The first level (L1), composed of custom hardware processors, uses information from the calorimeters and muon detectors to select events at a rate of around 100 kHz within a fixed latency of about $4\ \mu\text{s}$ [30]. The second level, known as the high-level trigger (HLT), consists of a farm of processors running a version of the full event reconstruction software optimized for fast processing, and reduces the event rate to around 1 kHz before data storage [31].

Channel	Year	L1 trigger	HLT
MET	2016	$p_{T,L1}^{\text{miss}} > 110 \text{ or } 120$	$p_T^{\text{miss}} > 170$
	2017/2018	$p_{T,L1}^{\text{miss}} > 120$	$p_T^{\text{miss}} > 180$
1 electron	2016	$E_{T,L1} > 27$	$p_T(e) > 32$
	2017/2018	$E_{T,L1} > 30$	$p_T(e) > 35$
1 muon	2017	$p_{T,L1}(\mu) > 22$	$p_T(\mu) > 24$
	2016/2018	$p_{T,L1}(\mu) > 25$	$p_T(\mu) > 27$
2 electrons	2016–2018	$E_{T,L1}(e_1) > 22 \text{ and } E_{T,L1}(e_2) > 10$	$p_T(e_1) > 22 \text{ and } p_T(e_2) > 10$
2 muons	2016–2018	$p_{T,L1}(\mu_1) > 15 \text{ and } p_{T,L1}(\mu_2) > 8$	$p_T(\mu_1) > 17 \text{ and } p_T(\mu_2) > 8$
FH	2016	$H_T > 280$	4 jets $p_T > 45$, 3 b tags
		$H_T > 280$	4 jets $p_T > (90, 90, 30, 30)$, 3 b tags
	2017	$H_T > 280 \text{ and } 4 \times E_{T,L1} > (70, 55, 40, 35)$	$H_T > 300 \text{ and } 4 \text{ jets } p_T > (75, 60, 45, 40)$, 3 b tags
	2018	$H_T > 320 \text{ and } 4 \times E_{T,L1} > (70, 55, 40, 40)$	$H_T > 330 \text{ and } 4 \text{ jets } p_T > (75, 60, 45, 40)$, 3 b tags

Table 2. Kinematic thresholds for L1 triggers and for the HLT are listed for each analysis channel with variations per year as needed. HLT reconstruction is very similar to that for the offline reconstruction. The L1 reconstruction does not include any information from tracking in the inner detector. Transverse energy from ECAL plus HCAL systems is referred to as $E_{T,L1}$. The scalar sum of $E_{T,L1}$ from all energy deposits over a threshold of 30 GeV is denoted by H_T . The scalar sum of $E_{T,L1}$ from all energy deposits over a threshold of 30 GeV is H_T . The p_T , $E_{T,L1}$, and H_T thresholds are reported in GeV. The multiplicities of b-tagged jets used in the FH triggers are reported as n b tags.

3 Data and simulated samples

The search for the VHH signature entails exploration through four distinct channels: the missing transverse energy (MET), 1-lepton (1L), 2-lepton (2L), and fully hadronic (FH) channels. Each is designed to probe specific decay modes of W and/or Z bosons: $Z \rightarrow v\bar{v}$, $W \rightarrow \ell\bar{v}$, $Z \rightarrow \ell\ell$, and $Z/W \rightarrow q\bar{q}/q\bar{q}'$. Therefore, dedicated trigger strategies are implemented.

The selection requirements at the trigger level are listed in table 2. QCD multijet events, characterized by the exclusive production of jets through strong interactions, are large cross section backgrounds for the FH and MET channels at lower transverse momentum (p_T) scales. On the other hand, backgrounds for the 1L and 2L channels are mostly from electroweak processes with much lower cross sections. Thus, FH and MET channels’ triggers require more stringent p_T requirements than those in the 1L and 2L channels.

Selection criteria for the triggers used in this analysis evolved with data-taking conditions in the 2016 (36.3 fb^{-1}), 2017 (41.5 fb^{-1}), and 2018 (59.8 fb^{-1}) data sets, where the number between parentheses refer to integrated luminosities [32–34]. The MET channel requires a large ($> 120 \text{ GeV}$; $> 110 \text{ GeV}$ for early 2016) L1 p_T^{miss} signature from coarsely reconstructed calorimeter energy deposits. The minimum p_T^{miss} threshold at the HLT is 170 (180) GeV for 2016 (2017–2018) data. Anomalous high- p_T^{miss} events can be due to a variety of reconstruction failures, detector malfunctions, or noncollision backgrounds. Such events are rejected by event filters that are designed to identify more than 85–90% of the spurious high- p_T^{miss} events with a mistagging rate less than 0.1% [35]. In the 1L channel, a single electron or muon is required,

while the 2L channel requires two electrons or muons. The p_T criteria for these leptons vary from year to year, with muons having less stringent requirements compared to electrons due to the higher likelihood of jets being misidentified as electrons rather than muons.

The trigger strategy in the FH channel targets directly the decay products of the Higgs boson. Events are selected at L1 using triggers requiring the presence of at least four jets in the tracker acceptance ($|\eta| < 2.5$) and large H_T , defined as the scalar sum of the p_T of the reconstructed jets in the event. During the 2016 data taking, events are required to have $H_T > 280 \text{ GeV}$. In the 2017 data set, events are required to have $H_T > 280 \text{ GeV}$ and the four leading jets are required to pass staggered p_T thresholds of 70, 55, 40, and 35 GeV. In the 2018 data set, the H_T requirement was raised to 320 GeV and the lowest jet p_T threshold was raised to 40 GeV.

Events in the FH channel are selected in the HLT using a combination of triggers requiring the presence of jets coming from the hadronization of b quarks (b jets). Events are required to have at least four jets, at least three of which are identified as arising from a bottom quark (b tagged). In the 2016 data set, events are required to have either at least four jets with transverse momentum $p_T > 45 \text{ GeV}$, or two or more jets with $p_T > 90 \text{ GeV}$ and two or more jets with $p_T > 30 \text{ GeV}$. In the 2017 data set, an H_T requirement of 300 GeV was added to match the threshold at L1, and the four highest- p_T jets were required to pass staggered p_T thresholds of 75, 60, 45, and 40 GeV. The H_T threshold was raised to 330 GeV in 2018. The b tagging was performed in the HLT using the csv algorithm [36] in 2016–2017, and with the DEEPCSV algorithm [37] in 2018.

In the leptonic channels (MET, 1L, and 2L), the background model is based on shapes derived from Monte Carlo (MC) simulation. However, in the FH channel, the background model comprises two components: MC simulation for $t\bar{t}$ events and a data-driven multi-jet background. The MC simulated samples of VHH production are generated at LO in a fixed-order perturbative QCD calculation of up to four noncollinear high- p_T partons with MADGRAPH5_aMC@NLO (v2.6.5) [38]. The pp interaction simulation is supplemented with parton showering and multiparton interactions with PYTHIA (v8.240) [39]. The NNPDF3.1 [40] PDF is used in the simulation. The underlying event description tuned with CMS data is CP5 [41].

Additionally, samples at next-to-LO (NLO) and NNLO are generated to study the impact of higher-order corrections on kinematics. While the kinematic distributions at NLO are found to be similar to LO, the NNLO ggF ZHH process ($gg \rightarrow ZHH$) exhibits, on average, higher $p_T(Z)$ compared to ZHH production at NLO. A representative Feynman diagram for $gg \rightarrow ZHH$ is illustrated in figure 2 (left panel). The LO simulated signals are first scaled to NLO in perturbative QCD with a constant. To incorporate the $gg \rightarrow ZHH$ contributions, the LO ZHH samples are further corrected. They are reweighted as functions of $p_T(Z)$ to differentially account for the $gg \rightarrow ZHH$ cross section enhancement. The comparison between NLO and NLO+gg → ZHH is presented in figure 2 (right panel), and the ratios shown in the lower panel represent the functions used to reweight the NLO signals.

In order to correctly infer the kinematic properties and the inclusive cross section of a VHH signal with arbitrary coupling modifiers (i.e., κ_λ , κ_{2V} , and κ_V), at least six samples, which are linearly independent in the three-dimensional coupling space, must be generated and combined (i.e., weighted and summed). Assuming the matrix elements of the three LO

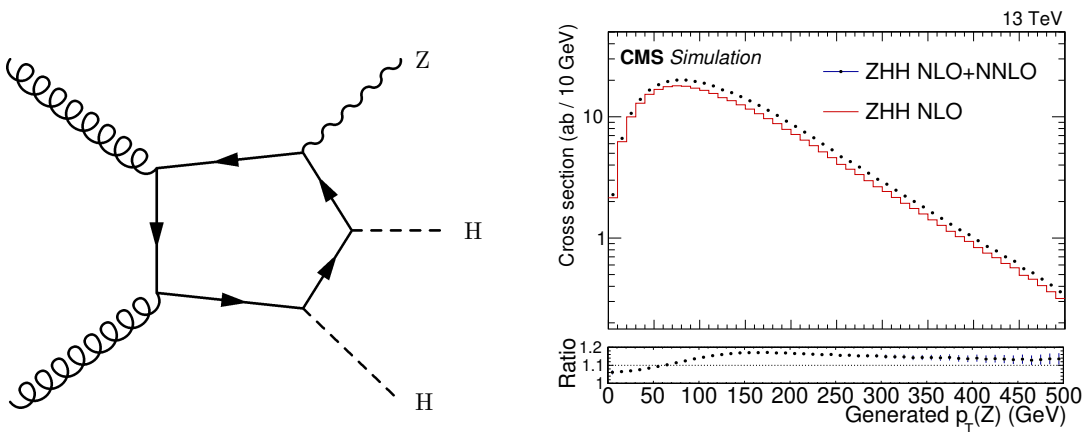


Figure 2. Left: representative Feynman diagram for ggF ZHH production, which represents approximately 14% of the total cross section for ZHH production. Right: distribution of $p_T(Z)$ with and without $gg \rightarrow ZHH$ process. The ratio is applied to NLO to incorporate the $gg \rightarrow ZHH$ cross section enhancement.

Feynman diagrams illustrated in figure 1 are denoted as A , B , and C under the SM, the cross section follows a relationship defined by:

$$\sigma(\kappa_\lambda, \kappa_{2V}, \kappa_V) \propto |\kappa_V \kappa_\lambda A + \kappa_{2V} B + \kappa_V^2 C|^2. \quad (3.1)$$

Six is the minimum number of samples required, arising from the three LO Feynman diagrams yielding three squared and three interference terms. In regions of coupling space beyond the generated values, improved statistical precision is facilitated by generating additional samples beyond the minimum. This is achieved using the Moore-Penrose inverse method [42, 43], where this analysis uses eight independent samples that are generated and combined with appropriate weights.

The $t\bar{t}$ +jets process simulated in POWHEG (v2.0) [44–47] is the dominant background in the MET and 1L channels, and is a significant background in the 2L channel. A dedicated $t\bar{t}b\bar{b}$ MC sample is generated in a four-flavor scheme (4FS) with dedicated POWHEG-BOX-RES and OPENLOOPs programs [48, 49], where the b quark is not considered a sea quark but kinematic effects due to the b quark mass are included. A complementary sample of simulated $t\bar{t}$ +jets events is generated using a five-flavor scheme (5FS) with POWHEG (v2.0), where the b quark is included in the sea but considered massless. For both samples, the pp interaction simulation is supplemented with PYTHIA (v8.230) CP5 tune [39, 41] and NNPDF3.1 PDF. The $t\bar{t}b\bar{b}$ process is defined as events having additional b jets at the particle level that do not originate from the top quark decays and that fulfill the acceptance requirements of $p_T > 20$ GeV and $|\eta| < 2.4$. The other events that do not fulfill this requirement are included in the $t\bar{t}$ process, and thus $t\bar{t}b\bar{b}$ and $t\bar{t}$ are mutually exclusive. The $t\bar{t}b\bar{b}$ process in the 4FS sample is combined with the $t\bar{t}$ process in the 5FS sample to yield the complete $t\bar{t}$ +jets process.

While Z+jets events are a negligible background to the FH and 1L channels, the Drell-Yan and Z+jets processes are substantial background in the 2L and MET channels. Drell-Yan production is generated with MADGRAPH5_amc@NLO (v2.6.5) [50] using the MLM [51] matching prescription at LO with up to 4 jets in the matrix element and is corrected to

NLO kinematics with $p_T(Z)$ reweighting. The samples are normalized to the cross section at NNLO [52–55].

Other background processes generated by the MADGRAPH5_aMC@NLO (v2.6.5) [50] are $t\bar{t}V$ (where V is W or Z and FxFx matching [56] is used for $t\bar{t}W$), and single top s -channel. The single top t -channel is generated with COMPHEP (v4.4) [57]. The POWHEG (v2.0) [44–47] generator is used to simulate events for single top quark tW and $t\bar{t}H$ production. All the samples are interfaced with PYTHIA (v8.240) [39] CP5 [41] tune and NNPDF3.1 [40] PDF for parton showering, fragmentation, and hadronization. In the MC that has Higgs boson production, the m_H is set to be 125 GeV. A full detector simulation is performed for all MC samples with GEANT4 [58].

Processes involving a W boson with additional jets, two top quarks with two vector bosons, two vector bosons, three vector bosons, one top quark with a Z boson, and one Higgs boson with a vector boson are negligible in all analysis channels based on simulations at NLO.

4 Event reconstruction

Global event reconstruction, utilizing the particle-flow (PF) algorithm [59], is designed to reconstruct and identify individual particles within an event (PF candidates) by optimizing information from subdetectors. Particle identification, in this process, plays an important role in the determination of the particle direction and energy. Photons are identified as ECAL energy clusters not associated with charged particle trajectories. Electrons are identified as primary tracks with corresponding ECAL energy clusters, accounting for bremsstrahlung photons within the tracker material. Muons are recognized as tracks consistent with either muon system hits or tracks with calorimeter deposits in line with the muon hypothesis. Charged hadrons are identified as tracks distinct from electrons or muons, while neutral hadrons are recognized as HCAL energy clusters without associated charged hadron trajectories or as an aggregate of ECAL and HCAL energy exceeding the expected charged hadron energy deposit.

The primary vertex (PV) is taken to be the vertex corresponding to the hardest scattering in the event, evaluated using tracking information alone [60]. For each event, hadronic jets are clustered from the reconstructed PF particles using the infrared and collinear safe anti- k_T algorithm [61, 62] with a distance parameter of 0.4 (denoted small-radius jets). As the Lorentz boost increases, hadron pairs from single-particle decays become more collimated, rendering the reconstruction of separate small-radius jets inefficient as the outer perimeters start to overlap. To enhance efficiency in this high signal-to-background scenario, an alternative reconstruction of hadronic jets with the anti- k_T algorithm with a distance parameter of 0.8 (denoted large-radius jets) is used.

For small-radius jets, jet momentum is determined as the vectorial sum of all particle momenta in the jet, and is found from simulation to be, on average, within 5–10% of the true momentum over the whole p_T spectrum and detector acceptance. Additional pp interactions within the same or nearby bunch crossings (pileup) can contribute additional tracks and calorimetric energy depositions to the jet momentum. To mitigate this effect, charged particles identified to be originating from pileup vertices are discarded and an offset correction is applied to correct for remaining contributions. Jet energy corrections are derived from simulation to bring the measured response of jets to that of particle level jets on

average. In situ measurements of the momentum balance in dijet, photon + jets, Z + jets, and multijet events are used to account for any residual differences in the jet energy scale between data and simulation [63]. The jet energy resolution amounts typically to 15–20% at 30 GeV, 10% at 100 GeV, and 5% at 1 TeV [63]. Additional selection criteria are applied to each jet to remove jets potentially dominated by anomalous contributions from various subdetector components or reconstruction failures. All selected jets in this analysis have an additional b jet energy regression applied [64]. The regression improves the resolution of the dijet mass of reconstructed Higgs boson candidates in signal simulation by 10–15%, as a function of the dijet p_T .

Reconstructed jets must have sufficient fractions of energy from various PF candidates (i.e., neutral hadron, charged hadron, and neutral electromagnetic) required via JETID thresholds [65] and the medium working point for the PILEUPJETID [65]. Since \vec{p}_T^{miss} represents the negative vector sum of momenta from all reconstructed particles in an event, the jet energy corrections are propagated to \vec{p}_T^{miss} for the energy balance.

For large-radius jets, the pileup-per-particle identification algorithm [65, 66] is used to mitigate the effect of pileup at the reconstructed-particle level, making use of local shape information, event pileup properties, and tracking information. A local shape variable is defined that distinguishes between collinear and soft diffuse distributions of other particles surrounding the particle under consideration; the former is attributed to particles originating from the hard scatter and the latter to particles originating from pileup interactions. Charged particles originating from pileup vertices are discarded. For each neutral particle, a local shape variable is evaluated using the surrounding charged particles compatible with the PV within the tracker acceptance ($|\eta| < 2.5$), and using both charged and neutral particles in the region outside of the tracker coverage. The momenta of the neutral particles are then rescaled according to their probability to originate from the PV deduced from the local shape variable, obviating the need for jet-based pileup corrections [65].

Small-radius b jets are identified with a deep neural network (DEEPJET) trained on all PF inputs [37, 67], achieving an expected selection efficiency of 80% with misidentification rate of 1 (15)% of light-flavor (charm-flavor) jets per selected jet for the medium working point [36]. The number of b-tagged small-radius jets, denoted by N_b , is defined as the number of jets passing a certain working point of this tagger. For the channels with large-radius jets, a graph neural network called PARTICLENET [68] is used to identify large-radius jets originating from the hadronization of two b quarks. The PARTICLENET algorithm outputs $D_{b\bar{b}}$, which represents the probability that a given jet originates from the hadronization of a b quark pair. For the tight, medium, and loose working points, PARTICLENET achieves expected selection efficiencies of 60, 80, and 90%, with misidentification rate of 0.3, 1, and 2%, respectively [17].

5 Event selection

In the scenario of SM couplings, only about 40 events would be produced in the $b\bar{b}b\bar{b}$ decay channel of VHH production for the integrated luminosity of 138 fb^{-1} without any selection applied. In the leptonic channels, to maximize signal efficiency, offline thresholds on the objects used in the trigger selection are close to the trigger thresholds. The trigger efficiencies are measured in data, and simulation is corrected to match data as a function of relevant

object p_T , η , and azimuthal angle ϕ . The FH channel uses offline jet thresholds below the trigger thresholds; including events that pass the trigger but are below the region that is fully efficient leads to a significant increase in signal acceptance. The efficiency of the H_T (jet-level p_T and b-tagging) requirements used in the trigger are measured as a function of the offline H_T (jet p_T). These efficiency measurements, referred to as trigger turn-ons, are measured in data and simulation using leptonic (electron + muon) $t\bar{t}$ events, triggered by the leptons. The H_T and jet-level trigger turn-ons are combined to correct the per-event trigger efficiency in simulation to match that of data.

In order to reduce contribution from backgrounds with misidentified leptons, electrons and muons in the 1L and 2L channels are required to be isolated. The specific isolation variable computed for this analysis is:

$$I_{\text{PF}} \equiv \frac{1}{p_T(\ell)} \left(\sum_{\text{in cone}} p_T^{\text{charged PF}} + \max \left[0, \sum_{\text{in cone}} p_T^{\text{neutral PF}} + \sum_{\text{in cone}} p_T^{\gamma \text{ PF}} - p_T^{\text{PU}}(\ell) \right] \right), \quad (5.1)$$

where $p_T^{\text{charged PF}}$, $p_T^{\text{neutral PF}}$, and $p_T^{\gamma \text{ PF}}$ are the reconstructed p_T of the charged, neutral, and photon PF candidates inside the cone centered on (but not including) the lepton track. The $p_T^{\text{PU}}(\ell)$ term is a pileup contribution, which is subtracted to remove momenta from particles not originating from the lepton's pp collision. The separation from the lepton track is measured as $\Delta R = \sqrt{(\Delta\eta)^2 + (\Delta\phi)^2}$, where $\Delta\eta$ and $\Delta\phi$ are the η and ϕ differences, respectively. The cone size is $\Delta R = 0.4$ (0.3) for electrons (muons), and the isolation variable is normalized by the lepton p_T . In the 1L channel, leptons must have $I_{\text{PF}} < 0.06$, which is a stringent selection criterion to remove any QCD multijet background in this channel. Furthermore, to ensure compatibility with a W boson, the lepton and \vec{p}_T^{miss} must satisfy the requirement $\Delta\phi(\vec{p}_T(\ell), \vec{p}_T^{\text{miss}}) < 2.0$. In the 2L channel, the isolation requirement is $I_{\text{PF}} < 0.15$ (0.25) for electrons (muons), which is much less stringent due to the intrinsic absence of substantial reducible backgrounds in the 2L channel.

Electrons are required to pass selection criteria based on the ECAL energy shape, compatibility of the associated track momentum and ECAL energy, and the absence of energy deposition in the HCAL. These criteria are optimized with a boosted decision tree (BDT) [69, 70]. In the 2L (1L) channel, the medium (tight) BDT working point is required. Muons in both 1L and 2L channels are required to pass the “tight” identification requirements, as detailed in ref. [71].

To further eliminate reducible backgrounds, such as QCD multijet events in MET and 1L channels and $t\bar{t}$ events in the 2L channel, the vector boson is reconstructed using \vec{p}_T^{miss} , $\vec{p}_T(\ell) + \vec{p}_T^{\text{miss}}$, $\vec{p}(\ell_1) + \vec{p}(\ell_2)$, and $\vec{p}(j_1) + \vec{p}(j_2)$ in the E_T^{miss} , 1L, 2L, and FH channels where j_1 and j_2 stand for the leading and subleading jets ordered by their p_T , respectively. Kinematic thresholds on leptons, jets, p_T^{miss} , and reconstructed vector bosons are described in table 3.

When jet p_T is inaccurately estimated, it can result in large p_T^{miss} . These events are vetoed from the MET channel by requiring that the $\Delta\phi$ between \vec{p}_T^{miss} and all Higgs boson decay candidate jets must be above a \vec{p}_T^{miss} -dependent threshold:

$$\Delta\phi > 0.4 \exp(4 - p_T^{\text{miss}}/50 \text{ GeV}) + 0.07. \quad (5.2)$$

Channel	Vector boson decay products selection	Vector boson selection	Jet selection
MET small-radius		$p_T^{\text{miss}} > 150 \text{ GeV}$	≥ 4 small-radius jets with $p_T > 35 \text{ GeV}$
MET large-radius		$p_T^{\text{miss}} > 250 \text{ GeV}$	≥ 2 large-radius jets with $p_T > 200 \text{ GeV}$
1L	$p_T(e) > 32 \text{ (28) GeV}$ $2018/2017 \text{ (2016)}$ OR $p_T(\mu) > 25 \text{ GeV}$	$p_T(W) > 125 \text{ GeV}$	≥ 3 small-radius jets with $p_T > 25 \text{ GeV}$ AND ≥ 4 small-radius jets with $p_T > 15 \text{ GeV}$ OR ≥ 2 large-radius jets with $p_T > 200 \text{ GeV}$
2L	$p_T(\mu_{1[2]}) > 20 \text{ [20] GeV}$ OR $p_T(e_{1[2]}) > 25 \text{ [20] GeV}$	$p_T(\ell\ell) > 50 \text{ GeV}$	≥ 4 small-radius jets with $p_T > 20 \text{ GeV}$
FH	$p_T(j_i) > 20 \text{ GeV}$	$65 < m_{jj,V} < 105 \text{ GeV}$	≥ 4 small-radius jets with $p_T > 40 \text{ GeV}$ and ≥ 6 small-radius jets with $p_T > 20 \text{ GeV}$

Table 3. Thresholds on kinematic variables for all selected objects are listed for each channel. Objects are always required to be within the acceptance of the CMS subdetectors, which is $|\eta| < 2.5$ for electrons and 2.4 for all other objects, as well as outside of barrel-endcap transition regions near $|\eta| \sim 1.5$. The dijet mass of the two jets with lower b tagging scores than the Higgs candidate jets in the FH channel is denoted $m_{jj,V}$.

Since the \vec{p}_T^{miss} spatial resolution is worse at lower values of p_T^{miss} , this function is designed to impose a larger $\Delta\phi$ criteria at lower values of \vec{p}_T^{miss} . This selection removes events with wrongly reconstructed p_T^{miss} that are not modeled in the simulation.

Jets in all channels have standard quality selection criteria applied to avoid selecting reconstructed jets resulting from noise in the HCAL or ECAL [65]. All leptonic channels require at least four small-radius jets or two large-radius jets. These jets are ordered by DEEPJET b tagger score or D_{bb^-} . The leading four small-radius jets or two large-radius jets are selected as the Higgs boson candidate jets. In the FH channel, at least six small-radius jets are needed. The four jets with the highest DEEPJET score are considered to be the Higgs boson candidate jets and at least three of them must pass a threshold of 0.6 in the

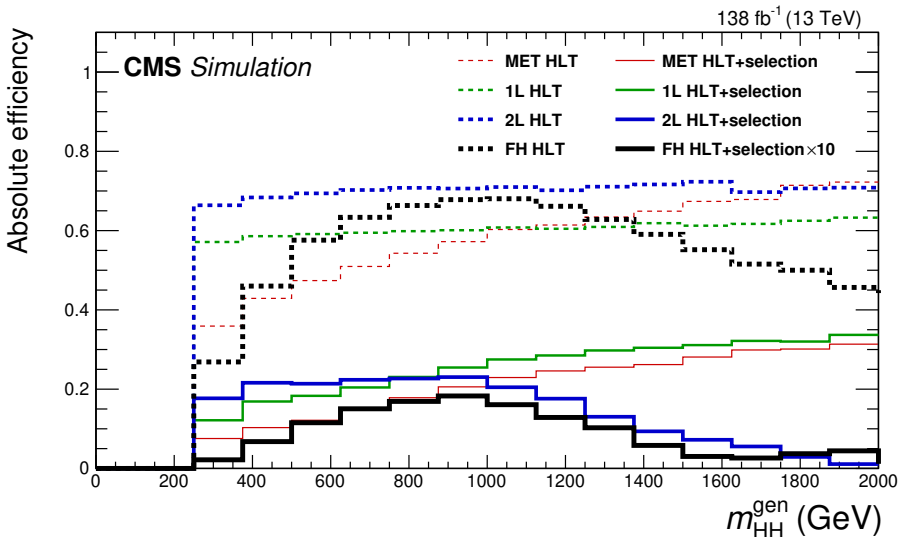


Figure 3. The SM VHH efficiencies of trigger selections (dashed lines) and full selections (solid lines) are shown for all four analysis channels. Decays involving tau lepton decays are not considered for the 1L and 2L channel efficiencies. The full selection efficiency in the FH channel is scaled up by 10 for visibility. Both sets of efficiencies are absolute efficiencies (acceptance times selections efficiencies).

DEEPJET b tagging score optimized to maximize the expected significance; this threshold is more stringent than the medium working point used in the leptonic channels. In other jets (excluding the Higgs boson candidates), at least one pair must be able to form a dijet with invariant mass $65 < m_{jj,V} < 105$ GeV. Among the candidates, the pair with leading p_T is selected to reconstruct the vector boson.

Figure 3 shows the dependence of the absolute efficiencies (acceptance times trigger and analysis selections efficiencies) on the mass of HH at generator level, $m_{\text{HH}}^{\text{gen}}$. The leptonic channels generally have high efficiency after HLT selection because no jets are required. The FH selection requires four jets at the HLT and thus its efficiency is generally lower. After applying all the analysis selections, the 1L and MET channel still maintain relatively high efficiencies at high $m_{\text{HH}}^{\text{gen}}$ because of the inclusion of the large-radius jet regions.

In channels featuring four small-radius jets, there exist three combinations of dijet pairings for reconstructing the two Higgs boson candidates. To optimize the selection of signal events and prevent biasing kinematic features of background processes, a metric is employed that aims to balance the masses of the two Higgs boson candidates. For each pairing, the variable D_{HH} is calculated as $D_{\text{HH}} = |m_{jj,1} - cm_{jj,2}|$, where $m_{jj,1}$ and $m_{jj,2}$ represent the masses of the Higgs boson candidates [16], and c is a correction factor between $m_{jj,1}$ and $m_{jj,2}$. The pairing with the smallest value of D_{HH} is chosen.

6 Categorization and analysis strategy

Categorization is a critical aspect of the VHH analysis. The kinematic distributions of the VHH process vary differently for κ_λ or κ_{2V} enhancements. The general strategy is to separate the regions that are most important for the two types of signal enhancements and to optimize in each region separately. Instead of creating categories based on simple kinematic properties,

a categorization BDT (BDT_{Cat.}) is used in most channels to define two signal regions: one with enhanced signal for large κ_{2V} couplings and another for large κ_λ couplings. In each of these categories, a multivariate algorithm, either a BDT (BDT_{SvB}) or neural network (NN_{SvB}), is used as fit observable for signal vs background separation.

Events are subdivided into different regions based on the invariant mass of the Higgs boson pair m_{HH} , the number of b-tagged jets N_b , and further into regions enhanced in sensitivity to κ_λ and κ_{2V} , and, for the 2L channel, a t̄t-enhanced region. In the 2L channel, we define an additional t̄t-enriched category by selecting all events that fall outside a Z boson mass window in the dilepton mass $m_{\ell\ell}$: $80 < m_{\ell\ell} < 100$ GeV. This category constrains some systematic uncertainties in the t̄t process simulations. The regions where all four jets are b-tagged are the most significant.

When correctly reconstructed, the HH signal is concentrated in the region where both Higgs boson candidates have masses near 125 GeV. There are reconstruction effects that cause the peak value of the Higgs boson candidates to not be reconstructed at 125 GeV. The candidate mass is corrected by a factor r so that the peak value of the signal is at generator mass of 125 GeV. These simulation-based correction factors r_1 (r_2) for the first (second) Higgs boson candidate are determined to be $r_1 = r_2 = 1$ for the leptonic channels, and $r_1 = 1.02$ and $r_2 = 0.98$ for the FH channel. To quantify how close a given event is to the expected HH signature, we then define two variables r_{HH} and δ_{HH} quantifying the distance of the reconstructed candidate masses to the expected Higgs boson mass in simulation:

$$r_{HH} = \sqrt{(m_{H_1} - 125 \text{ GeV } r_1)^2 + (m_{H_2} - 125 \text{ GeV } r_2)^2},$$

and

$$\delta_{HH} = \sqrt{\left(\frac{m_{H_1} - 125 \text{ GeV } r_1}{m_{H_1}}\right)^2 + \left(\frac{m_{H_2} - 125 \text{ GeV } r_2}{m_{H_2}}\right)^2},$$

where m_{H_1} and m_{H_2} are the masses of the Higgs boson candidates.

Signal regions (SRs), control regions (CRs), and sideband regions (SBs) are defined by requirements on r_{HH} or δ_{HH} : for the leptonic channels, the SRs are defined by $r_{HH} < 25$ GeV, the CRs by $25 < r_{HH} < 50$ GeV, and the SBs by $50 < r_{HH} < 75$ GeV, similar to ref. [16]. For the FH channel, the SR is defined by $\delta_{HH} < 0.19$, while the region beyond that defines the SB. In the leptonic channels, SRs with three or four b jets have significant signal yields, and are thus used for signal extraction. As expected, the category with $N_b = 4$ is the most significant. In the 2L channel, $N_b = 4$ and 3 are optimized and statistically analyzed separately, while in other leptonic channels they are validated separately but analyzed together. The electron and muon channels are merged in 1L and 2L channels. In the 2L channel, data (and simulation) from all years are merged to improve statistical precision in the background estimation.

In all channels, we maximize the sensitivity for enhanced SM coupling strengths, particularly on κ_λ and κ_{2V} , by leveraging kinematic variables whose distributions are significantly different when one or the other coupling of interest is larger than the SM prediction. To optimize the separation of these kinematic regions, a BDT is trained to separate events according to the signal kinematics into a category with enhanced κ_λ contribution ($\kappa_\lambda = 20$ in training) and one with enhanced κ_{2V} contribution ($\kappa_\lambda = 0$ in training) using the SCIKIT-LEARN

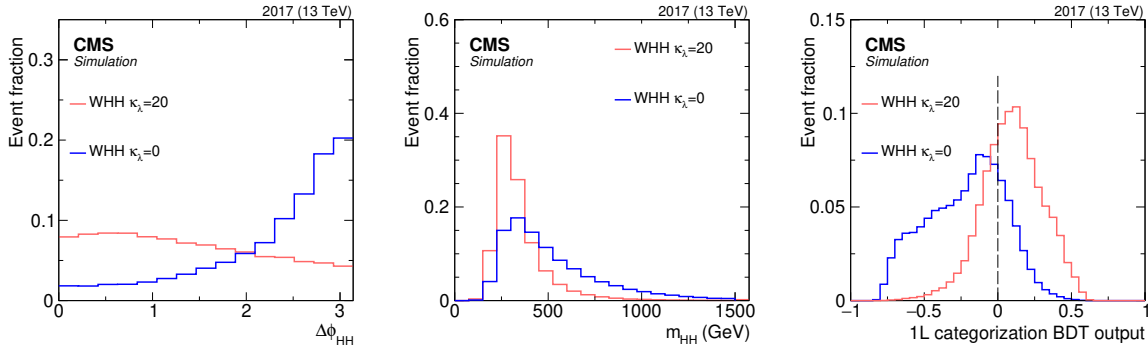


Figure 4. Kinematic distributions of the HH signal for different coupling strengths. Left and middle: azimuthal angle between the two reconstructed Higgs boson candidates, $\Delta\phi_{\text{HH}}$, and the reconstructed HH mass, m_{HH} , in the 1L SR for two different coupling values, $\kappa_\lambda = 20$ and 0. Right: the categorization BDT output for the same two models. The dashed vertical line shows where the categorization boundary is set.

software [72]. In the latter case, reducing the κ_λ coupling to zero effectively enhances κ_{2V} . Other pairs of enhanced coupling samples were tested in the training of candidate $\text{BDT}_{\text{Cat.}}$. The selected pair, $\kappa_\lambda = 20$ and 0, was among several that were equally performant in the separation of signal kinematics. The categorization BDT is used to define κ_λ -enriched and κ_{2V} -enriched SRs, which are distinct and optimized separately for signal versus background separation. Figure 4 highlights one of many kinematic inputs to a categorization BDT (from the 1L channel as an example), as well as the BDT output, for two simulated signal samples. Separate BDTs are trained for each channel due to the varying mass resolution and kinematic effects of the trigger and selection criteria. The categorization boundary value in the $\text{BDT}_{\text{Cat.}}$ is optimized to separate the signal models in the training. This procedure was validated by varying the boundary and comparing final results. The same procedure is implemented in each channel. The variables used as input to the BDT trainings are listed in table 4.

In the large-radius jet analysis in the MET and 1L channels, events are divided into three regions using the $D_{b\bar{b}}$ of each Higgs boson candidate jet: $\min(D_{b\bar{b},1}, D_{b\bar{b},2}) > 0.94$ defines high-purity regions (HP), $0.90 < \min(D_{b\bar{b},1}, D_{b\bar{b},2}) < 0.94$ defines low-purity regions (LP), and $\min(D_{b\bar{b},1}, D_{b\bar{b},2}) < 0.90$ and $\max(D_{b\bar{b},1}, D_{b\bar{b},2}) > 0.80$ define failing regions. No κ_λ -enrichment is possible in this topology because the two large-radius jets tend to have $\Delta\phi \sim \pi$, which corresponds both to enhanced κ_{2V} , shown in figure 4, and larger values of m_{HH} . These regions are therefore considered κ_{2V} -enriched by construction, and thus no additional categorization based on $\text{BDT}_{\text{Cat.}}$ is considered. Separate BDT_{SvB} are optimized in the LP and HP regions.

For the signal extraction, the output of a dedicated machine learning classifier trained to separate signal and background is used. In the leptonic channels, BDT_{SvB} s are used to separate signal-like events from background-like events. Simulated signal samples with corresponding enhancements (i.e., κ_{2V} -enriched or κ_λ -enriched) are used in the training for the different regions. The variables used as input to the BDT are listed in table 4.

In the FH channel, the NN_{SvB} classifier is a neural network discriminant with residual learning [74]. The neural network contains multiple convolutional layers where all combinations

Input variable	BDT _{Cat.}			BDT _{SvB}			NN _{SvB}	
	MET/1L	2L	FH	MET (S)	1L (S)	MET/1L (L)	2L	FH
$p_T(V), p_T(H_1)$	✓	✓	✓	✓	✓	✓	✓	✓
$p_T(HH)$	✓			✓	✓	✓	✓	✓
$p_T(H_2)$	✓			✓	✓	✓	✓	
m_{H_1}	✓			✓	✓	✓	✓	
m_{H_2}	✓			✓	✓	✓	✓	
m_{HH}	✓	✓	✓	✓	✓	✓	✓	
$\Delta R(H_1, H_2)$	✓			✓				
$\Delta\phi(V, H_2)$	✓			✓	✓		✓	
$p_T(H_2)/p_T(H_1)$	✓	✓	✓					
$\Delta\eta(H_1, H_2)$	✓			✓				
$\Delta\phi(H_1, H_2)$	✓			✓	✓	✓	✓	
Energy of H_1	✓						✓	
Energy of H_2	✓				✓			
Energy of HH	✓						✓	
η_{HH}	✓			✓				
η_{H_1}			✓		✓			
$\phi(V)$				✓	✓	✓	✓	
$s_{b\text{-tag}}(j_{1,2,3,4})$				✓	✓			
H_T^{ex}				✓				
m_V				✓			✓	
$\Delta R(H_1, H_2)$		✓		✓			✓	
$\Delta\phi(V, H_2)$		✓		✓			✓	
$\Delta R(H_1, H_2)$				✓			✓	
N_{jets}				✓				✓
$\tau_2/\tau_1(H_1, H_2)$						✓		
$\tau_3/\tau_2(H_1, H_2)$						✓		
$p_T(\ell_2)/p_T(\ell_1)$			✓				✓	
$\Delta\phi(\ell_1, \ell_2)$			✓				✓	
$\Delta\eta(\ell_1, \ell_2)$			✓				✓	
$\Delta R(j_{1,H_2}, j_{2,H_2})$			✓				✓	
$\Delta R(j_{1,H_1}, j_{2,H_1})$			✓				✓	
$p_T(\ell_1)/m_V$			✓					
$p_T(\ell_1)$			✓					
$p_T(j_{3,4})$						✓		
H_T^{VHH}						✓		
$p_T(V)/p_T(HH)$						✓		
$\Delta\phi(V, HH)$						✓		
$p_T(\ell_1)/m_V$						✓		
$\eta/\phi/m/p_T(j_{1,2,3,4,\text{other}})$							✓	
$m_{j_i j_k}$							✓	
$\Delta\phi(j_i, j_k)$							✓	
Year							✓	

Table 4. Variables used in the categorization BDTs for the separation of the κ_λ - and κ_{2V} -enriched regions, as well as in BDT_{SvB} and NN_{SvB} for extracting signal-like events. The ✓ symbol indicates that the BDTs include the variable. These variables include the reconstructed Higgs boson with leading (H_1) and subleading (H_2) transverse momentum, the Higgs boson candidate jets ordered by the DEEPJET b tagging score ($j_{1,2,3,4}$), the other jets (j_{other}), the dijets formed by any two jets ($j_i j_k$ with $i, k \in \{1, 2, 3, 4\}$), the scalar sum of the transverse energy of all the jets excluding $j_{1,2,3,4}$ (H_T^{ex}), the number of jets (N_{jets}), the selected leptons in the 2L channel (ℓ_1, ℓ_2), the N -subjettiness [73] ratio τ_2/τ_1 and τ_3/τ_2 . The small-radius (large-radius) regions are designated with an “S” (“L”) in parentheses.

Variable for categorization	BDT _{Cat.}	$N_b, D_{b\bar{b}}$	r_{HH}, δ_{HH}, m_V	Year split	$N(\text{regions})$	Observable
Signal regions						
MET small-radius	$\kappa_\lambda, \kappa_{2V}$	$N_b \geq 3$	SR+CR	Per year	6	BDT _{SvB}
MET large-radius	κ_{2V}	HP, LP	SR+CR	Per year	6	BDT _{SvB}
1L small-radius	$\kappa_\lambda, \kappa_{2V}$	$N_b \geq 3$	SR+CR	Per year	6	BDT _{SvB}
1L large-radius	κ_{2V}	HP, LP	SR+CR	Per year	6	BDT _{SvB}
2L	$\kappa_\lambda, \kappa_{2V}$	$N_b = 3 \text{ or } 4$	SR, CR	Combined	8	BDT _{SvB}
FH	$\kappa_\lambda, \kappa_{2V}$	$N_b = 4$	SR	Per year	6	NN _{SvB}
Control regions						
MET small-radius	—	$N_b \geq 3$	SB	Per year	3	$p_T(V)$
MET large-radius	—	HP, LP	SB	Per year	6	m_{H_2}
1L small-radius	—	$N_b \geq 3$	SB	Per year	3	$p_T(V)$
1L large-radius	—	HP, LP	SB	Per year	6	m_{H_2}
2L (DY)	—	$N_b = 3 \text{ or } 4$	DY CR	Combined	2	$p_T(V)$
2L (TT)	—	$N_b \geq 3$	t \bar{t} CR	Combined	1	$p_T(V)$

Table 5. A summary of the categorization used in all of the channels, where DY denotes Drell-Yan production. The first row outlines the variables used for the categorization. HP and LP are regions defined based on $D_{b\bar{b}}$ cuts: $\min(D_{b\bar{b},1}, D_{b\bar{b},2}) > 0.94$ (HP), and $0.90 < \min(D_{b\bar{b},1}, D_{b\bar{b},2}) < 0.94$ (LP). N_b is the number of jets that pass DEEPJET b tagging score medium working point.

of the four Higgs boson candidate jets are considered. A multi-head attention block [75] in the neural network considers the kinematic variables associated with additional jets.

In the SB regions, the observables are kinematic variables with significant systematic uncertainties that can be constrained with a fit to data. The observable in all small-radius leptonic SBs and in the t \bar{t} CR is the reconstructed $p_T(V)$. In the large-radius SBs, the mass of the subleading large-radius jet is the observable. Overall, 59 distinct regions are used. Table 5 summarizes the categories used in each channel.

7 Background estimation methods

A variety of background estimate strategies are employed in this analysis. In the FH channel, a data-driven technique is used to create a background estimate from a region with an inverted b tagging selection directly from reweighted data. In the leptonic channels, simulation is used to model the various background processes.

Because of the limited statistical precision of background simulations, a reweighting method exploiting a BDT is used in some regions [76]. The technique is to invert part of the event selection to define an “inverted” region where MC events are numerous and reweight events from the inverted region such that analysis variables, as well as the correlations among them, match those of the signal selection. Similar approaches were also adapted in other analyses, as demonstrated in refs. [77, 78]. In practice, the BDTs are trained to distinguish between the inverted and signal regions. The BDT output scores are used to produce the reweighting function between the inverted and signal regions. The BDT output distribution

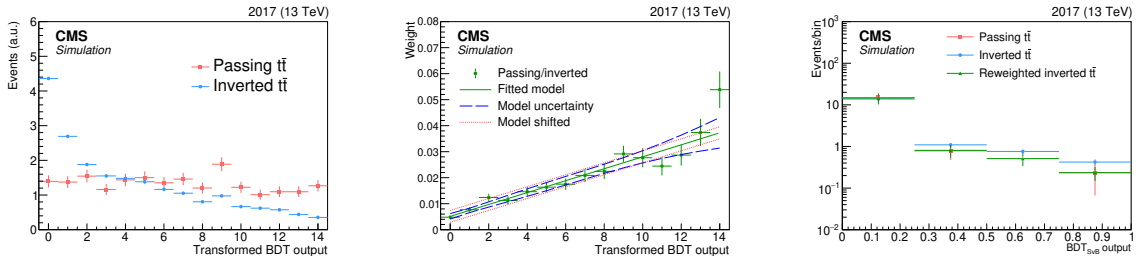


Figure 5. Left: a reweighting BDT in the 1L LP region for the $t\bar{t}$ process that is transformed such that the limited-precision passing $t\bar{t}$ sample, shown as red squares, is approximately evenly distributed across all bins. In blue circles is the same process where the b tagging selections are inverted. Middle: the ratio is shown of passing $t\bar{t}$ to inverted $t\bar{t}$ (green points) as a function of the transformed reweighting BDT score. The solid line is the second-order polynomial fit of the green points, which is used for the reweighting. In dotted red and dashed blue are the associated systematic uncertainties, which are obtained from shifting the BDT score bin in evaluation of the model and the evaluation of the fit uncertainties on the weight, respectively. These systematic variations account for finite binning and limited statistical precision of the passing events, and they enhance the flexibility of the model. Right: the distribution of BDT_{SvB} from passing (red squares), inverted (blue points), and reweighted inverted $t\bar{t}$ (green triangles) sample in the 1L LP region. The inverted $t\bar{t}$ is normalized to make it the same yield as the reweighted inverted $t\bar{t}$. The uncertainty of reweighted inverted $t\bar{t}$ distribution includes both statistical and systematic uncertainties on the reweighting.

is binned such that each bin has approximately the same yield in the sample passing the full selection. The ratio of passing events to inverted events as a function of the BDT output with this binning is used to derive a parametrized weighting to be applied to the inverted region. The parametrization is performed using a first- or second-order polynomial to provide a smooth reweighting function. Two systematic uncertainties are assessed for these reweightings: shifting the parametrization left and right along BDT scores and evaluating the fit uncertainty directly. In all cases, all of the input variables of the reweighted inverted samples are compared with the distributions of the passing samples as a closure test. The distributions match within statistical uncertainty and the systematic uncertainties previously described generously cover any discrepancy. Figure 5 shows this procedure for the $t\bar{t}$ process simulation in the 1L large-radius SR.

The primary backgrounds in the MET and 1L channels are $t\bar{t}b\bar{b}$, inclusive $t\bar{t}$, and single t production. In the small-radius jet analyses, the statistical precision is sufficient to use the simulation with nominal selection to directly produce the templates for these processes in the analysis regions. The number of selected simulated events in the large-radius channels is so small that the reweighting procedure is used in these regions instead. The inverted region, which is the previously mentioned failing region, is trained separately against both HP and LP regions. The small-radius 2L channel uses this technique for main backgrounds (Drell-Yan $\ell\ell$ and inclusive $t\bar{t}$) in all regions, as well as for $N_b = 3$ and 4 regions separately. The inverted region for the 2L channel is a region with exactly two b tagged jets.

In the FH channel, the dominant background processes are QCD multijet followed by $t\bar{t}$ (including $t\bar{t}b\bar{b}$) production. The QCD multijet background is estimated by reweighting $N_b = 3$ data to mimic the $N_b = 4$ QCD multijet background, while the $t\bar{t}$ templates are

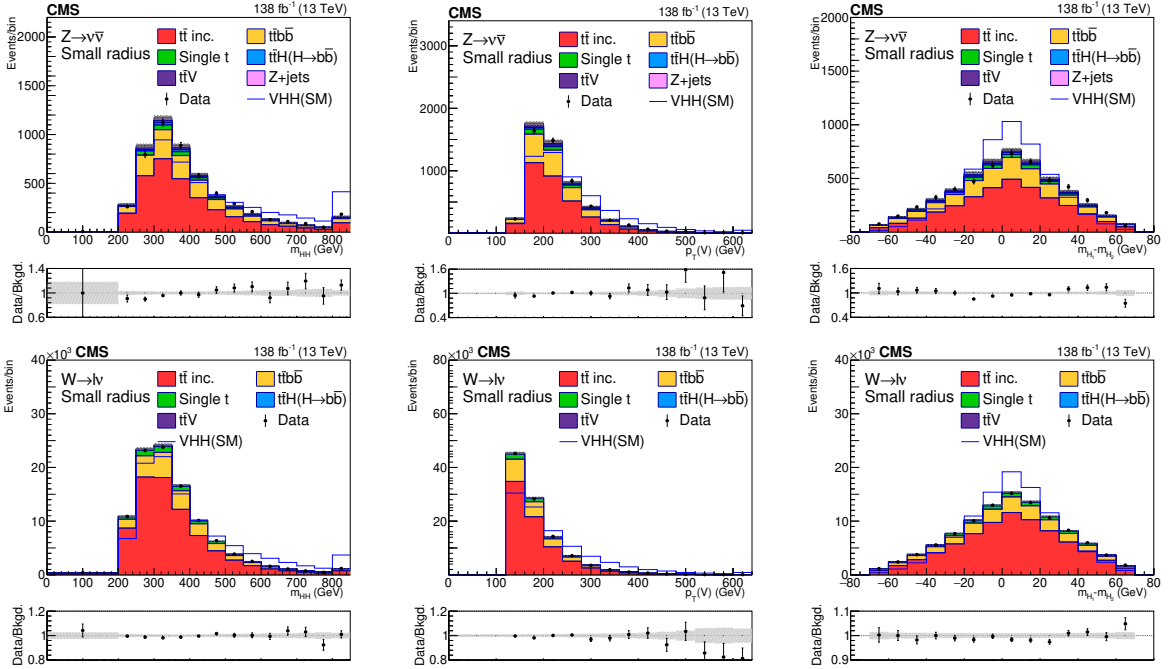


Figure 6. Postfit distributions of kinematic variables in the small-radius jet regions. The upper (lower) row shows the MET (1L) channel. The variables in each channel are m_{HH} , $p_T(\text{V})$, and $m_{\text{H}_1} - m_{\text{H}_2}$. The fit is done with the background-only hypotheses and the final bin in each plot includes overflows. The ratios of data to the total expected background are shown in the lower panel of each plot and the hatched bands are the combined statistical and systematic uncertainties of total background. The blue lines are SM signal distributions, which are scaled to have the same number of events as the background.

produced using nominally selected simulation directly. The signal purity in $N_b = 4$ is about 18 times higher than in $N_b = 3$, so the signal contamination in the reweighted $N_b = 3$ data is negligible. A two-step approach is used to reweight $N_b = 3$ to $N_b = 4$ kinematics. First, a pseudo-tag rate f , which is the probability that an untagged jet would be b-tagged, a normalization factor t and pair-enhancement terms e and d [79] are used to account for the lower jet multiplicity in the $N_b = 3$ region comparing to the $N_b = 4$ region. The parameters are derived by fitting the jet multiplicity distribution in the SB region after subtracting the $t\bar{t}$ contribution, so that the weight for an event with n non-b-tagged jets is given by:

$$w_1 = t \sum_{i=1}^n \binom{n}{i} f^i (1-f)^{n-i} \times \begin{cases} 1 + e/n^d & (3+i) \text{ even} \\ 1 & (3+i) \text{ odd.} \end{cases} \quad (7.1)$$

Then, a neural network classifier is used to distinguish the remaining kinematic differences between $N_b = 3$ and $N_b = 4$ regions. The classifier is trained to predict the probabilities of an event to be $N_b = 4$ data, $N_b = 4$ $t\bar{t}$, $N_b = 3$ data or $N_b = 3$ $t\bar{t}$ using both data and simulated $t\bar{t}$ in SB region and the second weight is given by:

$$w_2 = \frac{P(N_b = 4 \text{ data}) - P(N_b = 4 \text{ } t\bar{t})}{P(N_b = 3 \text{ data})}. \quad (7.2)$$

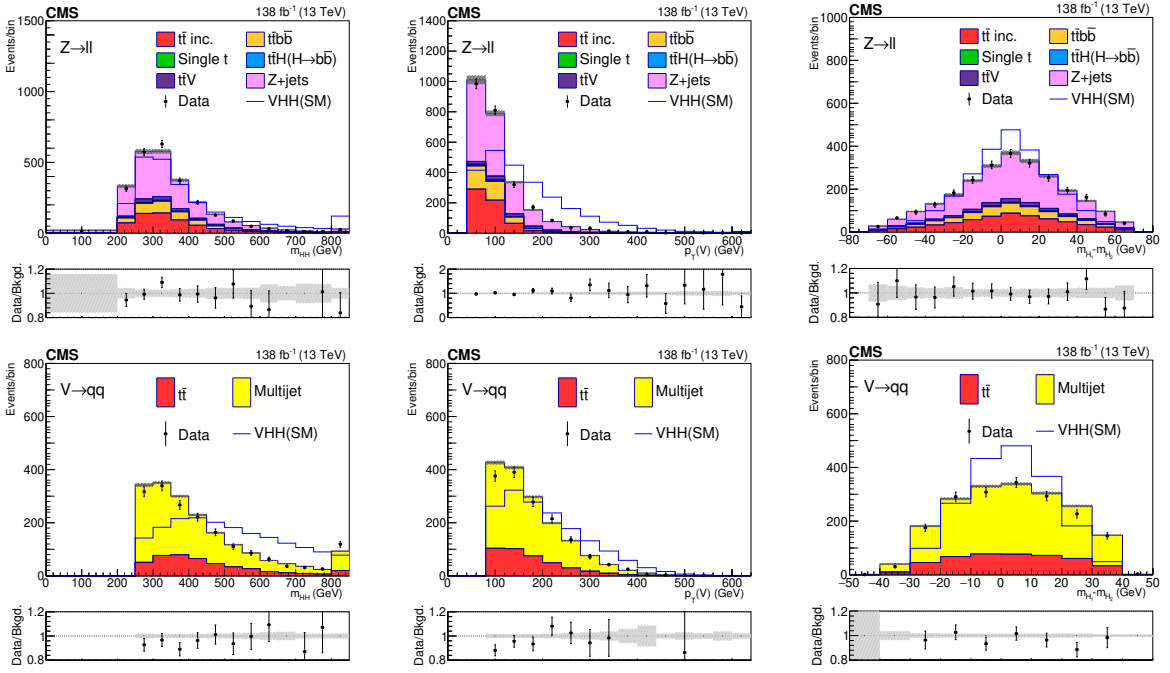


Figure 7. Postfit distributions of kinematic variables in the small-radius jet regions. The upper (lower) row shows the 2L (FH) channel. The variables in each channel are m_{HH} , $p_T(\text{V})$, and $m_{\text{H}_1} - m_{\text{H}_2}$. The fit is done with the background-only hypotheses and the final bin in each plot includes overflows. The ratios of data to the total expected background are shown in the lower panel of each plot and the hatched bands are the combined statistical and systematic uncertainties of total background. The blue lines are SM signal distributions, which are scaled to have the same number of events as the background.

The final weight is the product of w_1 and w_2 . Since only $t\bar{t}$ is subtracted explicitly during both fits, besides the QCD multijet, the contributions of all other processes and potential mismodeling of $t\bar{t}$ simulation are included in the weight.

Figures 6 and 7 compare the m_{HH} , $p_T(\text{V})$, and $m_{\text{H}_1} - m_{\text{H}_2}$ distributions of data with the expected distributions for events that pass the SR selections (MET, 1L, and FH) in the small-radius jet regions, based on their respective background estimates. The background distributions are obtained from the fit with the background-only hypothesis. SM signal distributions are also shown and they are scaled to have the same number of events as the background. Similarly, figure 8 shows the distribution of the same variables in the large-radius jet regions.

Moreover, the FH background model is validated using a synthetic data set, which is generated by splitting individual events into hemispheres and then combining similar hemispheres from different events following the method described in refs. [79, 80]. This mixing procedure removes event-level correlations from any signal events in the data, while preserving the kinematic distributions of the $N_b = 4$ background. The procedure is to divide events with $N_b = 3$ into two hemispheres: one with two b-tagged jets and the other one with two jets where only one is b-tagged. Similar hemispheres from different data events are combined to produce mixed $N_b = 4$ events. There are sufficient combinations of suitable hemispheres for mixing that 15 distinct data sets with the same statistical precision of the

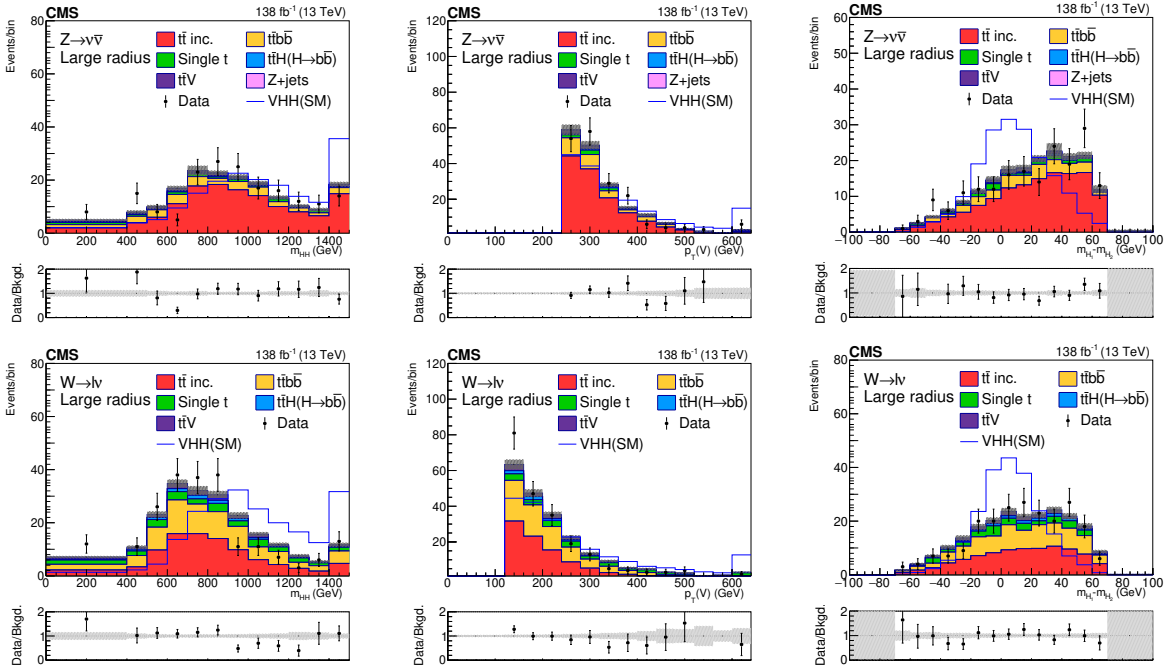


Figure 8. Postfit distributions of kinematic variables in the large-radius jet regions. The upper (lower) row shows the MET (1L) channel. The variables in each channel are m_{HH} , $p_{\text{T}}(\text{V})$, and $m_{\text{H}_1} - m_{\text{H}_2}$. The fit is done with the background-only hypotheses and the final bin in each plot includes overflows. The ratios of data to the total expected background are shown in the lower panel of each plot and the hatched bands are the combined statistical and systematic uncertainties of total background. The blue lines are SM signal distributions, which are scaled to have the same number of events as the background.

data are created. These samples provide a signal-free, data-driven data set that can be used to assess the background model directly in the SR. Figure 9 compares one of the 15 synthetic data sets to the background model and data in the SR. The background procedure is performed treating the mixed data as the four-tag data set. Systematic uncertainties are derived by comparing the predicted background to the observed yield in the signal region.

8 Systematic uncertainties

Uncertainties are categorized into theoretical and experimental uncertainties, and are described in section 8.1 and section 8.2, respectively. The signal extraction is performed with a maximum likelihood fit [81]. The signal strength is the additionally fitted normalization parameter relative to the nominal model. All uncertainties are implemented as penalty terms, known as “nuisance parameters”, to a likelihood function. Systematic uncertainties may affect the normalization of the different background processes, their shape, or both. We also include freely-floating nuisance parameters for the $t\bar{t}b\bar{b}$, inclusive $t\bar{t}$, and Drell-Yan background where a fixed background cross section is not assumed. Some uncertainties are fully correlated between event categories and data-taking periods, while other uncertainties only apply to specific categories. Correlations are described in the uncertainty descriptions.

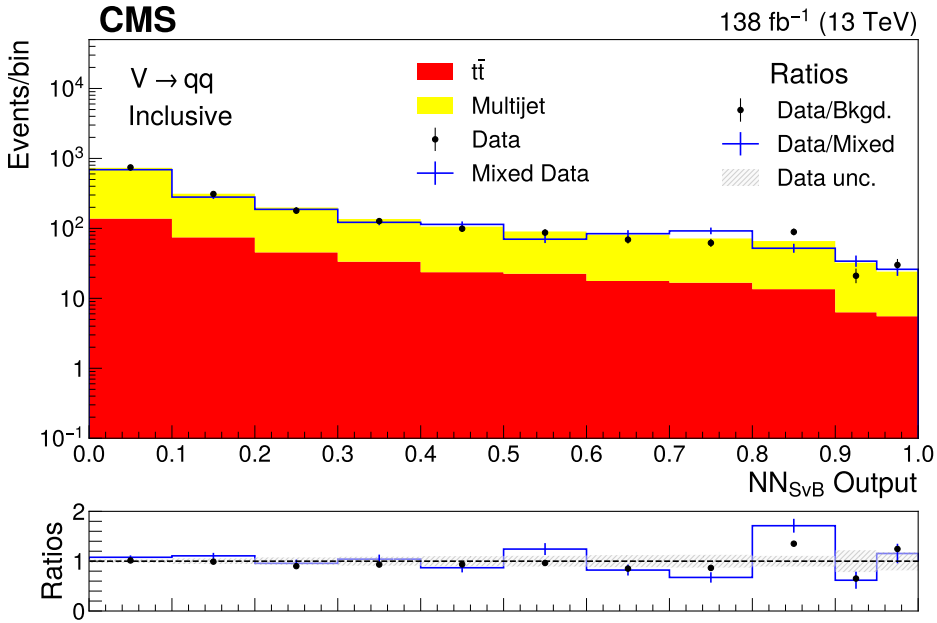


Figure 9. The prefit distribution of NN_{SvB} output in the FH channel including both κ_λ and κ_{2V} enriched categories. The ratios of data to the background model and data to one of the mixed data set is shown in the lower panel where the hatched band is the statistical uncertainty of data. The systematic uncertainty is then estimated based on the remaining discrepancy.

8.1 Theoretical uncertainties

Signal cross section predictions: the total signal cross section has been calculated at NNLO accuracy, and the total uncertainty is about 3.6% for both ZHH and WHH processes, including the effect of scale and PDF variation [11].

Branching fraction: the uncertainty in the $\text{HH} \rightarrow b\bar{b}b\bar{b}$ branching fraction is 2.5% [11].

Reweighting to include $gg \rightarrow ZHH$: as shown in figure 2 right, the LO ZHH simulation is initially scaled to NLO. Subsequently it is kinematically reweighted to NNLO to include the ggF ZHH contribution. These reweighting factors are established prior to any selection criteria being implemented. Despite this procedure, after the signal region selections, a discernible discrepancy emerges between the reweighted LO ZHH simulation and the real distributions arising from NNLO simulations. This observed discrepancy is used to produce a shape-based systematic uncertainty.

NLO Drell-Yan simulations reweighting: the LO and NLO Drell-Yan simulations are compared with minimal selection, and a shape discrepancy as a function of generator-level $p_T(Z)$ is observed. The LO simulation is reweighted as a function of generator-level $p_T(Z)$ to match the NLO generator-level $p_T(Z)$ distribution. While the reweighted LO sample matches the NLO with the minimal selection where the reweighting is defined, there is a discrepancy after full selection between the NLO and LO with reweighting. This discrepancy is linearly parameterized as a function of $p_T(Z)$ and implemented as a shape uncertainty.

Factorization and renormalization scales: the uncertainty from the choice of the factorization and renormalization scales, μ_F and μ_R , in the calculation of the matrix elements of the hard-scattering process is estimated by varying each scale by a factor of 0.5 and 2, excluding nonphysical anticorrelated combinations due to large logarithmic corrections $|\ln(\mu_R/\mu_F)| > 1$. The effects on different signal and background processes are considered uncorrelated. The normalization effect on the uncertainty due to the choice of scales is already included in the cross section uncertainty.

Proton PDF uncertainties: in order to estimate an impact on the limit due to the uncertainty in the proton PDFs, event weights corresponding to the set of NNPDF3.1 [40] MC replicas were applied to the simulation as a shape systematic uncertainty.

Parton shower uncertainty: in order to evaluate the impact of the α_S choice in the parton shower simulation, the renormalization scales in the shower simulation are varied by a factor 0.5 and 2 via weights obtained directly from the generator information. This is done independently for the initial- and final-state radiation showers, and treated as a shape systematic uncertainty.

8.2 Experimental uncertainties

Some of the most significant experimental systematic uncertainties come from the limited size of the simulation and data samples used to build the templates for each process. To account for this, the Barlow-Beeston-lite approach is used [83]. A dedicated Gaussian nuisance parameter is assigned to each histogram bin in every analysis region. The prior uncertainty of each nuisance parameter is set to the total statistical uncertainty obtained by combining all background processes in the corresponding bin.

Integrated luminosity: the integrated luminosity uncertainties for 2016, 2017, and 2018 are 1.2, 2.3, and 2.5%, respectively [32–34]. A correlation scheme is used for the three sets of uncertainties based on correlated features in calibration methods, measurements, and data set. Effectively, the uncertainty is about 1.6% for the full data set.

Lepton and trigger efficiencies: uncertainties from the choice of the lepton identification and reconstruction criteria in the baseline selection, as well as in the trigger efficiency in the leptonic channels, are also modeled as shape uncertainties. The efficiency corrections applied to simulated samples have uncertainties from bin-by-bin differences using alternative samples, alternative selections, alternative models, and the limited number of events in bins of η and p_T when measuring the efficiencies in data [69, 71]. All these sources are combined, and they are considered fully correlated across all bins of lepton η and p_T . These uncertainties are mostly in the range of 1–2%. They are uncorrelated by analysis channel and by year.

Trigger efficiencies in the FH channel: trigger efficiency uncertainties in the FH channel are evaluated for the signal, based on the systematic uncertainties arising from measured trigger turn-ons. There is an additional, small, non-closure uncertainty associated with the calculation of per-event trigger efficiencies using the measured per-jet efficiencies. The non-closure uncertainty was derived by comparing the event-level trigger efficiencies in

simulation to those derived using the per-jet efficiencies as measured in simulation. The total trigger efficiency uncertainties in the FH channel are in the range of 1–2% and are uncorrelated by year.

Pileup: the systematic uncertainty on the signal and background shapes introduced by the pileup reweighting procedure is quantified by varying the effective total inelastic cross section of 69.2 mb within its $\pm 4.6\%$ uncertainty. This is a shape uncertainty.

Small-radius jet: to evaluate the effect from the jet energy scale (JES) and resolution (JER) on the signal and background shapes, alternative templates (i.e., one standard deviation shape uncertainty templates) of all analysis region observables are obtained by varying absolute JES and JER within their uncertainties and propagating the events through the full reconstruction chain [63]. In total, 11 different sources of systematic uncertainty affecting the JES and one affecting JER were considered. A b jet energy regression is applied to improve small-radius b JER [64]. A further 2% scale uncertainty and 10% resolution uncertainty are also assigned to all small-radius jets.

b tagging: the b tagging algorithm plays a crucial role in distinguishing between jets that stem from b or c quarks (referred to as heavy-flavor jets) and those that originate from light-flavor quarks or gluons (referred to as light-flavor jets). The related efficiency and misidentification correction factors are applied per event with efficiencies measured in bins of jet p_T , η , and DEEPJET b tagging score. There are uncertainties from the fitting procedure used to derive the applied correction factors. The contamination from jets originating from non-b (c or b) partons but identified as heavy- (light-)flavor jets, and the statistical precision in both data and simulation samples are used to evaluate the uncertainty in these measurements [36]. That uncertainty is applied in a fully correlated manner for b and light-flavor jets and c jets have separate uncertainty. The resulting alternative templates are implemented as one standard deviation shape systematic uncertainties.

Large-radius jet: the $D_{b\bar{b}}$ tagger is used to select events in the large-radius channels and the correction factors of efficiency are applied in bins of jet p_T and $D_{b\bar{b}}$ score. The correction factors and associated uncertainties are consistent with those in the previous publications [17] where $D_{b\bar{b}}$ boundaries are aligned. Similar to b jet energy regression, a dedicated graph neural network mass regression is used in the large-radius jet analyses [84]. An additional 1% mass scale uncertainty and 5% resolution uncertainty are included for the regressed mass (m_{reg}). These are all shape uncertainties.

Normalization: the normalizations of the primary backgrounds in the leptonic channels are free parameters that are extracted and constrained in the likelihood fit. The $t\bar{t}$ process normalization is uncorrelated in each channel. However, the ratio of 4FS $t\bar{t}b\bar{b}$ to 5FS $t\bar{t}$ is correlated among all channels. In the 2L channel, the normalization of the Drell-Yan process background is also free and fit to data.

Inverted sample reweighting: where the BDT reweighting procedure from inverted-to-nominal region is used (i.e., MET and 1L large-radius channels and 2L small-radius channel), two

associated systematic uncertainties, as described in section 7, are implemented independently per channel. These uncertainties are independent per region and correlated among years.

Top quark p_T : the top quark p_T distribution in $t\bar{t}$ MC samples has a higher mean value in simulation than in data. To correct for this bias, a linear variation to the top quark p_T floats during the signal extraction fit. This correction is constrained in the SBs and in the $t\bar{t}$ region in the 2L channel where the observable is the reconstructed $p_T(V)$, which is correlated with the top quark p_T . This uncertainty is correlated across all regions.

FH background estimation cross check: the uncertainties in FH background estimation are derived by comparing the predicted background to the observed yield in the SR of the corresponding mixed data set, as described in section 7. The uncertainties are parameterized using a Fourier basis on the SR NN_{SvB} shape. Two Fourier terms ($\sin \pi x$, $\cos \pi x$) provide sufficient flexibility and no risk of spurious signal as estimated with an F -test [85]. Together with a constant term these three terms are orthonormalized to eliminate correlations among them. These systematic uncertainties are among the most significant for this channel.

For systematic variation templates of processes modeled with inverted reweighting, the alternative shapes are taken from propagating systematic uncertainties in the inverted samples directly. Comparisons with the variations from the passing events were performed. The size of the variations are compatible in nearly all cases, and the differences are negligible when there is any discrepancy.

Table 6 presents the contributions of various uncertainty sources to the overall uncertainty in the signal strength, when such signal strength is derived assuming a SM-like signal shape. Each group of uncertainties is quantified with respect to the total uncertainty as shown in the final line of the table. The impactful sources of uncertainty include statistical uncertainty, background modeling, b tagging, and JES/JER affecting the small-radius jets. The statistical uncertainty accounts for the limited size of both data and MC samples. The b tagging uncertainty corresponding to the contamination of light-quark-flavored jets in heavy flavor regions is the most impactful uncertainty, and it is pulled by about 1σ . Other impactful uncertainties that are pulled within 1σ include top quark p_T reweighting, b energy regression scale uncertainty, and inverted sample reweighting uncertainty.

9 Results

For the signal extraction we performed a binned maximum likelihood fit using the 59 regions for signal extraction and for background control altogether, as shown in the table 5. All regions for signal extraction are either κ_λ - or κ_{2V} -enriched by construction. The observables are machine learning scores, i.e., from BDT or neural networks, that distinguish signal from background. In the background control regions, the reconstructed $p_T(V)$ and m_{reg} of the subleading Higgs boson candidate are used as fitting variables in the small-radius and large-radius regions, respectively. The BDT distributions are divided to ensure a uniform distribution for the signal and also maintain background MC statistical uncertainties $<30\%$ in each bin.

The postfit distributions with the signal-plus-background hypotheses are shown in figures 10–11 with SR, CR, N_b , $D_{b\bar{b}}$ categories, and all data-taking periods summed up.

Uncertainty sources	2L	1L	MET	FH	Combined
Systematic uncertainty	+54%/-40%	+47%/-40%	+64%/-45%	+51%/-36%	+68%/-49%
Theory	+16%/-3%	+3%/-12%	+23%/-10%	+15%/-2%	+17%/-7%
Integrated luminosity	+6%/-0%	+5%/-1%	+8%/-1%	+4%/-0%	+6%/-4%
Lepton	+2%/-1%	+4%/-1%	+0%/-1%	+0%/-0%	+3%/-4%
Pileup	+3%/-6%	+4%/-2%	+8%/-7%	+3%/-0%	+9%/-14%
Small-radius jet	+17%/-5%	+15%/-5%	+26%/-23%	+21%/-2%	+26%/-16%
b tagging	+41%/-4%	+35%/-3%	+56%/-29%	+36%/-1%	+62%/-34%
Large-radius jet	+2%/-0%	+12%/-18%	+3%/-3%	+1%/-0%	+5%/-17%
Background modeling	+53%/-38%	+37%/-19%	+54%/-29%	+44%/-19%	+62%/-40%
Normalization	+40%/-12%	+34%/-4%	+52%/-25%	+35%/-0%	+58%/-32%
Reweighting	+34%/-36%	+13%/-17%	+22%/-13%	+12%/-1%	+25%/-19%
Kinematic	+11%/-10%	+17%/-3%	+13%/-4%	+24%/-24%	+19%/-14%
Statistical uncertainty	+84%/-91%	+88%/-92%	+77%/-89%	+86%/-93%	+73%/-87%
Signal strength and uncertainty	101 ⁺¹³⁶ ₋₉₉	12 ⁺¹¹¹ ₋₈₃	283 ⁺¹⁶¹ ₋₁₂₃	190 ⁺¹⁶³ ₋₁₃₂	145 ⁺⁸¹ ₋₆₃

Table 6. The contribution of each group of uncertainties is quantified relative to the total uncertainty in the signal strength, which is listed in the final line. To compute the relative contributions, the group of nuisance parameters is fixed to the best fit value while the likelihood is scanned again profiling all other nuisance parameters. The reductions in the upper and lower variations are shown in each line. The likelihood shape is asymmetric, and so the upper and lower variations are quantified separately.

For an accurate and simultaneous visualization, the SRs are combined by transforming all the discriminant outputs into bins of increasing signal purity, i.e., $\log_{10}(100(S_{\text{SM}}/B))$, where S_{SM} is the signal predicted by SM and B is estimated background, which are then summed separately for each enrichment type. Figure 12 shows these summed distributions, overlaid with data and signal models within the coupling sensitivity of this analysis. For better visualization, the single t , $t\bar{t}H$, and $t\bar{t}V$ backgrounds are grouped and labeled as “Other” in figure 12.

A test statistic based on the profile likelihood ratio [81] is used to determine the signal strength, with the combined signal strength as the parameter of interest (POI). Systematic uncertainties are incorporated as additional nuisance parameters. In the likelihood calculations, each of the nuisance parameter adds an additional multiplicative term to the total likelihood. Alternatively four signal strengths are assigned as POI to each channel and compared to the combined signal strength. Figure 13 shows the signal strengths per analysis channel, as well as the combined signal strengths.

A small excess of data over the background-only expectation in the most signal-like bins in κ_{2V} -enrichment region can be seen in figure 12, which is primarily from the MET channel κ_{2V} -enrichment region SRs shown in figure 11. For an SM-like signal, the observed significance is 2.6 standard deviations with a fitted signal strength of 145^{+81}_{-63} times the SM signal when all coupling modifiers are equal to 1. Figure 13 shows the results of two fits. The first one is the inclusive fit with a single signal strength modifier, and the second fit has separate signal strength modifiers per channel.

Two-dimensional likelihood scans of κ_λ versus κ_{2V} and κ_{2Z} versus κ_{2W} are shown in figure 14 and 15, respectively. Other couplings are fixed to their SM values.

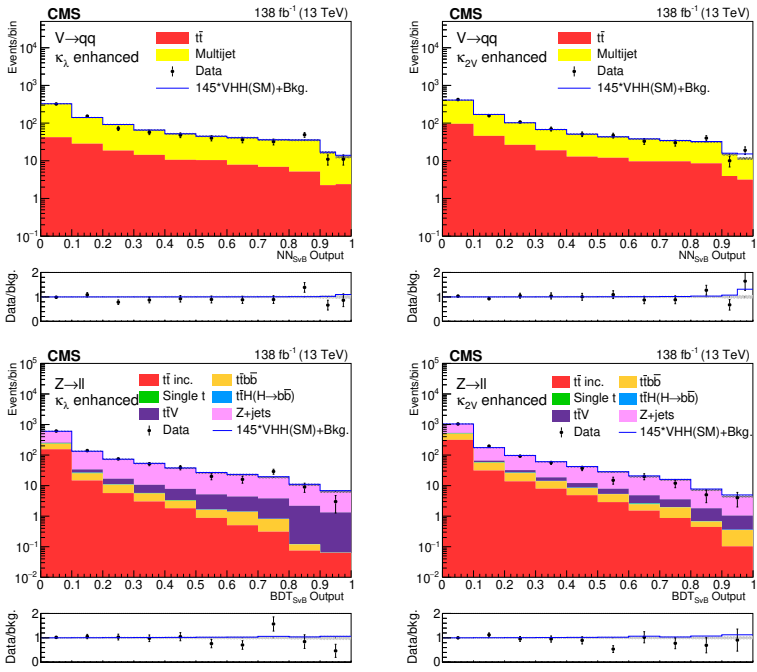


Figure 10. Postfit BDT distributions with the signal-plus-background hypotheses of the FH and 2L channels.

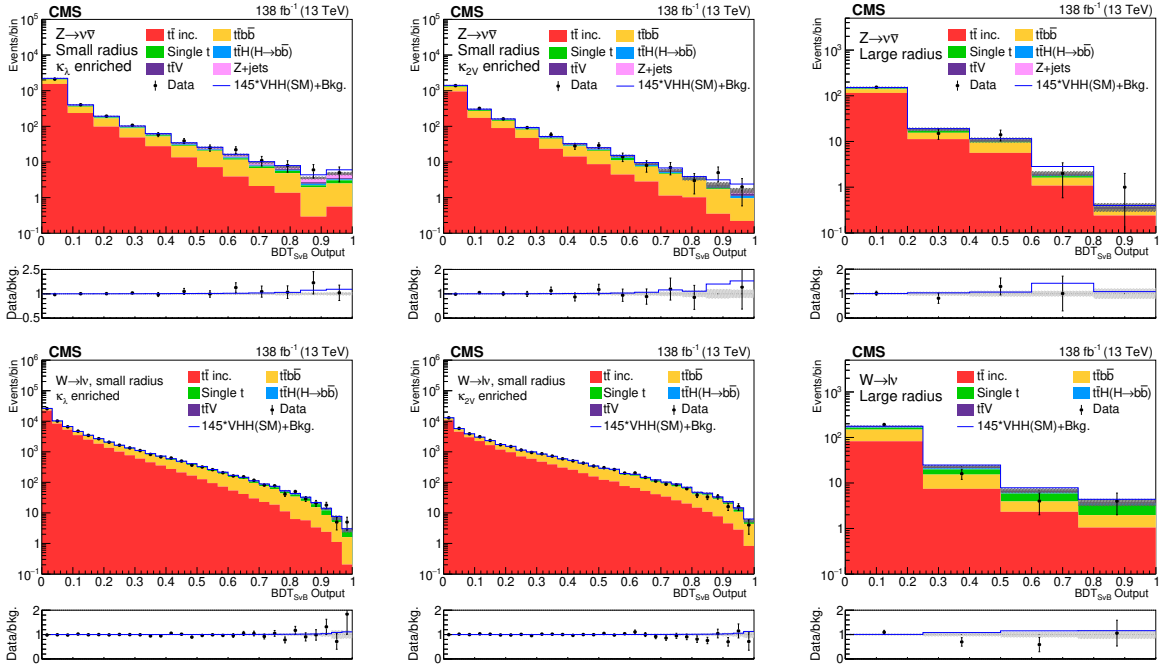


Figure 11. Postfit BDT distributions with the signal-plus-background hypotheses of the MET and 1L channels.

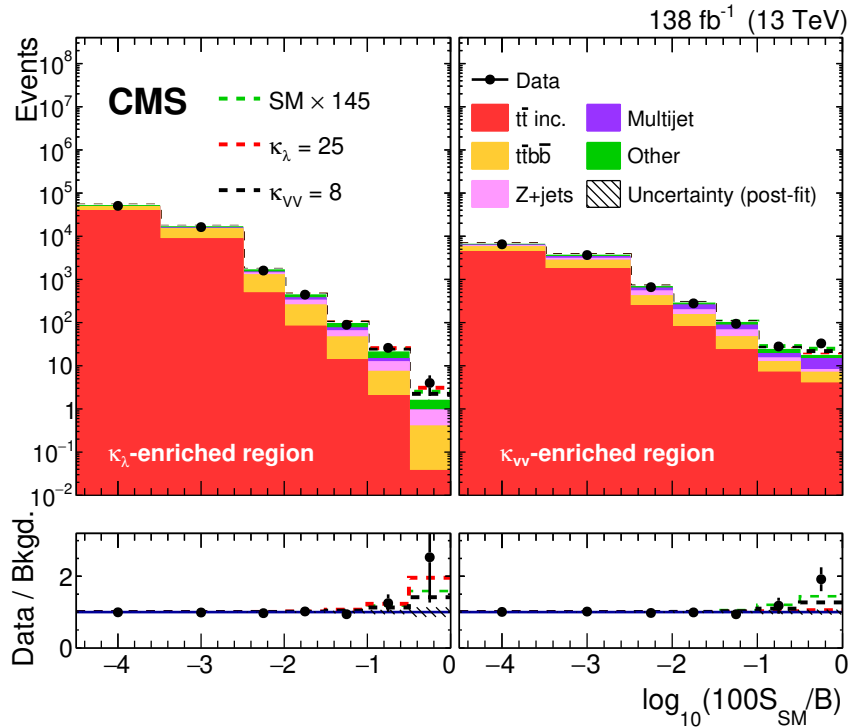


Figure 12. Machine learning output distributions are transformed to $\log_{10}(100(S_{SM}/B))$ and summed for κ_λ - and κ_{vv} -enriched SR samples separately. The filled histograms represent the postfit simulation. The total postfit uncertainty is represented by the hatched band. The SM contribution and two signal models near expected exclusion at the 95% CL, each assuming the other couplings to be SM-like, are shown with the dashed lines.

Based on the CL_s criterion [86, 87] and asymptotic formulas [88], the upper limits on the VHH cross section at 95% CL are extracted both with the SM couplings and with scans on the coupling modifiers. The upper limit at 95% CL of the VHH production cross section is observed (expected) to be at 294 (124) times the SM prediction. Because of destructive interference with positive κ_λ in leading HH production modes (ggF and VBF), VHH searches can make a significant contribution to the overall HH program near the corresponding minimum in HH sensitivity. In particular, in the range of $4 < \kappa_\lambda < 7$ this search has a sensitivity near other HH searches. Scaling cross sections by the ratio of $pp \rightarrow HH$ to $pp \rightarrow VHH$ with the same coupling modifiers is done to interpret the VHH results in the greater HH context. For example, the $pp \rightarrow HH$ cross section 95% CL expected limit from this VHH search is about 3–4 times the expected HH cross section limit from the $b\bar{b}\tau\bar{\tau}$ search in this range on the equivalent data set [18]. Figure 16 shows the SM 95% CL cross section upper limits, as well as those for $\kappa_\lambda = 5.5$, which is in the middle of the highlighted region, with other coupling modifiers set to unity. The upper limits on VHH and total HH cross section as functions of κ_λ , κ_{2V} , and κ_V are shown in Figs 17, 18, and 19. The theoretic prediction of VHH and inclusive HH production cross sections are shown with the red lines. The 95% CL upper limits are summarized in table 7.

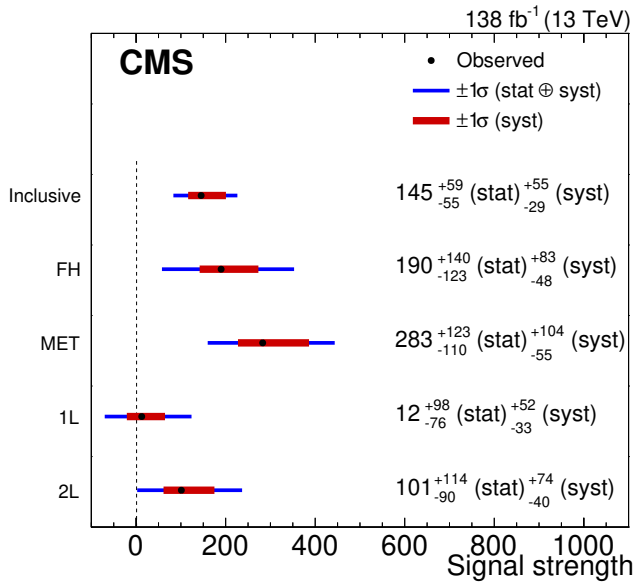


Figure 13. Results of two maximum likelihood fits. The top entry, labeled “Inclusive”, is the result of a single signal strength fit of all channels. The other four entries are from a fit of the same regions but with independent signal strengths in each channel. The thinner blue bands are one standard deviation from the full likelihood scan in that parameter, while the thicker red bands are one standard deviation bands of the systematic uncertainties only. The mutual compatibility of the multi-signal strength fit with the inclusive fit is 38%.

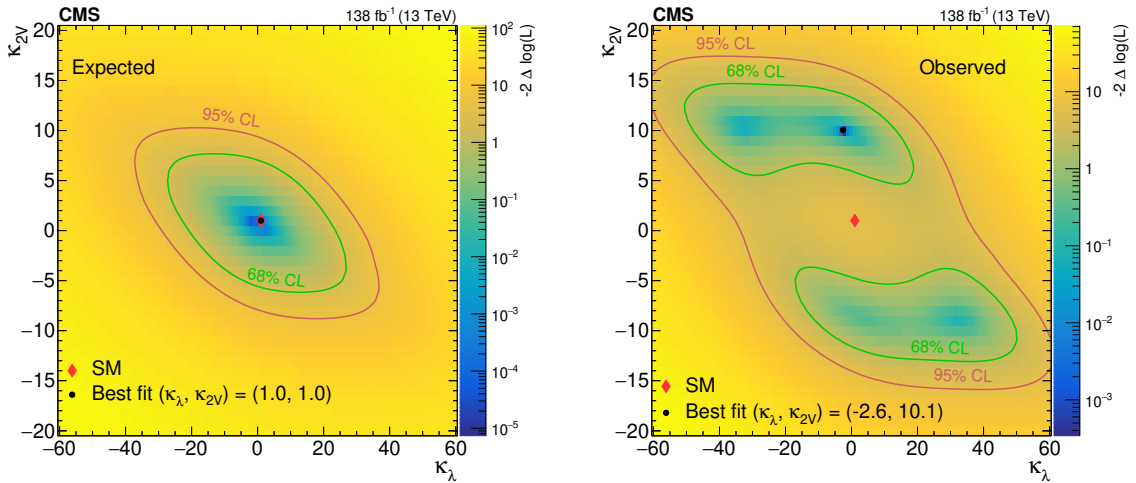


Figure 14. Expected (left) and observed (right) likelihood scans in κ_λ versus κ_{2V} are shown, with other couplings fixed to the SM predicted strength. The excess is most prominent in the κ_{2V} -enriched region, and so the most likely point of the scan at $\kappa_{2V} = 10.1$ and $\kappa_\lambda = -2.6$ is pulled from the SM mostly in the κ_{2V} dimension.

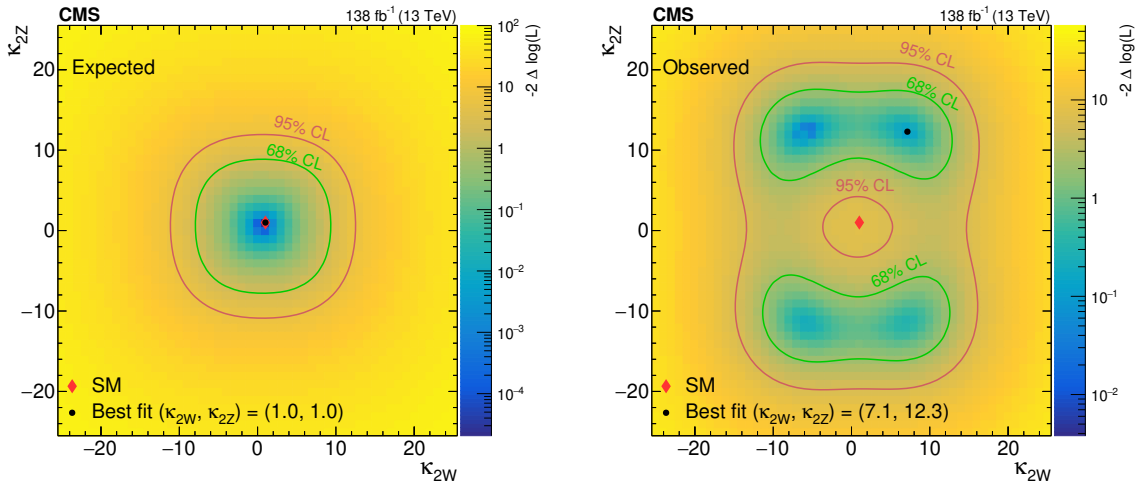


Figure 15. Expected (left) and observed (right) likelihood scans of κ_{2W} versus κ_{2Z} are shown, with other couplings fixed to the SM predicted strength. The excess is most prominent in the MET channel, and so the most likely point of the scan at $\kappa_{2W} = 7.1$ and $\kappa_{2Z} = 12.3$ is pulled from the SM mostly in the κ_{2Z} dimension, to which the signal in the MET channel is solely sensitive.

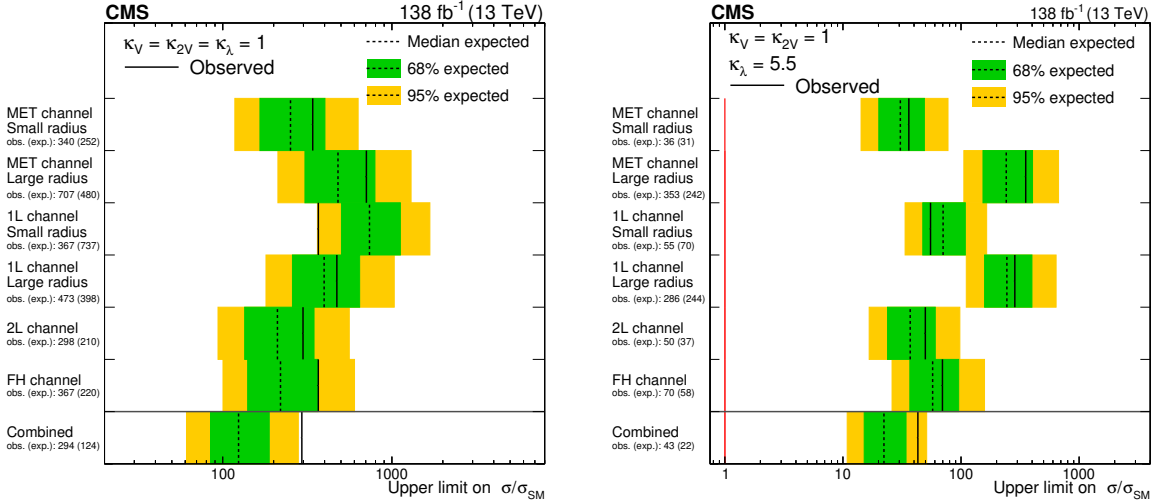


Figure 16. The left plot shows the VHH cross section upper limits per channel and combined for SM value couplings, while results with $\kappa_\lambda = 5.5$ and $\kappa_{2V} = \kappa_V = 1.0$ are shown on the right.

	κ_λ	κ_{2V}	κ_V	κ_{2Z}	κ_{2W}
Observed	(−37.7, 37.2)	(−12.2, 13.5)	(−3.7, 3.8)	(−17.4, 18.5)	(−14.0, 15.4)
Expected	(−30.1, 28.9)	(−7.2, 8.9)	(−3.1, 3.1)	(−10.5, 11.6)	(−10.2, 11.6)

Table 7. Observed and expected 95% CL upper limits on the coupling modifiers.

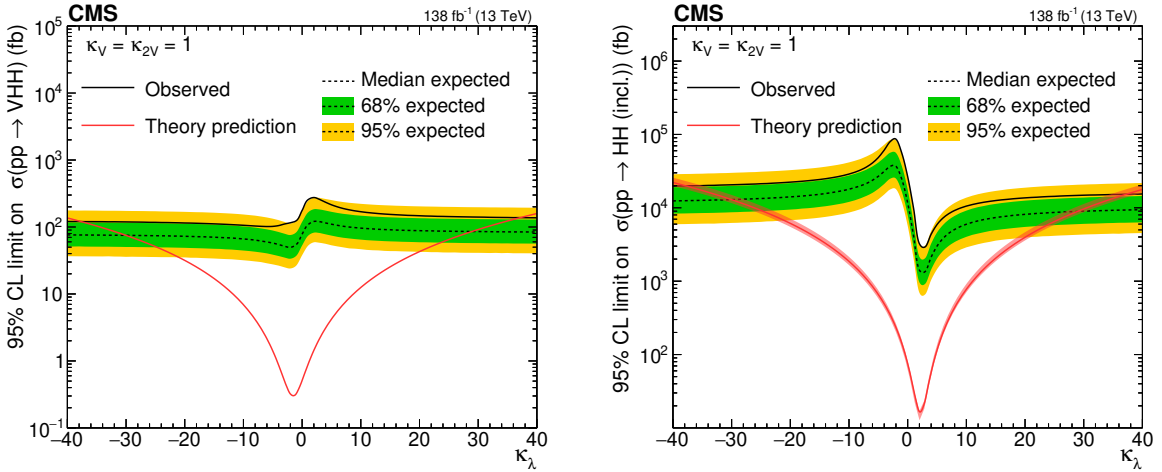


Figure 17. Upper 95% CL limits on VHH (left) and HH (right) signal cross section scanned over the κ_λ parameter while fixing the κ_{2V} and κ_V to their SM-predicted values. The independent axis is the scanned κ_λ parameter, and the dependent axis is the 95% CL upper limit on signal cross section. The theoretic prediction of VHH (left) and HH (right) production cross sections are shown with the red lines.

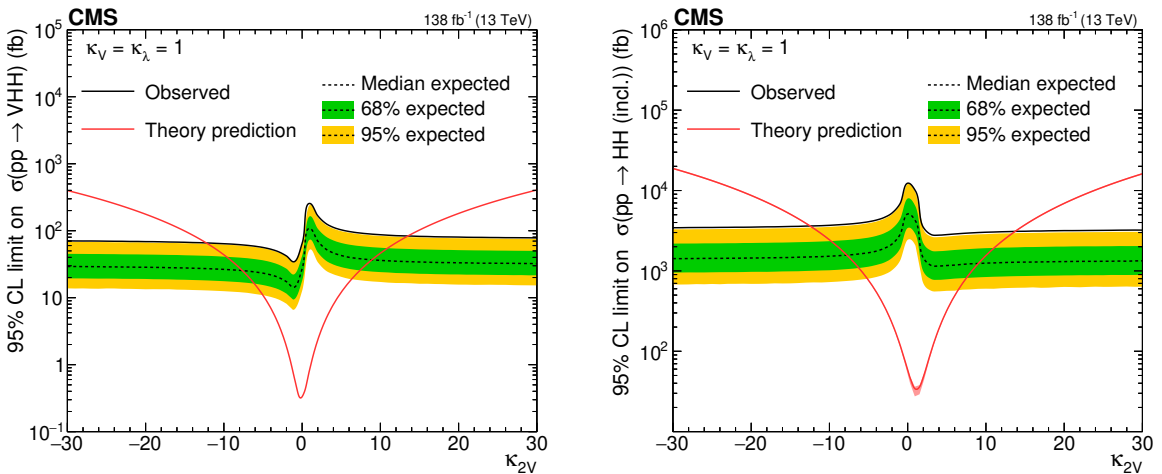


Figure 18. Upper 95% CL limits on VHH (left) and HH (right) signal cross section scanned over the κ_{2V} parameter while fixing the κ_λ and κ_V to their SM-predicted values. The independent axis is the scanned κ_{2V} parameter, and the dependent axis is the 95% CL upper limit on signal cross section. The theoretic prediction of VHH (left) and HH (right) production cross sections are shown with the red lines.

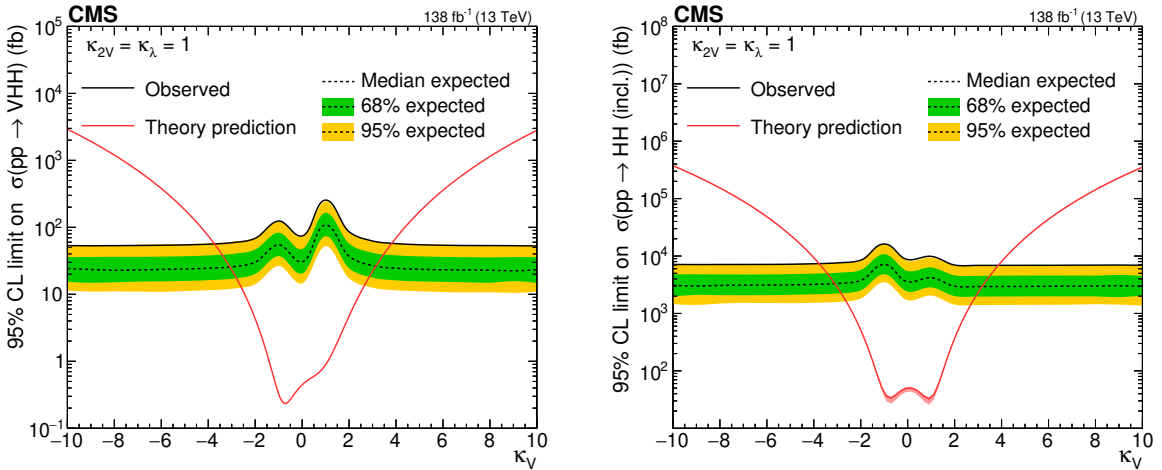


Figure 19. Upper 95% CL limits on VHH (left) and HH (right) signal cross section scanned over the κ_V parameter while fixing the κ_{2V} and κ_λ to their SM-predicted values. The independent axis is the scanned κ_V parameter, and the dependent axis is the 95% CL upper limit on signal cross section. The theoretic prediction of VHH (left) and HH (right) production cross sections are shown with the red lines.

10 Summary

A search for Higgs boson pair production in association with a vector boson (VHH) using a data set of proton-proton collisions at $\sqrt{s} = 13$ TeV, corresponding to an integrated luminosity of 138 fb^{-1} , is presented. Final states including Higgs boson decay to bottom quarks are analyzed in events where the W or Z boson decay to electrons, muons, neutrinos, and hadrons. An observed (expected) upper limit at 95% confidence level of VHH production cross section is set at 294 (124) times the standard model prediction. Coupling modifiers, defined relative to the standard model coupling strengths, are scanned and constrained for the Higgs boson trilinear coupling (κ_λ) and the coupling between two V bosons with two Higgs bosons (κ_{2V}). The observed (expected) 95% confidence level limits constrain κ_λ and κ_{2V} to be $-37.7 < \kappa_\lambda < 37.2$ ($-30.1 < \kappa_\lambda < 28.9$) and $-12.2 < \kappa_{2V} < 13.5$ ($-7.2 < \kappa_{2V} < 8.9$), respectively, where each of these constrains assumes the other couplings to be SM-like.

Acknowledgments

We congratulate our colleagues in the CERN accelerator departments for the excellent performance of the LHC and thank the technical and administrative staffs at CERN and at other CMS institutes for their contributions to the success of the CMS effort. In addition, we gratefully acknowledge the computing centers and personnel of the Worldwide LHC Computing Grid and other centers for delivering so effectively the computing infrastructure essential to our analyses. Finally, we acknowledge the enduring support for the construction and operation of the LHC, the CMS detector, and the supporting computing infrastructure provided by the following funding agencies: SC (Armenia), BMBWF and FWF (Austria); FNRS and FWO (Belgium); CNPq, CAPES, FAPERJ, FAPERGS, and FAPESP (Brazil); MES and BNSF (Bulgaria); CERN; CAS, MoST, and NSFC (China); MINCIENCIAS (Colombia); MSES and CSF (Croatia); RIF (Cyprus); SENESCYT (Ecuador); ERC PRG,

RVTT3 and MoER TK202 (Estonia); Academy of Finland, MEC, and HIP (Finland); CEA and CNRS/IN2P3 (France); SRNSF (Georgia); BMBF, DFG, and HGF (Germany); GSRI (Greece); NKFIH (Hungary); DAE and DST (India); IPM (Iran); SFI (Ireland); INFN (Italy); MSIP and NRF (Republic of Korea); MES (Latvia); LMELT (Lithuania); MOE and UM (Malaysia); BUAP, CINVESTAV, CONACYT, LNS, SEP, and UASLP-FAI (Mexico); MOS (Montenegro); MBIE (New Zealand); PAEC (Pakistan); MES and NSC (Poland); FCT (Portugal); MESTD (Serbia); MCIN/AEI and PCTI (Spain); MOSTR (Sri Lanka); Swiss Funding Agencies (Switzerland); MST (Taipei); MHESI and NSTDA (Thailand); TUBITAK and TENMAK (Turkey); NASU (Ukraine); STFC (United Kingdom); DOE and NSF (U.S.A.).

Individuals have received support from the Marie-Curie program and the European Research Council and Horizon 2020 Grant, contract Nos. 675440, 724704, 752730, 758316, 765710, 824093, 101115353, 101002207, and COST Action CA16108 (European Union); the Leventis Foundation; the Alfred P. Sloan Foundation; the Alexander von Humboldt Foundation; the Science Committee, project no. 22rl-037 (Armenia); the Belgian Federal Science Policy Office; the Fonds pour la Formation à la Recherche dans l’Industrie et dans l’Agriculture (FRIA-Belgium); the Agentschap voor Innovatie door Wetenschap en Technologie (IWT-Belgium); the F.R.S.-FNRS and FWO (Belgium) under the “Excellence of Science — EOS” — be.h project n. 30820817; the Beijing Municipal Science & Technology Commission, No. Z191100007219010 and Fundamental Research Funds for the Central Universities (China); the Ministry of Education, Youth and Sports (MEYS) of the Czech Republic; the Shota Rustaveli National Science Foundation, grant FR-22-985 (Georgia); the Deutsche Forschungsgemeinschaft (DFG), under Germany’s Excellence Strategy — EXC 2121 “Quantum Universe” — 390833306, and under project number 400140256 — GRK2497; the Hellenic Foundation for Research and Innovation (HFRI), Project Number 2288 (Greece); the Hungarian Academy of Sciences, the New National Excellence Program — ÚNKP, the NKFIH research grants K 131991, K 133046, K 138136, K 143460, K 143477, K 146913, K 146914, K 147048, 2020-2.2.1-ED-2021-00181, and TKP2021-NKTA-64 (Hungary); the Council of Science and Industrial Research, India; ICSC — National Research Center for High Performance Computing, Big Data and Quantum Computing, funded by the EU Next-Generation program (Italy); the Latvian Council of Science; the Ministry of Education and Science, project no. 2022/WK/14, and the National Science Center, contracts Opus 2021/41/B/ST2/01369 and 2021/43/B/ST2/01552 (Poland); the Fundação para a Ciência e a Tecnologia, grant CEECIND/01334/2018 (Portugal); the National Priorities Research Program by Qatar National Research Fund; MCIN/AEI/10.13039/501100011033, ERDF “a way of making Europe”, and the Programa Estatal de Fomento de la Investigación Científica y Técnica de Excelencia María de Maeztu, grant MDM-2017-0765 and Programa Severo Ochoa del Principado de Asturias (Spain); the Chulalongkorn Academic into Its 2nd Century Project Advancement Project, and the National Science, Research and Innovation Fund via the Program Management Unit for Human Resources & Institutional Development, Research and Innovation, grant B05F650021 (Thailand); the Kavli Foundation; the Nvidia Corporation; the SuperMicro Corporation; the Welch Foundation, contract C-1845; and the Weston Havens Foundation (U.S.A.).

Open Access. This article is distributed under the terms of the Creative Commons Attribution License ([CC-BY4.0](#)), which permits any use, distribution and reproduction in any medium, provided the original author(s) and source are credited.

References

- [1] ATLAS collaboration, *Observation of a new particle in the search for the Standard Model Higgs boson with the ATLAS detector at the LHC*, *Phys. Lett. B* **716** (2012) 1 [[arXiv:1207.7214](#)] [[INSPIRE](#)].
- [2] CMS collaboration, *Observation of a new boson at a mass of 125 GeV with the CMS experiment at the LHC*, *Phys. Lett. B* **716** (2012) 30 [[arXiv:1207.7235](#)] [[INSPIRE](#)].
- [3] CMS collaboration, *Observation of a new boson with mass near 125 GeV in pp collisions at $\sqrt{s} = 7$ and 8 TeV*, *JHEP* **06** (2013) 081 [[arXiv:1303.4571](#)] [[INSPIRE](#)].
- [4] CMS collaboration, *A portrait of the Higgs boson by the CMS experiment ten years after the discovery*, *Nature* **607** (2022) 60 [[arXiv:2207.00043](#)] [[INSPIRE](#)].
- [5] ATLAS collaboration, *A detailed map of Higgs boson interactions by the ATLAS experiment ten years after the discovery*, *Nature* **607** (2022) 52 [Erratum *ibid.* **612** (2022) E24] [[arXiv:2207.00092](#)] [[INSPIRE](#)].
- [6] A.G. Cohen, D.B. Kaplan and A.E. Nelson, *Baryogenesis at the weak phase transition*, *Nucl. Phys. B* **349** (1991) 727 [[INSPIRE](#)].
- [7] D.E. Morrissey and M.J. Ramsey-Musolf, *Electroweak baryogenesis*, *New J. Phys.* **14** (2012) 125003 [[arXiv:1206.2942](#)] [[INSPIRE](#)].
- [8] A. Noble and M. Perelstein, *Higgs self-coupling as a probe of electroweak phase transition*, *Phys. Rev. D* **78** (2008) 063518 [[arXiv:0711.3018](#)] [[INSPIRE](#)].
- [9] Q.-H. Cao, Y. Liu and B. Yan, *Measuring trilinear Higgs coupling in WHH and ZHH productions at the high-luminosity LHC*, *Phys. Rev. D* **95** (2017) 073006 [[arXiv:1511.03311](#)] [[INSPIRE](#)].
- [10] K. Nordström and A. Papaefstathiou, *VHH production at the high-luminosity LHC*, *Eur. Phys. J. Plus* **134** (2019) 288 [[arXiv:1807.01571](#)] [[INSPIRE](#)].
- [11] LHC HIGGS CROSS SECTION WORKING GROUP collaboration, *Handbook of LHC Higgs cross sections: 4. Deciphering the nature of the Higgs sector*, [arXiv:1610.07922](#) [[DOI:10.23731/CYRM-2017-002](#)] [[INSPIRE](#)].
- [12] J. Baglio et al., *The measurement of the Higgs self-coupling at the LHC: theoretical status*, *JHEP* **04** (2013) 151 [[arXiv:1212.5581](#)] [[INSPIRE](#)].
- [13] J. Baglio et al., *gg → HH: combined uncertainties*, *Phys. Rev. D* **103** (2021) 056002 [[arXiv:2008.11626](#)] [[INSPIRE](#)].
- [14] F.A. Dreyer and A. Karlberg, *Vector-boson fusion Higgs pair production at N³LO*, *Phys. Rev. D* **98** (2018) 114016 [[arXiv:1811.07906](#)] [[INSPIRE](#)].
- [15] CMS collaboration, *Search for nonresonant Higgs boson pair production in final states with two bottom quarks and two photons in proton-proton collisions at $\sqrt{s} = 13$ TeV*, *JHEP* **03** (2021) 257 [[arXiv:2011.12373](#)] [[INSPIRE](#)].
- [16] CMS collaboration, *Search for Higgs boson pair production in the four b quark final state in proton-proton collisions at $\sqrt{s} = 13$ TeV*, *Phys. Rev. Lett.* **129** (2022) 081802 [[arXiv:2202.09617](#)] [[INSPIRE](#)].

- [17] CMS collaboration, *Search for nonresonant pair production of highly energetic Higgs bosons decaying to bottom quarks*, *Phys. Rev. Lett.* **131** (2023) 041803 [[arXiv:2205.06667](#)] [[INSPIRE](#)].
- [18] CMS collaboration, *Search for nonresonant Higgs boson pair production in final state with two bottom quarks and two tau leptons in proton-proton collisions at $\sqrt{s} = 13$ TeV*, *Phys. Lett. B* **842** (2023) 137531 [[arXiv:2206.09401](#)] [[INSPIRE](#)].
- [19] CMS collaboration, *Search for nonresonant Higgs boson pair production in the four leptons plus two jets final state in proton-proton collisions at $\sqrt{s} = 13$ TeV*, *JHEP* **06** (2023) 130 [[arXiv:2206.10657](#)] [[INSPIRE](#)].
- [20] CMS collaboration, *Search for Higgs boson pairs decaying to WW^*WW^* , $WW^*\tau\tau$, and $\tau\tau\tau\tau$ in proton-proton collisions at $\sqrt{s} = 13$ TeV*, *JHEP* **07** (2023) 095 [[arXiv:2206.10268](#)] [[INSPIRE](#)].
- [21] ATLAS collaboration, *Search for Higgs boson pair production in the two bottom quarks plus two photons final state in pp collisions at $\sqrt{s} = 13$ TeV with the ATLAS detector*, *Phys. Rev. D* **106** (2022) 052001 [[arXiv:2112.11876](#)] [[INSPIRE](#)].
- [22] ATLAS collaboration, *Search for resonant and non-resonant Higgs boson pair production in the $b\bar{b}\tau^+\tau^-$ decay channel using 13 TeV pp collision data from the ATLAS detector*, *JHEP* **07** (2023) 040 [[arXiv:2209.10910](#)] [[INSPIRE](#)].
- [23] ATLAS collaboration, *Search for nonresonant pair production of Higgs bosons in the $b\bar{b}b\bar{b}$ final state in pp collisions at $\sqrt{s} = 13$ TeV with the ATLAS detector*, *Phys. Rev. D* **108** (2023) 052003 [[arXiv:2301.03212](#)] [[INSPIRE](#)].
- [24] ATLAS collaboration, *Search for non-resonant Higgs boson pair production in the $b\bar{b}\ell\nu\ell\nu$ final state with the ATLAS detector in pp collisions at $\sqrt{s} = 13$ TeV*, *Phys. Lett. B* **801** (2020) 135145 [[arXiv:1908.06765](#)] [[INSPIRE](#)].
- [25] ATLAS collaboration, *Constraints on the Higgs boson self-coupling from single- and double-Higgs production with the ATLAS detector using pp collisions at $\sqrt{s} = 13$ TeV*, *Phys. Lett. B* **843** (2023) 137745 [[arXiv:2211.01216](#)] [[INSPIRE](#)].
- [26] ATLAS collaboration, *Search for Higgs boson pair production in association with a vector boson in pp collisions at $\sqrt{s} = 13$ TeV with the ATLAS detector*, *Eur. Phys. J. C* **83** (2023) 519 [[arXiv:2210.05415](#)] [[INSPIRE](#)].
- [27] CMS collaboration, *Search for higgs boson pair production with one associated vector boson in proton-proton collisions at $\sqrt{s} = 13$ TeV*, CMS-HIG-22-006, CERN, Geneva, Switzerland (2024).
- [28] CMS collaboration, *The CMS experiment at the CERN LHC*, 2008 *JINST* **3** S08004 [[INSPIRE](#)].
- [29] CMS collaboration, *Development of the CMS detector for the CERN LHC run 3*, 2024 *JINST* **19** P05064 [[arXiv:2309.05466](#)] [[INSPIRE](#)].
- [30] CMS collaboration, *Performance of the CMS level-1 trigger in proton-proton collisions at $\sqrt{s} = 13$ TeV*, 2020 *JINST* **15** P10017 [[arXiv:2006.10165](#)] [[INSPIRE](#)].
- [31] CMS collaboration, *The CMS trigger system*, 2017 *JINST* **12** P01020 [[arXiv:1609.02366](#)] [[INSPIRE](#)].
- [32] CMS collaboration, *Precision luminosity measurement in proton-proton collisions at $\sqrt{s} = 13$ TeV in 2015 and 2016 at CMS*, *Eur. Phys. J. C* **81** (2021) 800 [[arXiv:2104.01927](#)] [[INSPIRE](#)].
- [33] CMS collaboration, *CMS luminosity measurement for the 2017 data-taking period at $\sqrt{s} = 13$ TeV*, CMS-PAS-LUM-17-004, CERN, Geneva, Switzerland (2018).

- [34] CMS collaboration, *CMS luminosity measurement for the 2018 data-taking period at $\sqrt{s} = 13$ TeV*, [CMS-PAS-LUM-18-002](#), CERN, Geneva, Switzerland (2019).
- [35] CMS collaboration, *Performance of missing transverse momentum reconstruction in proton-proton collisions at $\sqrt{s} = 13$ TeV using the CMS detector*, [2019 JINST 14 P07004 \[arXiv:1903.06078\]](#) [[INSPIRE](#)].
- [36] CMS collaboration, *Identification of heavy-flavour jets with the CMS detector in pp collisions at 13 TeV*, [2018 JINST 13 P05011 \[arXiv:1712.07158\]](#) [[INSPIRE](#)].
- [37] E. Bols et al., *Jet flavour classification using DeepJet*, [2020 JINST 15 P12012 \[arXiv:2008.10519\]](#) [[INSPIRE](#)].
- [38] J. Alwall et al., *The automated computation of tree-level and next-to-leading order differential cross sections, and their matching to parton shower simulations*, [JHEP 07 \(2014\) 079 \[arXiv:1405.0301\]](#) [[INSPIRE](#)].
- [39] T. Sjöstrand et al., *An introduction to PYTHIA 8.2*, [Comput. Phys. Commun. 191 \(2015\) 159 \[arXiv:1410.3012\]](#) [[INSPIRE](#)].
- [40] NNPDF collaboration, *Parton distributions from high-precision collider data*, [Eur. Phys. J. C 77 \(2017\) 663 \[arXiv:1706.00428\]](#) [[INSPIRE](#)].
- [41] CMS collaboration, *Extraction and validation of a new set of CMS PYTHIA8 tunes from underlying-event measurements*, [Eur. Phys. J. C 80 \(2020\) 4 \[arXiv:1903.12179\]](#) [[INSPIRE](#)].
- [42] A. Dresden, *The fourteenth western meeting of the American Mathematical Society*, [Bull. Amer. Math. Soc. 26 \(1920\) 385](#).
- [43] R. Penrose, *A generalized inverse for matrices*, [Proc. Cambridge Phil. Soc. 51 \(1955\) 406](#) [[INSPIRE](#)].
- [44] P. Nason, *A new method for combining NLO QCD with shower Monte Carlo algorithms*, [JHEP 11 \(2004\) 040 \[hep-ph/0409146\]](#) [[INSPIRE](#)].
- [45] S. Frixione, P. Nason and C. Oleari, *Matching NLO QCD computations with parton shower simulations: the POWHEG method*, [JHEP 11 \(2007\) 070 \[arXiv:0709.2092\]](#) [[INSPIRE](#)].
- [46] S. Alioli, P. Nason, C. Oleari and E. Re, *A general framework for implementing NLO calculations in shower Monte Carlo programs: the POWHEG BOX*, [JHEP 06 \(2010\) 043 \[arXiv:1002.2581\]](#) [[INSPIRE](#)].
- [47] T. Ježo and P. Nason, *On the treatment of resonances in next-to-leading order calculations matched to a parton shower*, [JHEP 12 \(2015\) 065 \[arXiv:1509.09071\]](#) [[INSPIRE](#)].
- [48] F. Buccioni et al., *OpenLoops 2*, [Eur. Phys. J. C 79 \(2019\) 866 \[arXiv:1907.13071\]](#) [[INSPIRE](#)].
- [49] T. Ježo, J.M. Lindert, N. Moretti and S. Pozzorini, *New NLOPS predictions for $t\bar{t} + b$ -jet production at the LHC*, [Eur. Phys. J. C 78 \(2018\) 502 \[arXiv:1802.00426\]](#) [[INSPIRE](#)].
- [50] J. Alwall et al., *MadGraph 5: going beyond*, [JHEP 06 \(2011\) 128 \[arXiv:1106.0522\]](#) [[INSPIRE](#)].
- [51] J. Alwall et al., *Comparative study of various algorithms for the merging of parton showers and matrix elements in hadronic collisions*, [Eur. Phys. J. C 53 \(2008\) 473 \[arXiv:0706.2569\]](#) [[INSPIRE](#)].
- [52] S. Kallweit et al., *NLO QCD+EW predictions for $V+jets$ including off-shell vector-boson decays and multijet merging*, [JHEP 04 \(2016\) 021 \[arXiv:1511.08692\]](#) [[INSPIRE](#)].
- [53] G. Ferrera, M. Grazzini and F. Tramontano, *Higher-order QCD effects for associated WH production and decay at the LHC*, [JHEP 04 \(2014\) 039 \[arXiv:1312.1669\]](#) [[INSPIRE](#)].

- [54] O. Brein, R.V. Harlander and T.J.E. Zirke, *vh@nnlo — Higgs strahlung at hadron colliders*, *Comput. Phys. Commun.* **184** (2013) 998 [[arXiv:1210.5347](#)] [[INSPIRE](#)].
- [55] G. Ferrera, M. Grazzini and F. Tramontano, *Associated ZH production at hadron colliders: the fully differential NNLO QCD calculation*, *Phys. Lett. B* **740** (2015) 51 [[arXiv:1407.4747](#)] [[INSPIRE](#)].
- [56] R. Frederix and S. Frixione, *Merging meets matching in MC@NLO*, *JHEP* **12** (2012) 061 [[arXiv:1209.6215](#)] [[INSPIRE](#)].
- [57] COMPHEP collaboration, *CompHEP 4.4: automatic computations from Lagrangians to events*, *Nucl. Instrum. Meth. A* **534** (2004) 250 [[hep-ph/0403113](#)] [[INSPIRE](#)].
- [58] GEANT4 collaboration, *GEANT4 — a simulation toolkit*, *Nucl. Instrum. Meth. A* **506** (2003) 250 [[INSPIRE](#)].
- [59] CMS collaboration, *Particle-flow reconstruction and global event description with the CMS detector*, *2017 JINST* **12** P10003 [[arXiv:1706.04965](#)] [[INSPIRE](#)].
- [60] D. Contardo et al., *Technical proposal for the phase-II upgrade of the CMS detector*, CERN-LHCC-2015-010, CERN, Geneva, Switzerland (2015) [[DOI:10.17181/CERN.VU8I.D59J](#)] [[literature/1614097](#)] [[INSPIRE](#)].
- [61] M. Cacciari, G.P. Salam and G. Soyez, *The anti- k_t jet clustering algorithm*, *JHEP* **04** (2008) 063 [[arXiv:0802.1189](#)] [[INSPIRE](#)].
- [62] M. Cacciari, G.P. Salam and G. Soyez, *FastJet user manual*, *Eur. Phys. J. C* **72** (2012) 1896 [[arXiv:1111.6097](#)] [[INSPIRE](#)].
- [63] CMS collaboration, *Jet energy scale and resolution in the CMS experiment in pp collisions at 8 TeV*, *2017 JINST* **12** P02014 [[arXiv:1607.03663](#)] [[INSPIRE](#)].
- [64] CMS collaboration, *A deep neural network for simultaneous estimation of b jet energy and resolution*, *Comput. Softw. Big Sci.* **4** (2020) 10 [[arXiv:1912.06046](#)] [[INSPIRE](#)].
- [65] CMS collaboration, *Pileup mitigation at CMS in 13 TeV data*, *2020 JINST* **15** P09018 [[arXiv:2003.00503](#)] [[INSPIRE](#)].
- [66] D. Bertolini, P. Harris, M. Low and N. Tran, *Pileup per particle identification*, *JHEP* **10** (2014) 059 [[arXiv:1407.6013](#)] [[INSPIRE](#)].
- [67] CMS collaboration, *Performance of the DeepJet b tagging algorithm using 41.9 fb^{-1} of data from proton-proton collisions at 13 TeV with phase 1 CMS detector*, CMS-DP-2018-058, CERN, Geneva, Switzerland (2018).
- [68] H. Qu and L. Gouskos, *ParticleNet: jet tagging via particle clouds*, *Phys. Rev. D* **101** (2020) 056019 [[arXiv:1902.08570](#)] [[INSPIRE](#)].
- [69] CMS collaboration, *Electron and photon reconstruction and identification with the CMS experiment at the CERN LHC*, *2021 JINST* **16** P05014 [[arXiv:2012.06888](#)] [[INSPIRE](#)].
- [70] CMS collaboration, *ECAL 2016 refined calibration and run 2 summary plots*, CMS-DP-2020-021, CERN, Geneva, Switzerland (2020).
- [71] CMS collaboration, *Performance of the CMS muon detector and muon reconstruction with proton-proton collisions at $\sqrt{s} = 13\text{ TeV}$* , *2018 JINST* **13** P06015 [[arXiv:1804.04528](#)] [[INSPIRE](#)].
- [72] F. Pedregosa et al., *Scikit-learn: machine learning in python*, *J. Machine Learning Res.* **12** (2011) 2825 [[arXiv:1201.0490](#)] [[INSPIRE](#)].

- [73] J. Thaler and K. Van Tilburg, *Identifying boosted objects with N-subjettiness*, *JHEP* **03** (2011) 015 [[arXiv:1011.2268](#)] [[INSPIRE](#)].
- [74] K. He, X. Zhang, S. Ren and J. Sun, *Deep residual learning for image recognition*, [[DOI:10.1109/CVPR.2016.90](#)] [[arXiv:1512.03385](#)] [[INSPIRE](#)].
- [75] A. Vaswani et al., *Attention is all you need*, in the proceedings of the 31st international conference on neural information processing systems, (2017) [[arXiv:1706.03762](#)] [[INSPIRE](#)].
- [76] A. Rogozhnikov, *Reweighting with boosted decision trees*, *J. Phys. Conf. Ser.* **762** (2016) 012036 [[arXiv:1608.05806](#)] [[INSPIRE](#)].
- [77] CMS collaboration, *Search for supersymmetry in pp collisions at $\sqrt{s} = 8$ TeV in events with a single lepton, large jet multiplicity, and multiple b jets*, *Phys. Lett. B* **733** (2014) 328 [[arXiv:1311.4937](#)] [[INSPIRE](#)].
- [78] ATLAS collaboration, *Measurements of WH and ZH production in the $H \rightarrow b\bar{b}$ decay channel in pp collisions at 13 TeV with the ATLAS detector*, *Eur. Phys. J. C* **81** (2021) 178 [[arXiv:2007.02873](#)] [[INSPIRE](#)].
- [79] CMS collaboration, *Search for ZZ and ZH production in the $b\bar{b}b\bar{b}$ final state using proton-proton collisions at $\sqrt{s} = 13$ TeV*, *Eur. Phys. J. C* **84** (2024) 712 [[arXiv:2403.20241](#)] [[INSPIRE](#)].
- [80] CMS collaboration, *Search for nonresonant Higgs boson pair production in the $b\bar{b}b\bar{b}$ final state at $\sqrt{s} = 13$ TeV*, *JHEP* **04** (2019) 112 [[arXiv:1810.11854](#)] [[INSPIRE](#)].
- [81] ATLAS, CMS collaborations and LHC Higgs Combination Group, *Procedure for the LHC Higgs boson search combination in Summer 2011*, [CMS-NOTE-2011-005](#), CERN, Geneva, Switzerland (2011).
- [82] NNPDF collaboration, *Parton distributions for the LHC run II*, *JHEP* **04** (2015) 040 [[arXiv:1410.8849](#)] [[INSPIRE](#)].
- [83] R.J. Barlow and C. Beeston, *Fitting using finite Monte Carlo samples*, *Comput. Phys. Commun.* **77** (1993) 219 [[INSPIRE](#)].
- [84] CMS collaboration, *Mass regression of highly-boosted jets using graph neural networks*, [CMS-DP-2021-017](#), CERN, Geneva, Switzerland (2021).
- [85] R.A. Fisher, *On the interpretation of χ^2 from contingency tables, and the calculation of P*, *J. Roy. Statist. Soc.* **85** (1922) 87.
- [86] T. Junk, *Confidence level computation for combining searches with small statistics*, *Nucl. Instrum. Meth. A* **434** (1999) 435 [[hep-ex/9902006](#)] [[INSPIRE](#)].
- [87] A.L. Read, *Presentation of search results: the CL_s technique*, *J. Phys. G* **28** (2002) 2693 [[INSPIRE](#)].
- [88] G. Cowan, K. Cranmer, E. Gross and O. Vitells, *Asymptotic formulae for likelihood-based tests of new physics*, *Eur. Phys. J. C* **71** (2011) 1554 [Erratum *ibid.* **73** (2013) 2501] [[arXiv:1007.1727](#)] [[INSPIRE](#)].

The CMS collaboration

Yerevan Physics Institute, Yerevan, Armenia

A. Hayrapetyan, A. Tumasyan¹

Institut für Hochenergiephysik, Vienna, Austria

W. Adam¹, J.W. Andrejkovic, T. Bergauer¹, S. Chatterjee¹, K. Damanakis¹, M. Dragicevic¹, A. Escalante Del Valle¹, P.S. Hussain¹, M. Jeitler^{1,2}, N. Krammer¹, D. Liko¹, I. Mikulec¹, J. Schieck^{1,2}, R. Schöfbeck¹, D. Schwarz¹, M. Sonawane¹, S. Templ¹, W. Waltenberger¹, C.-E. Wulz^{1,2}

Universiteit Antwerpen, Antwerpen, Belgium

M.R. Darwish³, T. Janssen¹, P. Van Mechelen¹

Vrije Universiteit Brussel, Brussel, Belgium

E.S. Bols¹, J. D'Hondt¹, S. Dansana¹, A. De Moor¹, M. Delcourt¹, H. El Faham¹, S. Lowette¹, I. Makarenko¹, D. Müller¹, A.R. Sahasransu¹, S. Tavernier¹, M. Tytgat^{1,4}, S. Van Putte¹, D. Vannerom¹

Université Libre de Bruxelles, Bruxelles, Belgium

B. Clerbaux¹, G. De Lentdecker¹, L. Favart¹, D. Hohov¹, J. Jaramillo¹, A. Khalilzadeh, K. Lee¹, M. Mahdavikhorrami¹, A. Malara¹, S. Paredes¹, L. Pétré¹, N. Postiau, L. Thomas¹, M. Vanden Bemden¹, C. Vander Velde¹, P. Vanlaer¹

Ghent University, Ghent, Belgium

M. De Coen¹, D. Dobur¹, Y. Hong¹, J. Knolle¹, L. Lambrecht¹, G. Mestdach, C. Rendón, A. Samalan, K. Skovpen¹, N. Van Den Bossche¹, L. Wezenbeek¹

Université Catholique de Louvain, Louvain-la-Neuve, Belgium

A. Benecke¹, G. Bruno¹, C. Caputo¹, C. Delaere¹, I.S. Donertas¹, A. Giammanco¹, K. Jaffel¹, Sa. Jain¹, V. Lemaitre, J. Lidrych¹, P. Mastrapasqua¹, K. Mondal¹, T.T. Tran¹, S. Wertz¹

Centro Brasileiro de Pesquisas Fisicas, Rio de Janeiro, Brazil

G.A. Alves¹, E. Coelho¹, C. Hensel¹, T. Menezes De Oliveira¹, A. Moraes¹, P. Rebello Teles¹, M. Soeiro

Universidade do Estado do Rio de Janeiro, Rio de Janeiro, Brazil

W.L. Aldá Júnior¹, M. Alves Gallo Pereira¹, M. Barroso Ferreira Filho¹, H. Brandao Malbouisson¹, W. Carvalho¹, J. Chinellato⁵, E.M. Da Costa¹, G.G. Da Silveira^{1,6}, D. De Jesus Damiao¹, S. Fonseca De Souza¹, J. Martins^{1,7}, C. Mora Herrera¹, K. Mota Amarilo¹, L. Mundim¹, H. Nogima¹, A. Santoro¹, S.M. Silva Do Amaral¹, A. Sznajder¹, M. Thiel¹, A. Vilela Pereira¹

Universidade Estadual Paulista, Universidade Federal do ABC, São Paulo, Brazil

C.A. Bernardes^{1,6}, L. Calligaris¹, T.R. Fernandez Perez Tomei¹, E.M. Gregores¹, P.G. Mercadante¹, S.F. Novaes¹, B. Orzari¹, Sandra S. Padula¹

Institute for Nuclear Research and Nuclear Energy, Bulgarian Academy of Sciences, Sofia, Bulgaria

A. Aleksandrov , G. Antchev , R. Hadjiiska , P. Iaydjiev , M. Misheva , M. Shopova , G. Sultanov 

University of Sofia, Sofia, Bulgaria

A. Dimitrov , T. Ivanov , L. Litov , B. Pavlov , P. Petkov , A. Petrov , E. Shumka 

Instituto De Alta Investigación, Universidad de Tarapacá, Casilla 7 D, Arica, Chile

S. Keshri , S. Thakur 

Beihang University, Beijing, China

T. Cheng , Q. Guo, T. Javaid , M. Mittal , L. Yuan 

Department of Physics, Tsinghua University, Beijing, China

G. Bauer^{8,9}, Z. Hu , K. Yi ^{8,10}

Institute of High Energy Physics, Beijing, China

G.M. Chen ¹¹, H.S. Chen ¹¹, M. Chen ¹¹, F. Iemmi , C.H. Jiang, A. Kapoor ¹², H. Liao , Z.-A. Liu ¹³, F. Monti , M.A. Shahzad¹¹, R. Sharma ¹⁴, J.N. Song¹³, J. Tao , C. Wang¹¹, J. Wang , Z. Wang¹¹, H. Zhang 

State Key Laboratory of Nuclear Physics and Technology, Peking University, Beijing, China

A. Agapitos , Y. Ban , A. Levin , C. Li , Q. Li , X. Lyu, Y. Mao, S.J. Qian , X. Sun , D. Wang , H. Yang, L. Zhang , C. Zhou 

Sun Yat-Sen University, Guangzhou, China

Z. You 

University of Science and Technology of China, Hefei, China

N. Lu 

Institute of Modern Physics and Key Laboratory of Nuclear Physics and Ion-beam Application (MOE) — Fudan University, Shanghai, China

X. Gao ¹⁵, D. Leggat, H. Okawa , Y. Zhang 

Zhejiang University, Hangzhou, Zhejiang, China

Z. Lin , C. Lu , M. Xiao 

Universidad de Los Andes, Bogota, Colombia

C. Avila , D.A. Barbosa Trujillo, A. Cabrera , C. Florez , J. Fraga , J.A. Reyes Vega

Universidad de Antioquia, Medellin, Colombia

J. Mejia Guisao , F. Ramirez , M. Rodriguez , J.D. Ruiz Alvarez 

University of Split, Faculty of Electrical Engineering, Mechanical Engineering and Naval Architecture, Split, Croatia

D. Giljanovic , N. Godinovic , D. Lelas , A. Sculac 

University of Split, Faculty of Science, Split, Croatia

M. Kovac , T. Sculac 

Institute Rudjer Boskovic, Zagreb, Croatia

P. Bargassa , V. Brigljevic , B.K. Chitroda , D. Ferencek , S. Mishra , A. Starodumov ¹⁶, T. Susa 

University of Cyprus, Nicosia, Cyprus

A. Attikis , K. Christoforou , S. Konstantinou , J. Mousa , C. Nicolaou, F. Ptochos , P.A. Razis , H. Rykaczewski, H. Saka , A. Stepennov 

Charles University, Prague, Czech Republic

M. Finger , M. Finger Jr. , A. Kveton 

Escuela Politecnica Nacional, Quito, Ecuador

E. Ayala 

Universidad San Francisco de Quito, Quito, Ecuador

E. Carrera Jarrin 

Academy of Scientific Research and Technology of the Arab Republic of Egypt, Egyptian Network of High Energy Physics, Cairo, Egypt

A.A. Abdelalim , E. Salama ^{19,20}

Center for High Energy Physics (CHEP-FU), Fayoum University, El-Fayoum, Egypt

A. Lotfy , M.A. Mahmoud 

National Institute of Chemical Physics and Biophysics, Tallinn, Estonia

R.K. Dewanjee , K. Ehataht , M. Kadastik, T. Lange , S. Nandan , C. Nielsen , J. Pata , M. Raidal , L. Tani , C. Veelken 

Department of Physics, University of Helsinki, Helsinki, Finland

H. Kirschenmann , K. Osterberg , M. Voutilainen 

Helsinki Institute of Physics, Helsinki, Finland

S. Bharthuar , E. Brücken , F. Garcia , J. Havukainen , K.T.S. Kallonen , M.S. Kim , R. Kinnunen, T. Lampén , K. Lassila-Perini , S. Lehti , T. Lindén , M. Lotti, L. Martikainen , M. Myllymäki , M.m. Rantanen , H. Siikonen , E. Tuominen , J. Tuominiemi 

Lappeenranta-Lahti University of Technology, Lappeenranta, Finland

P. Luukka , H. Petrow , T. Tuuva[†]

IRFU, CEA, Université Paris-Saclay, Gif-sur-Yvette, France

M. Besancon , F. Couderc , M. Dejardin , D. Denegri, J.L. Faure, F. Ferri , S. Ganjour , P. Gras , G. Hamel de Monchenault , V. Lohezic , J. Malcles , J. Rander, A. Rosowsky , M.Ö. Sahin , A. Savoy-Navarro ²², P. Simkina , M. Titov

Laboratoire Leprince-Ringuet, CNRS/IN2P3, Ecole Polytechnique, Institut Polytechnique de Paris, Palaiseau, France

C. Baldenegro Barrera , F. Beaudette , A. Buchot Perraguin , P. Busson , A. Cappati , C. Charlot , F. Damas , O. Davignon , A. De Wit , G. Falmagne , B.A. Fontana Santos Alves , S. Ghosh , A. Gilbert , R. Granier de Cassagnac , A. Hakimi , B. Harikrishnan , L. Kalipoliti , G. Liu , J. Motta , M. Nguyen , C. Ochando , L. Portales , R. Salerno , U. Sarkar , J.B. Sauvan , Y. Sirois , A. Tarabini , E. Vernazza , A. Zabi , A. Zghiche

Université de Strasbourg, CNRS, IPHC UMR 7178, Strasbourg, France

J.-L. Agram ²³, J. Andrea , D. Apparu , D. Bloch , J.-M. Brom , E.C. Chabert , C. Collard , S. Falke , U. Goerlach , C. Grimault, R. Haeberle , A.-C. Le Bihan , M.A. Sessini , P. Van Hove

Institut de Physique des 2 Infinis de Lyon (IP2I), Villeurbanne, France

S. Beauceron , B. Blancon , G. Boudoul , N. Chanon , J. Choi , D. Contardo , P. Depasse , C. Dozen ²⁴, H. El Mamouni, J. Fay , S. Gascon , M. Gouzevitch , C. Greenberg, G. Grenier , B. Ille , I.B. Laktineh, M. Lethuillier , L. Mirabito, S. Perries, M. Vander Donckt , P. Verdier , J. Xiao

Georgian Technical University, Tbilisi, Georgia

G. Adamov, I. Lomidze , Z. Tsamalaidze ¹⁶

RWTH Aachen University, I. Physikalisches Institut, Aachen, Germany

V. Botta , L. Feld , K. Klein , M. Lipinski , D. Meuser , A. Pauls , N. Röwert , M. Teroerde 

RWTH Aachen University, III. Physikalisches Institut A, Aachen, Germany

S. Diekmann , A. Dodonova , N. Eich , D. Eliseev , F. Engelke , M. Erdmann , P. Fackeldey , B. Fischer , T. Hebbeker , K. Hoepfner , F. Ivone , A. Jung , M.y. Lee , L. Mastrolorenzo, M. Merschmeyer , A. Meyer , S. Mukherjee , D. Noll , A. Novak , F. Nowotny, A. Pozdnyakov , Y. Rath, W. Redjeb , F. Rehm, H. Reithler , V. Sarkisovi , A. Schmidt , S.C. Schuler, A. Sharma , A. Stein , F. Torres Da Silva De Araujo ²⁵, L. Vigilante, S. Wiedenbeck , S. Zaleski

RWTH Aachen University, III. Physikalisches Institut B, Aachen, Germany

C. Dziwok , G. Flügge , W. Haj Ahmad ²⁶, T. Kress , A. Nowack , O. Pooth , A. Stahl , T. Ziemons , A. Zottz

Deutsches Elektronen-Synchrotron, Hamburg, Germany

H. Aarup Petersen , M. Aldaya Martin , J. Alimena , S. Amoroso, Y. An , S. Baxter , M. Bayatmakou , H. Becerril Gonzalez , O. Behnke , A. Belvedere , S. Bhattacharya

F. Blekman^{id}²⁷, K. Borras^{id}²⁸, D. Brunner^{id}, A. Campbell^{id}, A. Cardini^{id}, C. Cheng,
 F. Colombina^{id}, S. Consuegra Rodríguez^{id}, G. Correia Silva^{id}, M. De Silva^{id}, G. Eckerlin,
 D. Eckstein^{id}, L.I. Estevez Banos^{id}, O. Filatov^{id}, E. Gallo^{id}²⁷, A. Geiser^{id}, A. Giraldi^{id}, G. Greau,
 V. Guglielmi^{id}, M. Guthoff^{id}, A. Hinzmann^{id}, A. Jafari^{id}²⁹, L. Jeppe^{id}, N.Z. Jomhari^{id},
 B. Kaech^{id}, M. Kasemann^{id}, H. Kaveh^{id}, C. Kleinwort^{id}, R. Kogler^{id}, M. Komm^{id}, D. Krücker^{id},
 W. Lange, D. Leyva Pernia^{id}, K. Lipka^{id}³⁰, W. Lohmann^{id}³¹, R. Mankel^{id},
 I.-A. Melzer-Pellmann^{id}, M. Mendizabal Morentin^{id}, J. Metwally, A.B. Meyer^{id}, G. Milella^{id},
 A. Mussgiller^{id}, A. Nürnberg^{id}, Y. Otarid, D. Pérez Adán^{id}, E. Ranken^{id}, A. Raspereza^{id},
 B. Ribeiro Lopes^{id}, J. Rübenach, A. Saggio^{id}, M. Scham^{id}^{32,28}, S. Schnake^{id}²⁸, P. Schütze^{id},
 C. Schwanenberger^{id}²⁷, D. Selivanova^{id}, M. Shchedrolosiev^{id}, R.E. Sosa Ricardo^{id},
 L.P. Sreelatha Pramod^{id}, D. Stafford, F. Vazzoler^{id}, A. Ventura Barroso^{id}, R. Walsh^{id}, Q. Wang^{id},
 Y. Wen^{id}, K. Wichmann, L. Wiens^{id}²⁸, C. Wissing^{id}, S. Wuchterl^{id}, Y. Yang^{id},
 A. Zimermann Castro Santos^{id}

University of Hamburg, Hamburg, Germany

A. Albrecht^{id}, S. Albrecht^{id}, M. Antonello^{id}, S. Bein^{id}, L. Benato^{id}, M. Bonanomi^{id}, P. Connor^{id},
 M. Eich, K. El Morabit^{id}, Y. Fischer^{id}, A. Fröhlich, C. Garbers^{id}, E. Garutti^{id}, A. Grohsjean^{id},
 M. Hajheidari, J. Haller^{id}, H.R. Jabusch^{id}, G. Kasieczka^{id}, P. Keicher, R. Klanner^{id}, W. Korcari^{id},
 T. Kramer^{id}, V. Kutzner^{id}, F. Labe^{id}, J. Lange^{id}, A. Lobanov^{id}, C. Matthies^{id}, A. Mehta^{id},
 L. Moureaux^{id}, M. Mrowietz, A. Nigamova^{id}, Y. Nissan, A. Paasch^{id}, K.J. Pena Rodriguez^{id},
 T. Quadfasel^{id}, B. Raciti^{id}, M. Rieger^{id}, D. Savoiu^{id}, J. Schindler^{id}, P. Schleper^{id}, M. Schröder^{id},
 J. Schwandt^{id}, M. Sommerhalder^{id}, H. Stadie^{id}, G. Steinbrück^{id}, A. Tews, M. Wolf^{id}

Karlsruher Institut fuer Technologie, Karlsruhe, Germany

S. Brommer^{id}, M. Burkart, E. Butz^{id}, T. Chwalek^{id}, A. Dierlamm^{id}, A. Droll, N. Faltermann^{id},
 M. Giffels^{id}, A. Gottmann^{id}, F. Hartmann^{id}³³, R. Hofsaess^{id}, M. Horzela^{id}, U. Husemann^{id},
 M. Klute^{id}, R. Koppenhöfer^{id}, M. Link, A. Lintuluoto^{id}, S. Maier^{id}, S. Mitra^{id}, M. Mormile^{id},
 Th. Müller^{id}, M. Neukum, M. Oh^{id}, G. Quast^{id}, K. Rabbertz^{id}, B. Regnery^{id}, N. Shadskiy^{id},
 I. Shvetsov^{id}, H.J. Simonis^{id}, N. Trevisani^{id}, R. Ulrich^{id}, J. van der Linden^{id}, R.F. Von Cube^{id},
 M. Wassmer^{id}, S. Wieland^{id}, F. Wittig, R. Wolf^{id}, S. Wunsch, X. Zuo^{id}

Institute of Nuclear and Particle Physics (INPP), NCSR Demokritos, Aghia Paraskevi, Greece

G. Anagnostou, P. Assiouras^{id}, G. Daskalakis^{id}, A. Kyriakis, A. Papadopoulos³³, A. Stakia^{id}

National and Kapodistrian University of Athens, Athens, Greece

P. Kontaxakis^{id}, G. Melachroinos, A. Panagiotou, I. Papavergou^{id}, I. Paraskevas^{id}, N. Saoulidou^{id},
 K. Theofilatos^{id}, E. Tziaferi^{id}, K. Vellidis^{id}, I. Zisopoulos^{id}

National Technical University of Athens, Athens, Greece

G. Bakas^{id}, T. Chatzistavrou, G. Karapostoli^{id}, K. Kousouris^{id}, I. Papakrivopoulos^{id},
 E. Siamarkou, G. Tsipolitis, A. Zacharopoulou

University of Ioánnina, Ioánnina, Greece

K. Adamidis, I. Bestintzanos, I. Evangelou^{id}, C. Foudas, P. Gianneios^{id}, C. Kamtsikis, P. Katsoulis,
 P. Kokkas^{id}, P.G. Kosmoglou Kioglou^{id}, N. Manthos^{id}, I. Papadopoulos^{id}, J. Strologas^{id}

HUN-REN Wigner Research Centre for Physics, Budapest, HungaryM. Bartók ³⁴, C. Hajdu , D. Horvath ^{35,36}, F. Sikler , V. Veszpremi **MTA-ELTE Lendület CMS Particle and Nuclear Physics Group, Eötvös Loránd University, Budapest, Hungary**M. Csanád , K. Farkas , M.M.A. Gadallah ³⁷, Á. Kadlecik , P. Major , K. Mandal , G. Pásztor , A.J. Rádl ³⁸, G.I. Veres **Faculty of Informatics, University of Debrecen, Debrecen, Hungary**P. Raics, B. Ujvari ³⁹, G. Zilizi **Institute of Nuclear Research ATOMKI, Debrecen, Hungary**G. Bencze, S. Czellar, J. Karancsi ³⁴, J. Molnar, Z. Szillasi**Karoly Robert Campus, MATE Institute of Technology, Gyongyos, Hungary**T. Csorgo ³⁸, F. Nemes ³⁸, T. Novak **Panjab University, Chandigarh, India**J. Babbar , S. Bansal , S.B. Beri, V. Bhatnagar , G. Chaudhary , S. Chauhan , N. Dhingra ⁴⁰, R. Gupta, A. Kaur , A. Kaur , H. Kaur , M. Kaur , S. Kumar , M. Meena , K. Sandeep , T. Sheokand, J.B. Singh , A. Singla **University of Delhi, Delhi, India**A. Ahmed , A. Bhardwaj , A. Chhetri , B.C. Choudhary , A. Kumar , M. Naimuddin , K. Ranjan , S. Saumya **Saha Institute of Nuclear Physics, HBNI, Kolkata, India**S. Acharya ⁴¹, S. Baradja , S. Barman ⁴², S. Bhattacharya , D. Bhowmik, S. Dutta , S. Dutta, B. Gomber ⁴¹, P. Palit , G. Saha , B. Sahu ⁴¹, S. Sarkar**Indian Institute of Technology Madras, Madras, India**M.M. Ameen , P.K. Behera , S.C. Behera , S. Chatterjee , P. Jana , P. Kalbhor , J.R. Komaragiri ⁴³, D. Kumar ⁴³, L. Panwar ⁴³, R. Pradhan , P.R. Pujahari , N.R. Saha , A. Sharma , A.K. Sikdar , S. Verma **Tata Institute of Fundamental Research-A, Mumbai, India**T. Aziz, I. Das , S. Dugad, M. Kumar , G.B. Mohanty , P. Suryadevara**Tata Institute of Fundamental Research-B, Mumbai, India**A. Bala , S. Banerjee , R.M. Chatterjee, M. Guchait , S. Karmakar , S. Kumar , G. Majumder , K. Mazumdar , S. Mukherjee , A. Thachayath **National Institute of Science Education and Research, An OCC of Homi Bhabha National Institute, Bhubaneswar, Odisha, India**S. Bahinipati ⁴⁴, A.K. Das, C. Kar , D. Maity ⁴⁵, P. Mal , T. Mishra , V.K. Muraleedharan Nair Bindhu ⁴⁵, K. Naskar ⁴⁵, A. Nayak ⁴⁵, P. Sadangi, P. Saha , S.K. Swain , S. Varghese ⁴⁵, D. Vats ⁴⁵

Indian Institute of Science Education and Research (IISER), Pune, IndiaA. Alpana , S. Dube , B. Kansal , A. Laha , A. Rastogi , S. Sharma **Isfahan University of Technology, Isfahan, Iran**H. Bakhshiansohi ⁴⁶, E. Khazaie ⁴⁷, M. Zeinali ⁴⁸**Institute for Research in Fundamental Sciences (IPM), Tehran, Iran**S. Chenarani ⁴⁹, S.M. Etesami , M. Khakzad , M. Mohammadi Najafabadi **University College Dublin, Dublin, Ireland**M. Grunewald **INFN Sezione di Bari^a, Università di Bari^b, Politecnico di Bari^c, Bari, Italy**M. Abbrescia , R. Aly ^{a,c,17}, A. Colaleo , D. Creanza , B. D'Anzi , N. De Filippis , M. De Palma , A. Di Florio , W. Elmetenawee ^{a,b,17}, L. Fiore , G. Iaselli , G. Maggi , M. Maggi , I. Margjeka , V. Mastrapasqua , S. My , S. Nuzzo , A. Pellecchia , A. Pompili , G. Pugliese , R. Radogna , G. Ramirez-Sanchez , D. Ramos , A. Ranieri , L. Silvestris , F.M. Simone , Ü. Sözbilir , A. Stamerra , R. Venditti , P. Verwilligen , A. Zaza **INFN Sezione di Bologna^a, Università di Bologna^b, Bologna, Italy**G. Abbiendi , C. Battilana , D. Bonacorsi , L. Borgonovi , R. Campanini , P. Capiluppi , A. Castro , F.R. Cavallo , M. Cuffiani , G.M. Dallavalle , T. Diotalevi , F. Fabbri , A. Fanfani , D. Fasanella , P. Giacomelli , L. Giommi , L. Guiducci , S. Lo Meo ⁵⁰, L. Lunerti , S. Marcellini , G. Masetti , F.L. Navarria , A. Perrotta , F. Primavera , A.M. Rossi , T. Rovelli , G.P. Siroli **INFN Sezione di Catania^a, Università di Catania^b, Catania, Italy**S. Costa , A. Di Mattia , R. Potenza ^{a,b}, A. Tricomi ^{a,b,51}, C. Tuve **INFN Sezione di Firenze^a, Università di Firenze^b, Firenze, Italy**G. Barbagli , G. Bardelli , B. Camaiani , A. Cassese , R. Ceccarelli , V. Ciulli , C. Civinini , R. D'Alessandro , E. Focardi , T. Kello , G. Latino , P. Lenzi , M. Lizzo , M. Meschini , S. Paoletti , A. Papanastassiou , G. Sguazzoni , L. Viliani **INFN Laboratori Nazionali di Frascati, Frascati, Italy**L. Benussi , S. Bianco , S. Meola ⁵², D. Piccolo **INFN Sezione di Genova^a, Università di Genova^b, Genova, Italy**P. Chatagnon , F. Ferro , E. Robutti , S. Tosi **INFN Sezione di Milano-Bicocca^a, Università di Milano-Bicocca^b, Milano, Italy**A. Benaglia , G. Boldrini , F. Brivio , F. Cetorelli , F. De Guio , M.E. Dinardo , P. Dini , S. Gennai , A. Ghezzi ^{a,b}, P. Govoni , L. Guzzi , M.T. Lucchini , M. Malberti , S. Malvezzi , A. Massironi , D. Menasce , L. Moroni , M. Paganoni , D. Pedrini , B.S. Pinolini , S. Ragazzi ^{a,b}, N. Redaelli , T. Tabarelli de Fatis ^{a,b}, D. Zuolo 

INFN Sezione di Napoli^a, Università di Napoli ‘Federico II’^b, Napoli, Italy; Università della Basilicata^c, Potenza, Italy; Scuola Superiore Meridionale (SSM)^d, Napoli, Italy

S. Buontempo ^a, A. Cagnotta ^{a,b}, F. Carnevali ^{a,b}, N. Cavallo ^{a,c}, A. De Iorio ^{a,b}, F. Fabozzi ^{a,c}, A.O.M. Iorio ^{a,b}, L. Lista ^{a,b,53}, P. Paolucci ^{a,33}, B. Rossi ^a, C. Sciacca ^{a,b}

INFN Sezione di Padova^a, Università di Padova^b, Padova, Italy; Università di Trento^c, Trento, Italy

R. Ardino ^a, P. Azzi ^a, N. Bacchetta ^{a,54}, P. Bortignon ^a, A. Bragagnolo ^{a,b}, R. Carlin ^{a,b}, P. Checchia ^a, T. Dorigo ^a, F. Gasparini ^{a,b}, U. Gasparini ^{a,b}, G. Grossi ^a, L. Layer ^{a,55}, E. Lusiani ^a, M. Margoni ^{a,b}, G. Maron ^{a,56}, A.T. Meneguzzo ^{a,b}, M. Migliorini ^{a,b}, J. Pazzini ^{a,b}, P. Ronchese ^{a,b}, R. Rossin ^{a,b}, F. Simonetto ^{a,b}, G. Strong ^a, M. Tosi ^{a,b}, A. Triossi ^{a,b}, S. Ventura ^a, H. Yarar ^{a,b}, M. Zanetti ^{a,b}, P. Zotto ^{a,b}, A. Zucchetta ^{a,b}, G. Zumerle ^{a,b}

INFN Sezione di Pavia^a, Università di Pavia^b, Pavia, Italy

S. Abu Zeid ^{a,20}, C. Aimè ^{a,b}, A. Braghieri ^a, S. Calzaferri ^{a,b}, D. Fiorina ^{a,b}, P. Montagna ^{a,b}, V. Re ^a, C. Riccardi ^{a,b}, P. Salvini ^a, I. Vai ^{a,b}, P. Vitulo ^{a,b}

INFN Sezione di Perugia^a, Università di Perugia^b, Perugia, Italy

S. Ajmal ^{a,b}, P. Asenov ^{a,57}, G.M. Bilei ^a, D. Ciangottini ^{a,b}, L. Fanò ^{a,b}, M. Magherini ^{a,b}, G. Mantovani ^{a,b}, V. Mariani ^{a,b}, M. Menichelli ^a, F. Moscatelli ^{a,57}, A. Piccinelli ^{a,b}, M. Presilla ^{a,b}, A. Rossi ^{a,b}, A. Santocchia ^{a,b}, D. Spiga ^a, T. Tedeschi ^{a,b}

INFN Sezione di Pisa^a, Università di Pisa^b, Scuola Normale Superiore di Pisa^c, Pisa, Italy; Università di Siena^d, Siena, Italy

P. Azzurri ^a, G. Bagliesi ^a, R. Bhattacharya ^a, L. Bianchini ^{a,b}, T. Boccali ^a, E. Bossini ^a, D. Bruschini ^{a,c}, R. Castaldi ^a, M.A. Ciocci ^{a,b}, M. Cipriani ^{a,b}, V. D’Amante ^{a,d}, R. Dell’Orso ^a, S. Donato ^a, A. Giassi ^a, F. Ligabue ^{a,c}, D. Matos Figueiredo ^a, A. Messineo ^{a,b}, M. Musich ^{a,b}, F. Palla ^a, S. Parolia ^a, A. Rizzi ^{a,b}, G. Rolandi ^{a,c}, S. Roy Chowdhury ^a, T. Sarkar ^a, A. Scribano ^a, P. Spagnolo ^a, R. Tenchini ^a, G. Tonelli ^{a,b}, N. Turini ^{a,d}, A. Venturi ^a, P.G. Verdini ^a

INFN Sezione di Roma^a, Sapienza Università di Roma^b, Roma, Italy

P. Barria ^a, M. Campana ^{a,b}, F. Cavallari ^a, L. Cunqueiro Mendez ^{a,b}, D. Del Re ^{a,b}, E. Di Marco ^a, M. Diemoz ^a, F. Errico ^{a,b}, E. Longo ^{a,b}, P. Meridiani ^a, J. Mijuskovic ^{a,b}, G. Organtini ^{a,b}, F. Pandolfi ^a, R. Paramatti ^{a,b}, C. Quaranta ^{a,b}, S. Rahatlou ^{a,b}, C. Rovelli ^a, F. Santanastasio ^{a,b}, L. Soffi ^a, R. Tramontano ^{a,b}

INFN Sezione di Torino^a, Università di Torino^b, Torino, Italy; Università del Piemonte Orientale^c, Novara, Italy

N. Amapane ^{a,b}, R. Arcidiacono ^{a,c}, S. Argiro ^{a,b}, M. Arneodo ^{a,c}, N. Bartosik ^a, R. Bellan ^{a,b}, A. Bellora ^{a,b}, C. Biino ^a, N. Cartiglia ^a, M. Costa ^{a,b}, R. Covarelli ^{a,b}, N. Demaria ^a, L. Finco ^a, M. Grippo ^{a,b}, B. Kiani ^{a,b}, F. Legger ^a, F. Luongo ^{a,b}, C. Mariotti ^a, S. Maselli ^a, A. Mecca ^{a,b}, E. Migliore ^{a,b}, M. Monteno ^a, R. Mularia ^a,

M.M. Obertino ^{a,b}, G. Ortona ^a, L. Pacher ^{a,b}, N. Pastrone ^a, M. Pelliccioni ^a, M. Ruspa ^{a,c}, F. Siviero ^{a,b}, V. Sola ^{a,b}, A. Solano ^{a,b}, D. Soldi ^{a,b}, A. Staiano ^a, C. Tarricone ^{a,b}, M. Tornago ^{a,b}, D. Trocino ^a, G. Umoret ^{a,b}, E. Vlasov ^{a,b}

INFN Sezione di Trieste^a, Università di Trieste^b, Trieste, Italy

S. Belforte ^a, V. Candelise ^{a,b}, M. Casarsa ^a, F. Cossutti ^a, K. De Leo ^{a,b}, G. Della Ricca ^{a,b}

Kyungpook National University, Daegu, Korea

S. Dogra , J. Hong , C. Huh , B. Kim , D.H. Kim , J. Kim, H. Lee, S.W. Lee , C.S. Moon , Y.D. Oh , M.S. Ryu , S. Sekmen , Y.C. Yang

Chonnam National University, Institute for Universe and Elementary Particles, Kwangju, Korea

G. Bak , P. Gwak , H. Kim , D.H. Moon 

Hanyang University, Seoul, Korea

E. Asilar , D. Kim , T.J. Kim , J.A. Merlin, J. Park 

Korea University, Seoul, Korea

S. Choi , S. Han, B. Hong , K. Lee, K.S. Lee , S. Lee , J. Park, S.K. Park, J. Yoo 

Kyung Hee University, Department of Physics, Seoul, Korea

J. Goh 

Sejong University, Seoul, Korea

H. S. Kim , Y. Kim, S. Lee

Seoul National University, Seoul, Korea

J. Almond, J.H. Bhyun, J. Choi , W. Jun , J. Kim , J.S. Kim, S. Ko , H. Kwon , H. Lee , J. Lee , J. Lee , B.H. Oh , S.B. Oh , H. Seo , U.K. Yang, I. Yoon

University of Seoul, Seoul, Korea

W. Jang , D.Y. Kang, Y. Kang , S. Kim , B. Ko, J.S.H. Lee , Y. Lee , I.C. Park , Y. Roh, I.J. Watson , S. Yang 

Yonsei University, Department of Physics, Seoul, Korea

S. Ha , H.D. Yoo 

Sungkyunkwan University, Suwon, Korea

M. Choi , M.R. Kim , H. Lee, Y. Lee , I. Yu 

College of Engineering and Technology, American University of the Middle East (AUM), Dasman, Kuwait

T. Beyrouthy, Y. Maghrbi 

Riga Technical University, Riga, Latvia

K. Dreimanis , A. Gaile , G. Pikurs, A. Potrebko , M. Seidel , V. Veckalns ⁵⁸

University of Latvia (LU), Riga, LatviaN.R. Strautnieks **Vilnius University, Vilnius, Lithuania**M. Ambrozas , A. Juodagalvis , A. Rinkevicius , G. Tamulaitis **National Centre for Particle Physics, Universiti Malaya, Kuala Lumpur, Malaysia**N. Bin Norjoharuddeen , I. Yusuff ⁵⁹, Z. Zolkapli**Universidad de Sonora (UNISON), Hermosillo, Mexico**J.F. Benitez , A. Castaneda Hernandez , H.A. Encinas Acosta, L.G. Gallegos Maríñez, M. León Coello , J.A. Murillo Quijada , A. Sehrawat , L. Valencia Palomo **Centro de Investigacion y de Estudios Avanzados del IPN, Mexico City, Mexico**G. Ayala , H. Castilla-Valdez , E. De La Cruz-Burelo , I. Heredia-De La Cruz ⁶⁰, R. Lopez-Fernandez , C.A. Mondragon Herrera, A. Sánchez Hernández **Universidad Iberoamericana, Mexico City, Mexico**C. Oropeza Barrera , M. Ramírez García **Benemerita Universidad Autonoma de Puebla, Puebla, Mexico**I. Bautista , I. Pedraza , H.A. Salazar Ibarguen , C. Uribe Estrada **University of Montenegro, Podgorica, Montenegro**I. Bubanja , N. Raicevic **University of Canterbury, Christchurch, New Zealand**P.H. Butler **National Centre for Physics, Quaid-I-Azam University, Islamabad, Pakistan**A. Ahmad , M.I. Asghar, A. Awais , M.I.M. Awan, H.R. Hoorani , W.A. Khan **AGH University of Krakow, Faculty of Computer Science, Electronics and Telecommunications, Krakow, Poland**V. Avati, L. Grzanka , M. Malawski **National Centre for Nuclear Research, Swierk, Poland**H. Bialkowska , M. Bluj , B. Boimska , M. Górski , M. Kazana , M. Szleper , P. Zalewski **Institute of Experimental Physics, Faculty of Physics, University of Warsaw, Warsaw, Poland**K. Bunkowski , K. Doroba , A. Kalinowski , M. Konecki , J. Krolikowski , A. Muhammad **Warsaw University of Technology, Warsaw, Poland**K. Pozniak , W. Zabolotny 

Laboratório de Instrumentação e Física Experimental de Partículas, Lisboa, Portugal

M. Araujo , D. Bastos , C. Beirão Da Cruz E Silva , A. Boletti , M. Bozzo , P. Faccioli , M. Gallinaro , J. Hollar , N. Leonardo , T. Niknejad , A. Petrilli , M. Pisano , J. Seixas , J. Varela , J.W. Wulff

Faculty of Physics, University of Belgrade, Belgrade, Serbia

P. Adzic , P. Milenovic

VINCA Institute of Nuclear Sciences, University of Belgrade, Belgrade, Serbia

M. Dordevic , J. Milosevic , V. Rekovic

Centro de Investigaciones Energéticas Medioambientales y Tecnológicas (CIEMAT), Madrid, Spain

M. Aguilar-Benitez, J. Alcaraz Maestre , Cristina F. Bedoya , M. Cepeda , M. Cerrada , N. Colino , B. De La Cruz , A. Delgado Peris , D. Fernández Del Val , J.P. Fernández Ramos , J. Flix , M.C. Fouz , O. Gonzalez Lopez , S. Goy Lopez , J.M. Hernandez , M.I. Josa , J. León Holgado , D. Moran , C. M. Morcillo Perez , Á. Navarro Tobar , C. Perez Dengra , A. Pérez-Calero Yzquierdo , J. Puerta Pelayo , I. Redondo , D.D. Redondo Ferrero , L. Romero, S. Sánchez Navas , L. Urda Gómez , J. Vazquez Escobar , C. Willmott

Universidad Autónoma de Madrid, Madrid, Spain

J.F. de Trocóniz

Universidad de Oviedo, Instituto Universitario de Ciencias y Tecnologías Espaciales de Asturias (ICTEA), Oviedo, Spain

B. Alvarez Gonzalez , J. Cuevas , J. Fernandez Menendez , S. Folgueras , I. Gonzalez Caballero , J.R. González Fernández , E. Palencia Cortezon , C. Ramón Álvarez , V. Rodríguez Bouza , A. Soto Rodríguez , A. Trapote , C. Vico Villalba , P. Vischia

Instituto de Física de Cantabria (IFCA), CSIC-Universidad de Cantabria, Santander, Spain

S. Bhowmik , S. Blanco Fernández , J.A. Brochero Cifuentes , I.J. Cabrillo , A. Calderon , J. Duarte Campderros , M. Fernandez , C. Fernandez Madrazo , G. Gomez , C. Lasosa García , C. Martinez Rivero , P. Martinez Ruiz del Arbol , F. Matorras , P. Matorras Cuevas , E. Navarrete Ramos , J. Piedra Gomez , L. Scodellaro , I. Vila , J.M. Vizan Garcia

University of Colombo, Colombo, Sri Lanka

M.K. Jayananda , B. Kailasapathy ⁶¹, D.U.J. Sonnadara , D.D.C. Wickramarathna

University of Ruhuna, Department of Physics, Matara, Sri Lanka

W.G.D. Dharmaratna , K. Liyanage , N. Perera , N. Wickramage

CERN, European Organization for Nuclear Research, Geneva, Switzerland

D. Abbaneo , C. Amendola , E. Auffray , G. Auzinger , J. Baechler, D. Barney , A. Bermúdez Martínez , M. Bianco , B. Bilin , A.A. Bin Anuar , A. Bocci , E. Brondolin

C. Caillool , T. Camporesi , G. Cerminara , N. Chernyavskaya , D. d'Enterria ,
A. Dabrowski , A. David , A. De Roeck , M.M. Defranchis , M. Deile , M. Dobson ,
F. Fallavollita⁶³ , L. Forthomme , G. Franzoni , W. Funk , S. Giani, D. Gigi, K. Gill ,
F. Glege , L. Gouskos , M. Haranko , J. Hegeman , V. Innocente , T. James , P. Janot ,
J. Kieseler , S. Laurila , P. Lecoq , E. Leutgeb , C. Lourenço , B. Maier , L. Malgeri ,
M. Mannelli , A.C. Marini , F. Meijers , S. Mersi , E. Meschi , V. Milosevic , F. Moortgat ,
M. Mulders , S. Orfanelli, F. Pantaleo , M. Peruzzi , G. Petrucciani , A. Pfeiffer ,
M. Pierini , D. Piparo , H. Qu , D. Rabady , G. Reales Gutiérrez, M. Rovere , H. Sakulin ,
S. Scarfi , M. Selvaggi , A. Sharma , K. Shchelina , P. Silva , P. Sphicas⁶⁴ ,
A.G. Stahl Leiton , A. Steen , S. Summers , D. Treille , P. Tropea , A. Tsirou, D. Walter ,
J. Wanczyk , K.A. Wozniak⁶⁶ , P. Zehetner , P. Zejdl , W.D. Zeuner

Paul Scherrer Institut, Villigen, Switzerland

T. Bevilacqua , L. Caminada , A. Ebrahimi , W. Erdmann , R. Horisberger , Q. Ingram ,
H.C. Kaestli , D. Kotlinski , C. Lange , M. Missiroli , L. Noehte , T. Rohe

ETH Zurich — Institute for Particle Physics and Astrophysics (IPA), Zurich, Switzerland

T.K. Arrestad , K. Androssov⁶⁵ , M. Backhaus , A. Calandri , C. Cazzaniga , K. Datta ,
A. De Cosa , G. Dissertori , M. Dittmar, M. Donegà , F. Eble , M. Galli , K. Gedia ,
F. Glessgen , C. Grab , D. Hits , W. Lustermann , A.-M. Lyon , R.A. Manzoni ,
M. Marchegiani , L. Marchese , C. Martin Perez , A. Mascellani , F. Nessi-Tedaldi ,
F. Pauss , V. Perovic , S. Pigazzini , M.G. Ratti , M. Reichmann , C. Reissel ,
T. Reitenspiess , B. Ristic , F. Riti , D. Ruini, D.A. Sanz Becerra , R. Seidita ,
J. Steggemann , D. Valsecchi , R. Wallny

Universität Zürich, Zurich, Switzerland

C. Amsler , P. Bärtschi , C. Botta , D. Brzhechko, M.F. Canelli , K. Cormier , R. Del Burgo,
J.K. Heikkilä , M. Huwiler , W. Jin , A. Jofrehei , B. Kilminster , S. Leontsinis ,
S.P. Liechti , A. Macchiolo , P. Meiring , V.M. Mikuni , U. Molinatti , I. Neutelings ,
A. Reimers , P. Robmann, S. Sanchez Cruz , K. Schweiger , M. Senger , Y. Takahashi

National Central University, Chung-Li, Taiwan

C. Adloff⁶⁹ , C.M. Kuo, W. Lin, P.K. Rout , P.C. Tiwari ⁴³, S.S. Yu 

National Taiwan University (NTU), Taipei, Taiwan

L. Ceard, Y. Chao , K.F. Chen , P.s. Chen, Z.g. Chen, W.-S. Hou , T.h. Hsu, Y.w. Kao,
R. Khurana, G. Kole , Y.y. Li , R.-S. Lu , E. Paganis , A. Psallidas, X.f. Su ,
J. Thomas-Wilsker , H.y. Wu, E. Yazgan 

High Energy Physics Research Unit, Department of Physics, Faculty of Science, Chulalongkorn University, Bangkok, Thailand

C. Asawatangtrakuldee , N. Srimanobhas , V. Wachirapusanand 

Çukurova University, Physics Department, Science and Art Faculty, Adana, Turkey

D. Agyel , F. Boran , Z.S. Demiroglu , F. Dolek , I. Dumanoglu ⁷⁰, E. Eskut , Y. Guler ⁷¹, E. Gurpinar Guler ⁷¹, C. Isik , O. Kara, A. Kayis Topaksu , U. Kiminsu , G. Onengut , K. Ozdemir ⁷², A. Polatoz , B. Tali ⁷³, U.G. Tok , S. Turkcapar , E. Uslan , I.S. Zorbakir

Middle East Technical University, Physics Department, Ankara, Turkey

M. Yalvac ⁷⁴

Bogazici University, Istanbul, Turkey

B. Akgun , I.O. Atakisi , E. Gülmez , M. Kaya ⁷⁵, O. Kaya ⁷⁶, S. Tekten ⁷⁷

Istanbul Technical University, Istanbul, Turkey

A. Cakir , K. Cankocak ⁷⁰, Y. Komurcu , S. Sen ⁷⁸

Istanbul University, Istanbul, Turkey

O. Aydilek , S. Cerci ⁷³, V. Epshteyn , B. Hacisahinoglu , I. Hos ⁷⁹, B. Isildak ⁸⁰, B. Kaynak , S. Ozkorucuklu , O. Potok , H. Sert , C. Simsek , D. Sunar Cerci ⁷³, C. Zorbilmez

Institute for Scintillation Materials of National Academy of Science of Ukraine, Kharkiv, Ukraine

A. Boyaryntsev , B. Grynyov 

National Science Centre, Kharkiv Institute of Physics and Technology, Kharkiv, Ukraine

L. Levchuk 

University of Bristol, Bristol, United Kingdom

D. Anthony , J.J. Brooke , A. Bundock , F. Bury , E. Clement , D. Cussans , H. Flacher , M. Glowacki, J. Goldstein , H.F. Heath , L. Kreczko , B. Krikler , S. Paramesvaran , S. Seif El Nasr-Storey, V.J. Smith ,⁸¹ N. Stylianou , K. Walkingshaw Pass, R. White

Rutherford Appleton Laboratory, Didcot, United Kingdom

A.H. Ball, K.W. Bell , A. Belyaev ⁸², C. Brew , R.M. Brown , D.J.A. Cockerill , C. Cooke , K.V. Ellis, K. Harder , S. Harper , M.-L. Holmberg ⁸³, Sh. Jain , J. Linacre , K. Manolopoulos, D.M. Newbold , E. Olaiya, D. Petyt , T. Reis , G. Salvi , T. Schuh, C.H. Shepherd-Themistocleous , I.R. Tomalin , T. Williams

Imperial College, London, United Kingdom

R. Bainbridge , P. Bloch , C.E. Brown , O. Buchmuller, V. Cacchio, C.A. Carrillo Montoya , G.S. Chahal ⁸⁴, D. Colling , J.S. Danceu, P. Dauncey , G. Davies , J. Davies, M. Della Negra , S. Fayer, G. Fedi , G. Hall , M.H. Hassanshahi , A. Howard, G. Iles , M. Knight , J. Langford , L. Lyons , A.-M. Magnan , S. Malik, A. Martelli , M. Mieskolainen , J. Nash ⁸⁵, M. Pesaresi , B.C. Radburn-Smith , A. Richards, A. Rose , C. Seez , R. Shukla

A. Tapper^{ID}, K. Uchida^{ID}, G.P. Uttley^{ID}, L.H. Vage, T. Virdee^{ID}³³, M. Vojinovic^{ID}, N. Wardle^{ID}, D. Winterbottom^{ID}

Brunel University, Uxbridge, United Kingdom

K. Coldham, J.E. Cole^{ID}, A. Khan, P. Kyberd^{ID}, I.D. Reid^{ID}

Baylor University, Waco, Texas, U.S.A.

S. Abdullin^{ID}, A. Brinkerhoff^{ID}, B. Caraway^{ID}, J. Dittmann^{ID}, K. Hatakeyama^{ID}, J. Hiltbrand^{ID}, A.R. Kanuganti^{ID}, B. McMaster^{ID}, M. Saunders^{ID}, S. Sawant^{ID}, C. Sutantawibul^{ID}, M. Toms^{ID}⁸⁶, J. Wilson^{ID}

Catholic University of America, Washington, DC, U.S.A.

R. Bartek^{ID}, A. Dominguez^{ID}, C. Huerta Escamilla, A.E. Simsek^{ID}, R. Uniyal^{ID}, A.M. Vargas Hernandez^{ID}

The University of Alabama, Tuscaloosa, Alabama, U.S.A.

R. Chudasama^{ID}, S.I. Cooper^{ID}, S.V. Gleyzer^{ID}, C.U. Perez^{ID}, P. Rumerio^{ID}⁸⁷, E. Usai^{ID}, C. West^{ID}, R. Yi^{ID}

Boston University, Boston, Massachusetts, U.S.A.

A. Akpinar^{ID}, A. Albert^{ID}, D. Arcaro^{ID}, C. Cosby^{ID}, Z. Demiragli^{ID}, C. Erice^{ID}, E. Fontanesi^{ID}, D. Gastler^{ID}, S. Jeon^{ID}, J. Rohlf^{ID}, K. Salyer^{ID}, D. Sperka^{ID}, D. Spitzbart^{ID}, I. Suarez^{ID}, A. Tsatsos^{ID}, S. Yuan^{ID}

Brown University, Providence, Rhode Island, U.S.A.

G. Benelli^{ID}, X. Coubez²⁸, D. Cutts^{ID}, M. Hadley^{ID}, U. Heintz^{ID}, J.M. Hogan^{ID}⁸⁸, T. Kwon^{ID}, G. Landsberg^{ID}, K.T. Lau^{ID}, D. Li^{ID}, J. Luo^{ID}, S. Mondal^{ID}, M. Narain^{ID}[†], N. Pervan^{ID}, S. Sagir^{ID}⁸⁹, F. Simpson^{ID}, M. Stamenkovic^{ID}, W.Y. Wong, X. Yan^{ID}, W. Zhang

University of California, Davis, Davis, California, U.S.A.

S. Abbott^{ID}, J. Bonilla^{ID}, C. Brainerd^{ID}, R. Breedon^{ID}, M. Calderon De La Barca Sanchez^{ID}, M. Chertok^{ID}, M. Citron^{ID}, J. Conway^{ID}, P.T. Cox^{ID}, R. Erbacher^{ID}, G. Haza^{ID}, F. Jensen^{ID}, O. Kukral^{ID}, G. Mocellin^{ID}, M. Mulhearn^{ID}, D. Pellett^{ID}, W. Wei^{ID}, Y. Yao^{ID}, F. Zhang^{ID}

University of California, Los Angeles, California, U.S.A.

M. Bachtis^{ID}, R. Cousins^{ID}, A. Datta^{ID}, J. Hauser^{ID}, M. Ignatenko^{ID}, M.A. Iqbal^{ID}, T. Lam^{ID}, E. Manca^{ID}, W.A. Nash^{ID}, D. Saltzberg^{ID}, B. Stone^{ID}, V. Valuev^{ID}

University of California, Riverside, Riverside, California, U.S.A.

R. Clare^{ID}, M. Gordon, G. Hanson^{ID}, W. Si^{ID}, S. Wimpenny^{ID}[†]

University of California, San Diego, La Jolla, California, U.S.A.

J.G. Branson^{ID}, S. Cittolin^{ID}, S. Cooperstein^{ID}, D. Diaz^{ID}, J. Duarte^{ID}, R. Gerosa^{ID}, L. Giannini^{ID}, J. Guiang^{ID}, R. Kansal^{ID}, V. Krutelyov^{ID}, R. Lee^{ID}, J. Letts^{ID}, M. Masciovecchio^{ID}, F. Mokhtar^{ID}, M. Pieri^{ID}, M. Quinnan^{ID}, B.V. Sathia Narayanan^{ID}, V. Sharma^{ID}, M. Tadel^{ID}, E. Vourliotis^{ID}, F. Würthwein^{ID}, Y. Xiang^{ID}, A. Yagil^{ID}

University of California, Santa Barbara — Department of Physics, Santa Barbara, California, U.S.A.

A. Barzdukas , L. Brennan , C. Campagnari , G. Collura , A. Dorsett , J. Incandela , M. Kilpatrick , J. Kim , A.J. Li , P. Masterson , H. Mei , M. Oshiro , J. Richman , U. Sarica , R. Schmitz , F. Setti , J. Sheplock , D. Stuart , S. Wang

California Institute of Technology, Pasadena, California, U.S.A.

A. Bornheim , O. Cerri, A. Latorre, J.M. Lawhorn , J. Mao , H.B. Newman , T. Q. Nguyen , M. Spiropulu , J.R. Vlimant , C. Wang , S. Xie , R.Y. Zhu

Carnegie Mellon University, Pittsburgh, Pennsylvania, U.S.A.

J. Alison , S. An , M.B. Andrews , P. Bryant , V. Dutta , T. Ferguson , A. Harilal , C. Liu , T. Mudholkar , S. Murthy , M. Paulini , A. Roberts , A. Sanchez , W. Terrill

University of Colorado Boulder, Boulder, Colorado, U.S.A.

J.P. Cumalat , W.T. Ford , A. Hassani , G. Karathanasis , E. MacDonald, N. Manganelli , F. Marini , A. Perloff , C. Savard , N. Schonbeck , K. Stenson , K.A. Ulmer , S.R. Wagner , N. Zipper

Cornell University, Ithaca, New York, U.S.A.

J. Alexander , S. Bright-Thonney , X. Chen , D.J. Cranshaw , J. Fan , X. Fan , D. Gadkari , S. Hogan , J. Monroy , J.R. Patterson , J. Reichert , M. Reid , A. Ryd , J. Thom , P. Wittich , R. Zou

Fermi National Accelerator Laboratory, Batavia, Illinois, U.S.A.

M. Albrow , M. Alyari , O. Amram , G. Apollinari , A. Apresyan , L.A.T. Bauerick , D. Berry , J. Berryhill , P.C. Bhat , K. Burkett , J.N. Butler , A. Canepa , G.B. Cerati , H.W.K. Cheung , F. Chlebana , G. Cummings , J. Dickinson , I. Dutta , V.D. Elvira , Y. Feng , J. Freeman , A. Gandrakota , Z. Gecse , L. Gray , D. Green, A. Grummer , S. Grünendahl , D. Guerrero , O. Gutsche , R.M. Harris , R. Heller , T.C. Herwig , J. Hirschauer , L. Horyn , B. Jayatilaka , S. Jindariani , M. Johnson , U. Joshi , T. Klijnsma , B. Klima , K.H.M. Kwok , S. Lammel , D. Lincoln , R. Lipton , T. Liu , C. Madrid , K. Maeshima , C. Mantilla , D. Mason , P. McBride , P. Merkel , S. Mrenna , S. Nahn , J. Ngadiuba , D. Noonan , V. Papadimitriou , N. Pastika , K. Pedro , C. Pena ⁹⁰, F. Ravera , A. Reinsvold Hall ⁹¹, L. Ristori , E. Sexton-Kennedy , N. Smith , A. Soha , L. Spiegel , S. Stoynev , J. Strait , L. Taylor , S. Tkaczyk , N.V. Tran , L. Uplegger , E.W. Vaandering , I. Zoi

University of Florida, Gainesville, Florida, U.S.A.

C. Aruta , P. Avery , D. Bourilkov , L. Cadamuro , P. Chang , V. Cherepanov , R.D. Field, E. Koenig , M. Kolosova , J. Konigsberg , A. Korytov , K.H. Lo, K. Matchev , N. Menendez , G. Mitselmakher , A. Muthirakalayil Madhu , N. Rawal , D. Rosenzweig , S. Rosenzweig , K. Shi , J. Wang

Florida State University, Tallahassee, Florida, U.S.A.

T. Adams , A. Al Kadhim , A. Askew , N. Bower , R. Habibullah , V. Hagopian , R. Hashmi , R.S. Kim , S. Kim , T. Kolberg , G. Martinez, H. Prosper , P.R. Prova, O. Viazlo , M. Wulansatiti , R. Yohay , J. Zhang

Florida Institute of Technology, Melbourne, Florida, U.S.A.

B. Alsufyani, M.M. Baarmand , S. Butalla , T. Elkafrawy ²⁰, M. Hohlmann , R. Kumar Verma , M. Rahmani

University of Illinois Chicago, Chicago, U.S.A., Chicago, U.S.A.

M.R. Adams , C. Bennett, R. Cavanaugh , S. Dittmer , R. Escobar Franco , O. Evdokimov , C.E. Gerber , D.J. Hofman , J.h. Lee , D. S. Lemos , A.H. Merrit , C. Mills , S. Nanda , G. Oh , B. Ozek , D. Pilipovic , T. Roy , S. Rudrabhatla , M.B. Tonjes , N. Varelas , X. Wang , Z. Ye , J. Yoo

The University of Iowa, Iowa City, Iowa, U.S.A.

M. Alhusseini , D. Blend, K. Dilsiz ⁹², L. Emediato , G. Karaman , O.K. Köseyan , J.-P. Merlo, A. Mestvirishvili ⁹³, J. Nachtman , O. Neogi, H. Ogul ⁹⁴, Y. Onel , A. Penzo , C. Snyder, E. Tiras ⁹⁵

Johns Hopkins University, Baltimore, Maryland, U.S.A.

B. Blumenfeld , L. Corcodilos , J. Davis , A.V. Gritsan , L. Kang , S. Kyriacou , P. Maksimovic , M. Roguljic , J. Roskes , S. Sekhar , M. Swartz , T.Á. Vámi

The University of Kansas, Lawrence, Kansas, U.S.A.

A. Abreu , L.F. Alcerro Alcerro , J. Anguiano , P. Baringer , A. Bean , Z. Flowers , D. Grove , J. King , G. Krintiras , M. Lazarovits , C. Le Mahieu , C. Lindsey, J. Marquez , N. Minafra , M. Murray , M. Nickel , M. Pitt , S. Popescu ⁹⁶, C. Rogan , C. Royon , R. Salvatico , S. Sanders , C. Smith , Q. Wang , G. Wilson

Kansas State University, Manhattan, Kansas, U.S.A.

B. Allmond , A. Ivanov , K. Kaadze , A. Kalogeropoulos , D. Kim, Y. Maravin , K. Nam, J. Natoli , D. Roy , G. Sorrentino 

Lawrence Livermore National Laboratory, Livermore, California, U.S.A.

F. Rebassoo , D. Wright 

University of Maryland, College Park, Maryland, U.S.A.

E. Adams , A. Baden , O. Baron, A. Belloni , A. Bethani , Y.M. Chen , S.C. Eno , N.J. Hadley , S. Jabeen , R.G. Kellogg , T. Koeth , B. Kronheim, Y. Lai , S. Lascio , A.C. Mignerey , S. Nabili , C. Palmer , C. Papageorgakis , M.M. Paranjpe, L. Wang , K. Wong

Massachusetts Institute of Technology, Cambridge, Massachusetts, U.S.A.

J. Bendavid , W. Busza , I.A. Cali , Y. Chen , M. D'Alfonso , J. Eysermans , C. Freer , G. Gomez-Ceballos , M. Goncharov, P. Harris, D. Hoang, D. Kovalskyi , J. Krupa , L. Lavezzi

Y.-J. Lee , K. Long , C. Mironov , C. Paus , D. Rankin , C. Roland , G. Roland , S. Rothman , Z. Shi , G.S.F. Stephans , J. Wang, Z. Wang , B. Wyslouch , T. J. Yang

University of Minnesota, Minneapolis, Minnesota, U.S.A.

B. Crossman , B.M. Joshi , C. Kapsiak , M. Krohn , D. Mahon , J. Mans , B. Marzocchi , S. Pandey , M. Revering , R. Rusack , R. Saradhy , N. Schroeder , N. Strobbe , M.A. Wadud

University of Mississippi, Oxford, Mississippi, U.S.A.

L.M. Cremaldi

University of Nebraska-Lincoln, Lincoln, Nebraska, U.S.A.

K. Bloom , M. Bryson, D.R. Claes , C. Fangmeier , F. Golf , J. Hossain , C. Joo , I. Kravchenko , I. Reed , J.E. Siado , G.R. Snow[†], W. Tabb , A. Vagnerini , A. Wightman , F. Yan , D. Yu , A.G. Zecchinelli

State University of New York at Buffalo, Buffalo, New York, U.S.A.

G. Agarwal , H. Bandyopadhyay , L. Hay , I. Iashvili , A. Kharchilava , C. McLean , M. Morris , D. Nguyen , J. Pekkanen , S. Rappoccio , H. Rejeb Sfar, A. Williams

Northeastern University, Boston, Massachusetts, U.S.A.

G. Alverson , E. Barberis , Y. Haddad , Y. Han , A. Krishna , J. Li , M. Lu , G. Madigan , D.M. Morse , V. Nguyen , T. Orimoto , A. Parker , L. Skinnari , A. Tishelman-Charny , B. Wang , D. Wood

Northwestern University, Evanston, Illinois, U.S.A.

S. Bhattacharya , J. Bueghly, Z. Chen , K.A. Hahn , Y. Liu , Y. Miao , D.G. Monk , M.H. Schmitt , A. Taliercio , M. Velasco

University of Notre Dame, Notre Dame, Indiana, U.S.A.

R. Band , R. Bucci, S. Castells , M. Cremonesi, A. Das , R. Goldouzian , M. Hildreth , K.W. Ho , K. Hurtado Anampa , C. Jessop , K. Lannon , J. Lawrence , N. Loukas , L. Lutton , J. Mariano, N. Marinelli, I. Mcalister, T. McCauley , C. Mcgrady , K. Mohrman , C. Moore , Y. Musienko ¹⁶, H. Nelson , M. Osherson , R. Ruchti , A. Townsend , M. Wayne , H. Yockey, M. Zarucki , L. Zygalda

The Ohio State University, Columbus, Ohio, U.S.A.

A. Basnet , B. Bylsma, M. Carrigan , L.S. Durkin , C. Hill , M. Joyce , A. Lesauvage , M. Nunez Ornelas , K. Wei, B.L. Winer , B. R. Yates

Princeton University, Princeton, New Jersey, U.S.A.

F.M. Addesa , H. Bouchamaoui , P. Das , G. Dezoort , P. Elmer , A. Frankenthal , B. Greenberg , N. Haubrich , S. Higginbotham , G. Kopp , S. Kwan , D. Lange , A. Loeliger , D. Marlow , I. Ojalvo , J. Olsen , D. Stickland , C. Tully

University of Puerto Rico, Mayaguez, Puerto Rico, U.S.A.

S. Malik

Purdue University, West Lafayette, Indiana, U.S.A.

A.S. Bakshi , V.E. Barnes , S. Chandra , R. Chawla , S. Das , A. Gu , L. Gutay,
 M. Jones , A.W. Jung , D. Kondratyev , A.M. Koshy, M. Liu , G. Negro , N. Neumeister ,
 G. Paspalaki , S. Piperov , A. Purohit , V. Scheurer, J.F. Schulte , M. Stojanovic ,
 J. Thieman , A. K. Virdi , F. Wang , W. Xie

Purdue University Northwest, Hammond, Indiana, U.S.A.

J. Dolen , N. Parashar , A. Pathak 

Rice University, Houston, Texas, U.S.A.

D. Acosta , A. Baty , T. Carnahan , S. Dildick , K.M. Ecklund , P.J. Fernández Manteca ,
 S. Freed, P. Gardner, F.J.M. Geurts , A. Kumar , W. Li , O. Miguel Colin , B.P. Padley ,
 R. Redjimi, J. Rotter , E. Yigitbasi , Y. Zhang

University of Rochester, Rochester, New York, U.S.A.

A. Bodek , P. de Barbaro , R. Demina , J.L. Dulemba , C. Fallon, A. Garcia-Bellido ,
 O. Hindrichs , A. Khukhunaishvili , P. Parygin ⁸⁶, E. Popova ⁸⁶, R. Taus , G.P. Van Onsem

The Rockefeller University, New York, New York, U.S.A.

K. Goulianatos 

Rutgers, The State University of New Jersey, Piscataway, New Jersey, U.S.A.

B. Chiarito, J.P. Chou , Y. Gershtein , E. Halkiadakis , A. Hart , M. Heindl ,
 D. Jaroslawski , O. Karacheban ³¹, I. Laflotte , A. Lath , R. Montalvo, K. Nash, H. Routray ,
 S. Salur , S. Schnetzer, S. Somalwar , R. Stone , S.A. Thayil , S. Thomas, J. Vora ,
 H. Wang

University of Tennessee, Knoxville, Tennessee, U.S.A.

H. Acharya, D. Ally , A.G. Delannoy , S. Fiorendi , T. Holmes , N. Karunaratna , L. Lee ,
 E. Nibigira , S. Spanier

Texas A&M University, College Station, Texas, U.S.A.

D. Aebi , M. Ahmad , O. Bouhalil ⁹⁷, M. Dalchenko , R. Eusebi , J. Gilmore , T. Huang ,
 T. Kamon ⁹⁸, H. Kim , S. Luo , S. Malhotra, R. Mueller , D. Overton , D. Rathjens ,
 A. Safonov

Texas Tech University, Lubbock, Texas, U.S.A.

N. Akchurin , J. Damgov , V. Hegde , A. Hussain , Y. Kazhykarim, K. Lamichhane ,
 S.W. Lee , A. Mankel , T. Mengke, S. Muthumuni , T. Peltola , I. Volobouev , A. Whitbeck

Vanderbilt University, Nashville, Tennessee, U.S.A.

E. Appelt , S. Greene, A. Gurrola , W. Johns , R. Kunawalkam Elayavalli , A. Melo ,
 F. Romeo , P. Sheldon , S. Tuo , J. Velkovska , J. Viinikainen

University of Virginia, Charlottesville, Virginia, U.S.A.

B. Cardwell , B. Cox , J. Hakala , R. Hirosky , A. Ledovskoy , A. Li , C. Neu ,
 C.E. Perez Lara 

Wayne State University, Detroit, Michigan, U.S.A.

P.E. Karchin¹⁰

University of Wisconsin — Madison, Madison, Wisconsin, U.S.A.

A. Aravind, S. Banerjee¹⁰, K. Black¹⁰, T. Bose¹⁰, S. Dasu¹⁰, I. De Bruyn¹⁰, P. Everaerts¹⁰, C. Galloni, H. He¹⁰, M. Herndon¹⁰, A. Herve¹⁰, C.K. Koraka¹⁰, A. Lanaro, R. Loveless¹⁰, J. Madhusudanan Sreekala¹⁰, A. Mallampalli¹⁰, A. Mohammadi¹⁰, S. Mondal, G. Parida¹⁰, D. Pinna, A. Savin, V. Shang¹⁰, V. Sharma¹⁰, W.H. Smith¹⁰, D. Teague, H.F. Tsoi¹⁰, W. Vetens¹⁰, A. Warden¹⁰

Authors affiliated with an institute or an international laboratory covered by a cooperation agreement with CERN

S. Afanasiev¹⁰, V. Andreev¹⁰, Yu. Andreev¹⁰, T. Aushev¹⁰, M. Azarkin¹⁰, A. Babaev¹⁰, A. Belyaev¹⁰, V. Blinov⁹⁹, E. Boos¹⁰, V. Borshch¹⁰, D. Budkouski¹⁰, V. Bunichev¹⁰, V. Chekhovsky, R. Chistov⁹⁹, M. Danilov⁹⁹, A. Dermenev¹⁰, T. Dimova⁹⁹, D. Druzhkin¹⁰⁰, M. Dubinin⁹⁰, L. Dudko¹⁰, A. Ershov¹⁰, G. Gavrilov¹⁰, V. Gavrilov¹⁰, S. Gninenko¹⁰, V. Golovtcov¹⁰, N. Golubev¹⁰, I. Golutvin¹⁰, I. Gorbunov¹⁰, A. Gribushin¹⁰, Y. Ivanov¹⁰, V. Kachanov¹⁰, L. Kardapoltsev⁹⁹, V. Karjavine¹⁰, A. Karneyeu¹⁰, V. Kim⁹⁹, M. Kirakosyan, D. Kirpichnikov¹⁰, M. Kirsanov¹⁰, V. Klyukhin¹⁰, O. Kodolova¹⁰¹, D. Konstantinov¹⁰, V. Korenkov¹⁰, A. Kozyrev⁹⁹, N. Krasnikov¹⁰, A. Lanev¹⁰, P. Levchenko¹⁰², N. Lychkovskaya¹⁰, V. Makarenko¹⁰, A. Malakhov¹⁰, V. Matveev⁹⁹, V. Murzin¹⁰, A. Nikitenko^{103,101}, S. Obraztsov¹⁰, V. Oreshkin¹⁰, V. Palichik¹⁰, V. Perelygin¹⁰, M. Perfilov, S. Petrushanko¹⁰, S. Polikarpov⁹⁹, V. Popov¹⁰, O. Radchenko⁹⁹, M. Savina¹⁰, V. Savrin¹⁰, V. Shalaev¹⁰, S. Shmatov¹⁰, S. Shulha¹⁰, Y. Skovpen⁹⁹, S. Slabospitskii¹⁰, V. Smirnov¹⁰, D. Sosnov¹⁰, V. Sulimov¹⁰, E. Tcherniaev¹⁰, A. Terkulov¹⁰, O. Teryaev¹⁰, I. Tlisova¹⁰, A. Toropin¹⁰, L. Uvarov¹⁰, A. Uzunian¹⁰, A. Vorobyev[†], N. Voytishin¹⁰, B.S. Yuldashev¹⁰⁴, A. Zarubin¹⁰, I. Zhizhin¹⁰, A. Zhokin¹⁰

[†] Deceased

¹ Also at Yerevan State University, Yerevan, Armenia

² Also at TU Wien, Vienna, Austria

³ Also at Institute of Basic and Applied Sciences, Faculty of Engineering, Arab Academy for Science, Technology and Maritime Transport, Alexandria, Egypt

⁴ Also at Ghent University, Ghent, Belgium

⁵ Also at Universidade Estadual de Campinas, Campinas, Brazil

⁶ Also at Federal University of Rio Grande do Sul, Porto Alegre, Brazil

⁷ Also at UFMS, Nova Andradina, Brazil

⁸ Also at Nanjing Normal University, Nanjing, China

⁹ Now at Henan Normal University, Xinxiang, China

¹⁰ Now at The University of Iowa, Iowa City, Iowa, U.S.A.

¹¹ Also at University of Chinese Academy of Sciences, Beijing, China

¹² Also at China Center of Advanced Science and Technology, Beijing, China

¹³ Also at University of Chinese Academy of Sciences, Beijing, China

¹⁴ Also at China Spallation Neutron Source, Guangdong, China

¹⁵ Also at Université Libre de Bruxelles, Bruxelles, Belgium

¹⁶ Also at an institute or an international laboratory covered by a cooperation agreement with CERN

¹⁷ Also at Helwan University, Cairo, Egypt

¹⁸ Now at Zewail City of Science and Technology, Zewail, Egypt

- ¹⁹ Also at British University in Egypt, Cairo, Egypt
²⁰ Now at Ain Shams University, Cairo, Egypt
²¹ Also at Birla Institute of Technology, Mesra, Mesra, India
²² Also at Purdue University, West Lafayette, Indiana, U.S.A.
²³ Also at Université de Haute Alsace, Mulhouse, France
²⁴ Also at Department of Physics, Tsinghua University, Beijing, China
²⁵ Also at The University of the State of Amazonas, Manaus, Brazil
²⁶ Also at Erzincan Binali Yildirim University, Erzincan, Turkey
²⁷ Also at University of Hamburg, Hamburg, Germany
²⁸ Also at RWTH Aachen University, III. Physikalisches Institut A, Aachen, Germany
²⁹ Also at Isfahan University of Technology, Isfahan, Iran
³⁰ Also at Bergische University Wuppertal (BUW), Wuppertal, Germany
³¹ Also at Brandenburg University of Technology, Cottbus, Germany
³² Also at Forschungszentrum Jülich, Juelich, Germany
³³ Also at CERN, European Organization for Nuclear Research, Geneva, Switzerland
³⁴ Also at Institute of Physics, University of Debrecen, Debrecen, Hungary
³⁵ Also at Institute of Nuclear Research ATOMKI, Debrecen, Hungary
³⁶ Now at Universitatea Babes-Bolyai — Facultatea de Fizica, Cluj-Napoca, Romania
³⁷ Also at Physics Department, Faculty of Science, Assiut University, Assiut, Egypt
³⁸ Also at HUN-REN Wigner Research Centre for Physics, Budapest, Hungary
³⁹ Also at Faculty of Informatics, University of Debrecen, Debrecen, Hungary
⁴⁰ Also at Punjab Agricultural University, Ludhiana, India
⁴¹ Also at University of Hyderabad, Hyderabad, India
⁴² Also at University of Visva-Bharati, Santiniketan, India
⁴³ Also at Indian Institute of Science (IISc), Bangalore, India
⁴⁴ Also at IIT Bhubaneswar, Bhubaneswar, India
⁴⁵ Also at Institute of Physics, Bhubaneswar, India
⁴⁶ Also at Deutsches Elektronen-Synchrotron, Hamburg, Germany
⁴⁷ Also at Department of Physics, Isfahan University of Technology, Isfahan, Iran
⁴⁸ Also at Sharif University of Technology, Tehran, Iran
⁴⁹ Also at Department of Physics, University of Science and Technology of Mazandaran, Behshahr, Iran
⁵⁰ Also at Italian National Agency for New Technologies, Energy and Sustainable Economic Development, Bologna, Italy
⁵¹ Also at Centro Siciliano di Fisica Nucleare e di Struttura Della Materia, Catania, Italy
⁵² Also at Università degli Studi Guglielmo Marconi, Roma, Italy
⁵³ Also at Scuola Superiore Meridionale, Università di Napoli ‘Federico II’, Napoli, Italy
⁵⁴ Also at Fermi National Accelerator Laboratory, Batavia, Illinois, U.S.A.
⁵⁵ Also at Università di Napoli ‘Federico II’, Napoli, Italy
⁵⁶ Also at Laboratori Nazionali di Legnaro dell’INFN, Legnaro, Italy
⁵⁷ Also at Consiglio Nazionale delle Ricerche — Istituto Officina dei Materiali, Perugia, Italy
⁵⁸ Also at Riga Technical University, Riga, Latvia
⁵⁹ Also at Department of Applied Physics, Faculty of Science and Technology, Universiti Kebangsaan Malaysia, Bangi, Malaysia
⁶⁰ Also at Consejo Nacional de Ciencia y Tecnología, Mexico City, Mexico
⁶¹ Also at Trincomalee Campus, Eastern University, Sri Lanka, Nilaveli, Sri Lanka
⁶² Also at Saegis Campus, Nugegoda, Sri Lanka
⁶³ Also at INFN Sezione di Pavia, Università di Pavia, Pavia, Italy
⁶⁴ Also at National and Kapodistrian University of Athens, Athens, Greece
⁶⁵ Also at Ecole Polytechnique Fédérale Lausanne, Lausanne, Switzerland
⁶⁶ Also at University of Vienna Faculty of Computer Science, Vienna, Austria
⁶⁷ Also at Universität Zürich, Zurich, Switzerland
⁶⁸ Also at Stefan Meyer Institute for Subatomic Physics, Vienna, Austria
⁶⁹ Also at Laboratoire d’Annecy-le-Vieux de Physique des Particules, IN2P3-CNRS, Annecy-le-Vieux, France

- ⁷⁰ Also at Near East University, Research Center of Experimental Health Science, Mersin, Turkey
⁷¹ Also at Konya Technical University, Konya, Turkey
⁷² Also at Izmir Bakircay University, Izmir, Turkey
⁷³ Also at Adiyaman University, Adiyaman, Turkey
⁷⁴ Also at Bozok Universitetesi Rektörlüğü, Yozgat, Turkey
⁷⁵ Also at Marmara University, Istanbul, Turkey
⁷⁶ Also at Milli Savunma University, Istanbul, Turkey
⁷⁷ Also at Kafkas University, Kars, Turkey
⁷⁸ Also at Hacettepe University, Ankara, Turkey
⁷⁹ Also at Istanbul University — Cerrahpasa, Faculty of Engineering, Istanbul, Turkey
⁸⁰ Also at Yildiz Technical University, Istanbul, Turkey
⁸¹ Also at Vrije Universiteit Brussel, Brussel, Belgium
⁸² Also at School of Physics and Astronomy, University of Southampton, Southampton, United Kingdom
⁸³ Also at University of Bristol, Bristol, United Kingdom
⁸⁴ Also at IPPP Durham University, Durham, United Kingdom
⁸⁵ Also at Monash University, Faculty of Science, Clayton, Australia
⁸⁶ Now at an institute or an international laboratory covered by a cooperation agreement with CERN
⁸⁷ Also at Università di Torino, Torino, Italy
⁸⁸ Also at Bethel University, St. Paul, Minnesota, U.S.A.
⁸⁹ Also at Karamanoğlu Mehmetbey University, Karaman, Turkey
⁹⁰ Also at California Institute of Technology, Pasadena, California, U.S.A.
⁹¹ Also at United States Naval Academy, Annapolis, Maryland, U.S.A.
⁹² Also at Bingöl University, Bingöl, Turkey
⁹³ Also at Georgian Technical University, Tbilisi, Georgia
⁹⁴ Also at Sinop University, Sinop, Turkey
⁹⁵ Also at Erciyes University, Kayseri, Turkey
⁹⁶ Also at Horia Hulubei National Institute of Physics and Nuclear Engineering (IFIN-HH), Bucharest, Romania
⁹⁷ Also at Texas A&M University at Qatar, Doha, Qatar
⁹⁸ Also at Kyungpook National University, Daegu, Korea
⁹⁹ Also at another institute or international laboratory covered by a cooperation agreement with CERN
¹⁰⁰ Also at Universiteit Antwerpen, Antwerpen, Belgium
¹⁰¹ Also at Yerevan Physics Institute, Yerevan, Armenia
¹⁰² Also at Northeastern University, Boston, Massachusetts, U.S.A.
¹⁰³ Also at Imperial College, London, United Kingdom
¹⁰⁴ Also at Institute of Nuclear Physics of the Uzbekistan Academy of Sciences, Tashkent, Uzbekistan